Final Master's Thesis

Master's Degree in Industrial Engineering (ETSEIB)

Reversible Solid Oxide Cell modelling and characterisation in customized experimental station

Author: Ignasi Lleonsí Carrillo
Director: Maria Serra Prat
2020/2021 Q2

Escola Tècnica Superior
d'Enginyeria Industrial de Barcelona

ETSEIB

UPC

ETSEIB

ABSTRACT

Electrical energy use is rapidly increasing in most countries. At the same time, concerns about climate change call for renewable solutions instead of using traditional electrical energy sources (coal, petroleum, natural gas, etc.).

A promising solution to the intermittency of renewable energy sources (solar, wind) can be found in Reversible Solid Oxide Cells (RSOC). RSOC can operate in fuel cell mode (Solid Oxide Fuel Cell, SOFC) and electrolysis mode (Solid Oxide Electrolyser Cell, SOEC) interchangeably. SOFC delivers electrical energy by transforming hydrogen into water, a process that results in electrical energy and heat. SOEC uses electrical energy to split water into hydrogen and oxygen, allowing for the storage of green hydrogen.

This work has been elaborated within the HyBCN project, which intends to develop a working RSOC prototype with a high operating efficiency. Different groups collaborated in this project: *Institut de Recerca en Energia de Catalunya* (IREC), *Institut de Robòtica I Informàtica Industrial* (IRI) and *Asesoría Energética S.A.* (AESA).

In this thesis, an experimental station situated in IREC's facilities equipped with a similar stack to the prototype's is programmed and a series of experiments are performed to obtain relevant data in SOFC and SOEC modes. Then, a RSOC Simulink model is used as a starting point and an improved version is developed, which includes the stack auxiliary equipment (heat exchangers, fuel mixer). A simple control system is developed, which allows the control of temperature (heating or cooling) and gas mass flow rates. Finally, a first approach to parameter estimation with experimental data is made, using the Particle Swarm Optimization method.

ETSEIB

CONTENTS

ETSEIB

1. Introduction

As renewable energy is becoming more and more relevant in modern society, its challenges are becoming more obvious and important to solve. The U.S. Energy Information Administration (EIA) projects that world energy consumption will grow by nearly 50% between 2018 and 2050. Worldwide renewable energy consumption increases by 3.1% per year between 2018 and 2050, compared with 0.6% annual growth in petroleum, 0.4% growth in coal, and 1.1% annual growth in natural gas consumption. [1]

Climate change and its derivates will force humanity to rely on renewable energy for this future increase in utilization. Therefore, new technologies are being studied, attempting to find solutions to the different problems renewable energy brings to the table. One of these problems is that renewable energy relies on natural factors (sun, wind, etc.) to produce energy, making its availability intermittent and unpredictable. This characteristic means it is necessary to store it in order to make it more useful.

Solid oxide cells (RSOC) are reversible devices that can convert chemical energy to electrical energy and vice versa with high efficiency. This means they can operate in two different modes, fuel cell mode or electrolysis mode. Electrolysis is a process that uses electrical energy to separate molecules with a redox reaction, such as hydrogen and oxygen from water, resulting in the production of hydrogen, which can be stored. Fuel cells perform the opposite reaction, using fuel (e.g. hydrogen) and an oxidizing agent (e.g. oxygen) to get a product (e.g. water) plus electricity via an electrochemical reaction. Effectively, this makes a RSOC system a "green battery", that can make green hydrogen for storage or produce energy by consuming it, depending on availability of energy sources and demand.

1.1. Project origin and context

This master's thesis has been elaborated within HyBCN, a project carried out by *Institut de Robòtica i Informàtica Industrial* (IRI), *Catalonia Energy Research Institute* (IREC) and *Asesoría Energética S.A.* (AESA). HyBCN goal is to develop an integrated system that converts water into green hydrogen (electrolyser operation mode), stores it and produces renewable energy for on-demand use (fuel cell operation mode). HyBCN project started in January 2020 and lasted for 18 months.

The developed system will be an affordable RSOC prototype that can perform in both electrolysis and fuel cell modes with a relatively high energy efficiency. The results obtained with HyBCN will therefore allow for a better efficiency and management of renewable energy in Barcelona.[2]

This master's thesis has been developed in IRI. IRI has collaborated in different previous projects related to solid oxide cells, like the REFER and the COSIN projects, both part of the RIS3CAT program. These projects are the cornerstone for IRI's participation in HyBCN, and have provided useful resources and information for the elaboration of this thesis.

REFER stands for Energetic Reduction and Flexibility in Rehabilitated Buildings. The project aims to improve the energetic alternatives available for buildings, granting them flexibility with different options to face renewable energy generation and energetic efficiency introducing new technologies like SOFC and others, not limiting them to solar panels and well-known batteries. In this work, a solid oxide fuel cell dynamic model has been developed by IRI. The model was calibrated using experimental data. A strategy is proposed for the thermal management of the stack and a control system is designed to keep the operating temperature of the system at the desired setpoint. This implemented strategy and controller is evaluated through simulation. [3] This model has been used later to design the RSOC model used and furtherly developed in this work.

COSIN stands for Synthetic Fuels, and among other things it focuses on the design of efficient systems based on electrolysis and co-electrolysis. In this project, the IRI research team developed a dynamic model of a SOEC implemented in MATLAB and compared it with experimental data. The analysis of the experimental data in the COSIN project suggested a hydrogen leak. Based on the SOEC thermal model, a methodology to quantify the flow of hydrogen that is leaked out is proposed and applied to the experimental system. [4]

1.2. Motivation

The HyBCN project involves different fields of knowledge, namely energy management, renewable energy sources, chemistry, control theory, system modelling and design and development of a physical prototype. The author showed significant interest in these topics in the past and decided that the opportunity to participate in this project is a good way to get involved and learn more about many of them.

As mentioned before, the collaboration between different research institutes is a very positive aspect, and the author hopes it will give him good experience working with a team involving many different professionals.

The main goal of the HyBCN project originates from environmental needs that involve a modern society's energy management. This is among the most pressing challenges humanity is currently facing. Currently, great quantities of readily available renewable energy are not being used because of, among other reasons, its intermittent nature. The proposed reversible solid oxide cell is a very promising technology to solve this problem because it can store or produce energy depending on the power the grid demands.

For these reasons, the HyBCN project and this work are very motivating goals to work towards for the author.

1.3. Project objectives

- ### Programming IREC's experimental station

This refers to the instrumentation and programming of an experimental station of a reversible solid oxide cell located in IREC's facilities.

The programming is done using the LabVIEW software, by NI (National Instruments). An existing program created by a previous student will be used and improved to add more features, as well making it more reliable and safer for experiments. The program has a user interface, and a CompactRIO real-time controller is used to establish communications with the different elements of the system and the acquisition of data. It must allow the laboratory worker to control the system manually, as well as automatically perform the set of programmed experiments.

- ### Modelling of a reversible solid oxide cell

The work will address the modelling of a reversible solid oxide cell using MATLAB and Simulink. An existing reversible solid oxide cell model will be used as a starting point and modified to include all relevant elements in the prototype's balance of plant (BOP): boiler, fuel channel heat exchanger, air side heat exchanger, and efficiency calculation.

The experimental data obtained will be used to improve the model's representation of a real system using parameter estimation methods.

- ### Design of control system

A simple gas flows and temperature control system for the prototype will be designed in Simulink to fit the completed model's needs. It must ensure maximum efficiency, and, if possible, minimum degradation of the fuel cell.

ETSEIB

1.4. Project scope

The scope of the project can refer directly to the main objectives.

- **Programming scope**

The LabVIEW program that will be used to run the experiments will have to meet the following requirements:

- **Complete:** It must be able to automatically perform the set of experiments designed by IREC and IRI.

- **Friendly user interface**: The laboratory worker, with previous RSOC knowledge, should find it easy to understand and navigate.

- **Safe**: The program must include the safety measures necessary to avoid danger for the laboratory worker and the excessive degradation of the RSOC.

- **Efficient**: The efficiency of the program is key to avoid memory problems during the hours-long experiments of a RSOC.

- **Model scope**

The model, after parameter identification based on experimental data, must be a reasonably accurate simulation of the real system. This will be key to design a validated control system, that is expected to perform on the prototype.

- **Control system scope**

The design of the RSOC controllers for maximum efficiency in MATLAB/Simulink is to be achieved. The implementation of the control system on the real system (RSOC prototype) will be carried out by a third party and is not considered in this thesis.

ETSEIB

2. Solid oxide cells state of the art

In this chapter the history and context of reversible solid oxide cells will be introduced, to understand its differences with similar devices for energy management as well as its advantages and disadvantages.

Later, the general concepts that define a solid oxide's cell behaviour will be explained. Chemical reaction's relation to voltage, thermodynamics, and other aspects are important to define the conditions that affect the fuel cell operation and efficiency, and a good understanding is necessary to achieve the project's objectives.

2.1. Fuel cell history

The invention of the fuel cell is generally credited to William Grove, in 1839, when he proved that electric current could be obtained from an electrochemical reaction ($H_2 + O_2$) with a platinum catalyst. However, its development was slow due to the better alternative offered by thermal machines.

In the 1960s, NASA developed the technology and used proton-exchange membrane fuel cells (PEMFC) in its space flights to provide power. The crucial characteristic of PEMFC was that they did not emit pollution, which was essential in a spacecraft. Because of NASA's success case with fuel cell technology, it caught the attention of the industry and market, but economic reasons prevented it from competing with existing energy solutions. [5]

In the 70s and 80s, environmental concerns grew, and clean air legislation was approved in Europe and the United States. This, coupled with energy efficiency, worries about oil prices and energy shortages, prompted large companies and governments to invest in research projects that included fuel cells. During this time, significant advances were made in the phosphoric acid fuel cell (PAFC) technology, to the point that thousands of units were predicted to be built for stationary use by the end of the century, but few were built.

In the 90s, PEMFC and solid oxide fuel cells (SOFC) got the most attention, with a focus on small stationary applications. Different countries started investing into research, expecting these technologies to have practical uses in the short term. With further restrictions being applied to internal combustion vehicles, companies like Toyota, General Motors and Daimler also invested in PEMFC research. Molten carbonate fuel cells (MCFC) and SOFC also experienced significant development for stationary applications.

After the year 2000 and until today, governments and large companies steadily increased funding of fuel cell technology research, as efficient, low-emission energy production

alternatives became more urgent. One of the first promising markets to be exploited was bus transportation in the mid-2000s, since the set routes made refuelling with hydrogen easy to predict. It is still one of the most spread use cases of fuel cell technology.[6]

In the late 2000s, fuel cells were commercialized in a variety of applications, such as leisure (boats, campervans), military applications and micro fuel cell units for educational kits or toys. Japan started a large-scale program called ENE-FARM, seen in Figure 1, focused on micro-cogeneration (micro combined heat and power, MCHP) using PEMFC technology, that lasted until 2019 and installed around 270.000 units in residential households. This program saved an estimated 324.000 tonnes of CO_2 each year. Their next focus are fuel cell vehicles as well as increasing the number of micro-cogeneration units to over 5 million by 2025.[7]
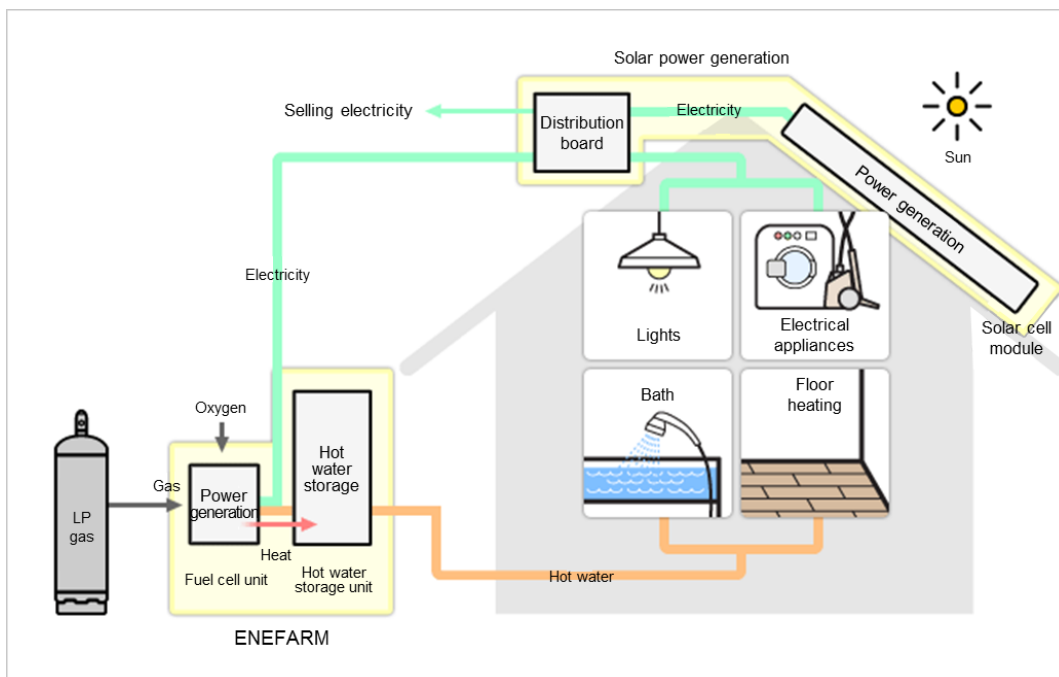
Figure 1. ENE-FARM installation sketch. Source: itcenex.com

In recent years, the effects of the global economic recession slowed down many research and development programs or caused them to be aborted. However, fuel cells are still seen as a promising alternative to conventional energy management systems. Governments around the world have kept investing resources in their development, followed closely by private companies. As fuel cell technology attempts the transition from research and development to commercialisation, predictions of a steady growth are widely accepted. The success of certain designs and applications, such as the hydrogen bus, has helped standard reference designs develop for different types of fuel cells, slowly inching closer to market production.

ETSEIB

2.2. Types of fuel cells

All fuel cells follow the same principle; therefore, they work in a similar way. Every design consists of an anode, cathode, and an electrolyte separating them. Two chemical reactions take place at the same time. Firstly, the fuel is oxidized in the cathode, making it a positively charged ion and generating a negatively charged electron. The electron travels through a wire towards the cathode, creating an electric current. In the cathode, the ions react with a third chemical, usually oxygen, and typically generate water or CO_2.

Different design and operational characteristics are what define the types of fuel cells. The most common characteristics that differ in each type are the electrolyte material, operating temperature, stack power and electrical efficiency. Table 1 is a good summary of the most common types of fuel cell and its characteristics.

FUEL CELL TYPE	COMMON ELECTROLYTE	OPERATING TEMPERATURE	TYPICAL STACK SIZE	ELECTRICAL EFFICIENCY
Polymer electrolyte membrane (PEMFC)	Perfluoro-sulfonic acid	<120ºC	<1 kW–100 kW	60% direct H2
				40% reformed fuel
Alkaline (AFC)	Aqueous potassium hydroxide soaked in a porous matrix, or alkaline polymer membrane	<100ºC	1–100 kW	60%
Phosphoric acid (PAFC)	Phosphoric acid soaked in a porous matrix or imbibed in a polymer membrane	150-200ºC	5–400 kW, 100 kW module (liquid PAFC) <10 kW (polymer membrane)	40%
Molten carbonate (MCFC)	Molten lithium, sodium, and/or potassium carbonates, soaked in a porous matrix	600-700ºC	300 kW–3 MW, 300 kW module	50%
Solid Oxide (SOFC)	Yttria stabilized zirconia (YSZ)	500-1000ºC	1 kW–2 MW	60%

Table 1. Comparison of fuel cell technologies. Source:energy.gov[8]

ETSEIB

2.3. Reversible RSOC description

A reversible solid oxide cell is an electrochemical conversion device characterized by a solid oxide or ceramic electrolyte separating two electrodes, operating at a high temperature (500-1000ºC). It can operate in two modes: SOFC (Solid Oxide Fuel Cell) and SOEC (Solid Oxide Electrolyser Cell). This is made possible by the construction materials and similar operating conditions between both modes, which does not hold true for other types of fuel cells.
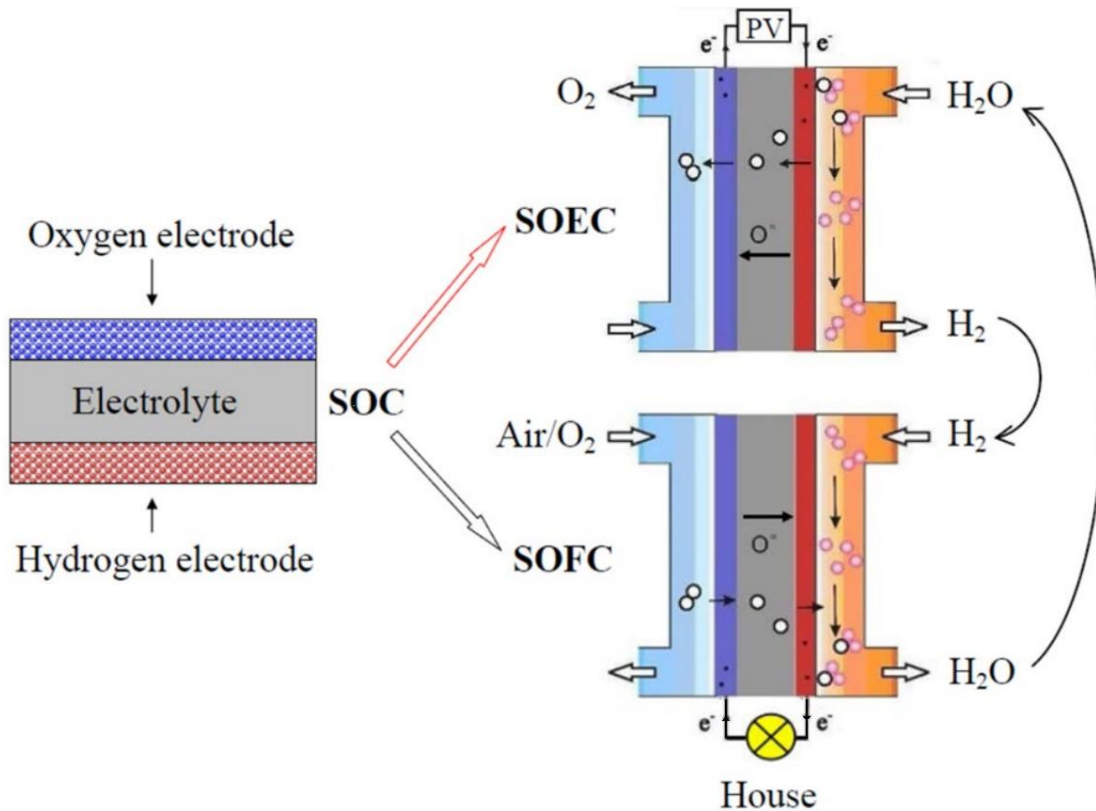
Figure 2. Operation of a RSOC in both modes. Adapted from [9]

As seen in Figure 2, in SOFC mode, the hydrogen combustion reaction is split into two electrochemical half reactions. The fuel (Hydrogen) gives away electrons in the porous anode, which travel towards the cathode via an external circuit, doing useful work before completing the reaction. These electrons reduce oxygen molecules inside the porous cathode, and oxygen ions travel through the dense electrolyte towards the anode, forming water:

$$H_2 \rightarrow 2H^+ + 2e^- \qquad (1)$$

$$\frac{1}{2}O_2 + 2H^+ + 2e^- \rightarrow H_2O \qquad (2)$$

In SOEC mode, the chemical reactions (1) and (2) happen in reverse. The fuel (steam) is introduced into the porous cathode, and a voltage is applied to force electron circulation. This causes the steam to be reduced in the electrolyte surface into H_2 and oxygen ions. The oxygen ions travel through the dense electrolyte, while H_2 gas flows out of the porous cathode and is collected at its surface. This redox reaction is endothermic and consumes electricity to separate steam into H_2 and oxygen. Figure 3 shows the gases flow and an example of construction of a fuel cell.
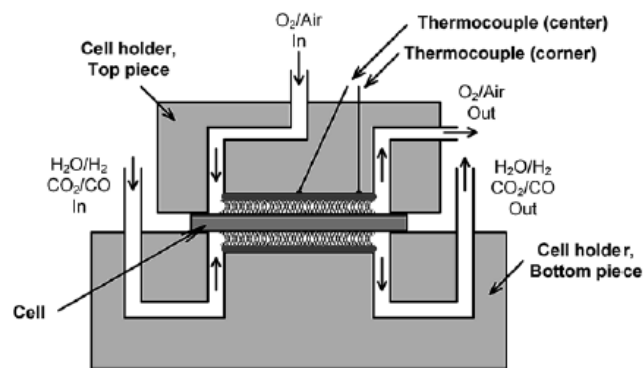
Figure 3. Example of a single-cell fuel cell assembly. From [10]

The biggest advantages of a solid oxide cell device are high efficiency (with co-generation potential and not limited by Carnot efficiency), long-term stability for stationary applications[11], very low emissions and relatively low cost.

The disadvantages include its high operational temperature (500 to 1000ºC), which result in long start-up times, and the use of materials that can withstand harsh conditions.[12] They can also be very sensible to fast changes of operating conditions, leading to faster degradation.

2.4. Electrochemical calculation

In this section the different electrochemical aspects that occur in a reversible solid oxide cell will be explained thoroughly.

As we can see in Figure 4, a typical fuel cell under current demand experiences different types of energetic losses (polarizations), caused by diverse phenomena occurring within the fuel cell. The first effect is by partial pressure of gases in the stack and calculated by the Nernst equation. Other effects such as activation polarization, ohmic polarization and concentration polarization depend on current density, and produce different voltage drops (overpotentials), explained in this chapter.
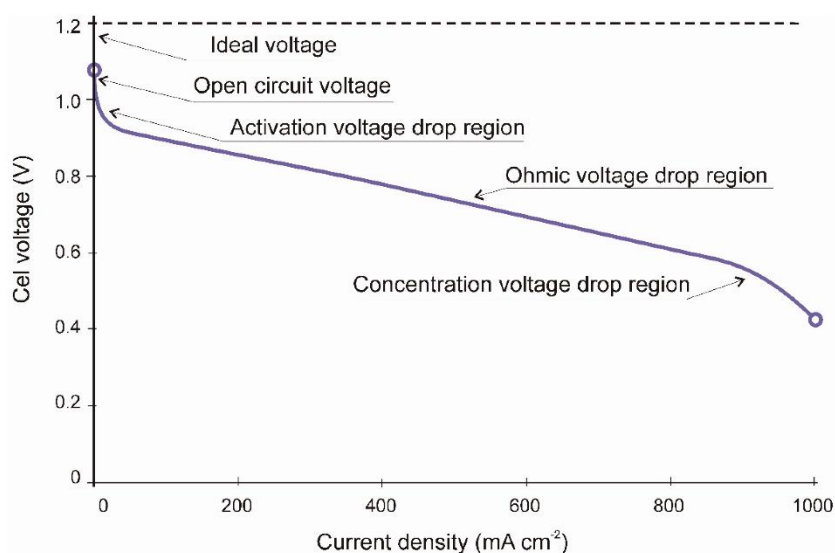

*Figure 4. Typical SOFC voltage-current graph, operating at about 800ºC*

2.4.1. Gibbs free energy

The behaviour of a fuel cell is ruled by the chemical reactions that occur within it. To quantify the energy generated by these chemical reactions, the Gibbs free energy represents the maximum reversible work a thermodynamic system at constant temperature and pressure can perform, measured in Joules. Therefore, the change in the Gibbs free energy will be directly related to the power that can be obtained from a fuel cell system.

The resulting energy of the reaction will be the difference between the Gibbs free energies of reactants and products, in the form:

$$\Delta G_f = \Delta G_{f,products} - \Delta G_{f,reactants}$$

Considering the RSOC operates in SOFC mode, the global reaction is the following:

$$SOFC: H_2 + \frac{1}{2}O_2 \rightarrow H_2O \tag{3}$$

$$SOEC: H_2O \rightarrow H_2 + \frac{1}{2}O_2 \tag{4}$$
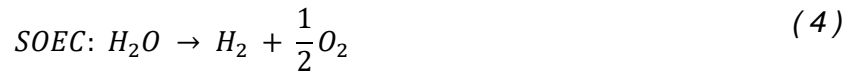
The change in the Gibbs free energy of formation can be defined as explained before, as the difference of energies, resulting in:

$$\Delta G_f = G_{f,H_2O} - G_{f,H_2} - \frac{1}{2}G_{f,O_2} \tag{5}$$

And, in molar form, which is the most typical expression to be used in calculations, the expression is as follows:

$$\Delta \hat{g}_{f,FC} = \hat{g}_{f,H_2O} - \hat{g}_{f,H_2} - \frac{1}{2}\hat{g}_{f,O_2} \tag{6}$$

Where $\hat{g}_f$ refers to the molar energy for each species that constitutes the reaction, while $\Delta \hat{g}_{f,FC}$ and $\Delta \hat{g}_{f,E}$ are the change in molar free Gibbs energy in fuel cell and electrolyser mode respectively. One can easily reach the conclusion that the relation between the Gibbs free energy in fuel cell and electrolyser mode is that one is the opposite sign of the other, while the absolute value remains the same, in the form:

$$\Delta \hat{g}_{f,FC} = -\Delta \hat{g}_{f,E} \tag{7}$$

The Gibbs free energy is calculated assuming the process is isothermal and isobaric.

ETSEIB

Still, the temperature of the fuel cell has to be considered in the Gibbs free energy calculation since it is as following:

$$\Delta \hat{g}_f = \Delta \hat{h}_f + T\Delta \hat{s}$$

(8)

Where $\hat{h}_f$ is the enthalpy of formation, $\hat{s}$ is the entropy, and T is the temperature in Kelvin.

Now that we know how to calculate the Gibbs free energy of each component, and the total change in energy with the balance equation, it is possible to determine the work potential of a fuel cell, which is typically the electrical work that it can perform.

The ideal (or reversible) voltage is the voltage that can be obtained from the reaction seen in (3) and (4) assuming there are no energy losses and is referenced to as E_0.

As seen before, for every mole of H_2 in the reaction, the number of electrons released is $2 \cdot N_A$, N_A being the Avogadro number ($6,022 \cdot 10^{23}$), the number of atoms, molecules, electrons, or other particles in 1 mol. Knowing that the electrical charge in each electron is of *-e*, the total electrical charge flow is of *-2·N_A·e*. The Faraday constant $96485,3329 \frac{C}{mol}$, equal to $|N_A \cdot e|$, allows us to relate this electrical work to the ideal voltage, in the form:

$$-2 \cdot F \cdot E_0 = \Delta \hat{g}_f$$

(9)

Therefore:

$$E_0 = \frac{-\Delta \hat{g}_f}{2 \cdot F}$$

(10)

ETSEIB

Temperature [ºC]	$\Delta \hat{h}_f$ [kJ·mol⁻¹]	$\Delta \hat{s}$ [kJ·(mol·K)⁻¹]	$\Delta \hat{g}_f$ [kJ·mol⁻¹]	E_0 [V]
100	-242,6	-0,0466	-225,2	1,17
300	-244,5	-0,0507	-215,4	1,12
500	-246,2	-0,0533	-205,0	1,06
700	-247,6	-0,0549	-194,2	1,01
900	-248,8	-0,0561	-183,1	0,95

Table 2. Values of enthalpy, entropy, Gibbs free energy and ideal voltage at different temperatures. Adapted from [13].

2.4.2. Nernst voltage

While the ideal voltage of a hydrogen fuel cell depends on its temperature, the concentration of reactants is also important for determining the open circuit voltage (OCV), also known as the Nernst voltage. Essentially, the Nernst equation allows the relation between partial pressures (directly related to their flow rates) of reactants and the Gibbs free energy variation they produce in the cell, resulting in a change of voltage.

In a chemical reaction where the reactants and products can be considered to behave like ideal gases, a certain "activity" can be linked to them in the form:

$$a = \frac{p}{P^0} \qquad (11)$$

Where p refers to the partial pressure of said gas, and P^0 refers to the reference pressure, which in a cell working under atmospheric pressure conditions is 1 *bar* = 1 *atm*.

In a chemical reaction of the form $jJ + kK \rightarrow mM$, the activities of the gas species that take part in it can be related to the total change in Gibbs free energy in the following manner:

$$\Delta \hat{g}_f = \Delta \hat{g}^0{}_f - \text{RT} \cdot \ln \left(\frac{a_J^j \cdot a_K^k}{a_M^m} \right) \qquad (12)$$

In the case of the reaction in fuel cell mode seen in (3), we get the new expressions of change in Gibbs free energy (13).

$$\Delta\hat{g}_{f,FC} = \Delta\hat{g}^0{}_f - \text{RT} \cdot \ln\left(\frac{a_{H_2}^1 \cdot a_{O_2}^{\frac{1}{2}}}{a_{H_2O}^1}\right) \qquad (13)$$

Therefore, by substituting using equations (10) and (11), we obtain the general expression for the total voltage of a RSOC depending on its temperature and gas flow rates, known as Nernst voltage:

$$E = E_0 + \frac{\text{RT}}{2F} \cdot \ln\left(\frac{p_{H_2} \cdot p_{O_2}^{\frac{1}{2}}}{p_{H_2O}}\right) \qquad (14)$$

Where E refers to the total cell voltage, E_0 is the ideal or reversible voltage, and p_x is the partial pressure of each gas component in the reaction, assumed to be an ideal gas under the working conditions, measured in *bar*.

It is important to note that partial pressures of gases inside the electrochemical cell stack will be directly related to their mass flow rates, therefore increasing or decreasing the Nernst voltage, as seen in Figure 5 in the case of increasing hydrogen mass flow rate without increasing the current. The current demand will also influence the partial pressures since it is related to the production or consumption of certain gases, as shown in Figure 6, where constant mass flow rates were kept while current increased in small steps. Both effects are clearly relevant in the results of the total voltage in the Nernst equation.

For this reason, it is typical for an electrochemical cell to work under constant fuel utilization (FU) conditions, measured in %. For example, a FU of 100% in SOFC mode would indicate that all the reactant gas entering the stack is reacting and being transformed into water. Such high utilizations are never reached, since starvation would become obvious due to diffusion issues, and the performance would be greatly reduced, as well as degradation being increased. The lower the FU, the easier it is for the gases to be diffused properly, and generally it results in better performance, but more reactants can be wasted. Typical FUs for an experimental system range from 40% to 80% or higher.
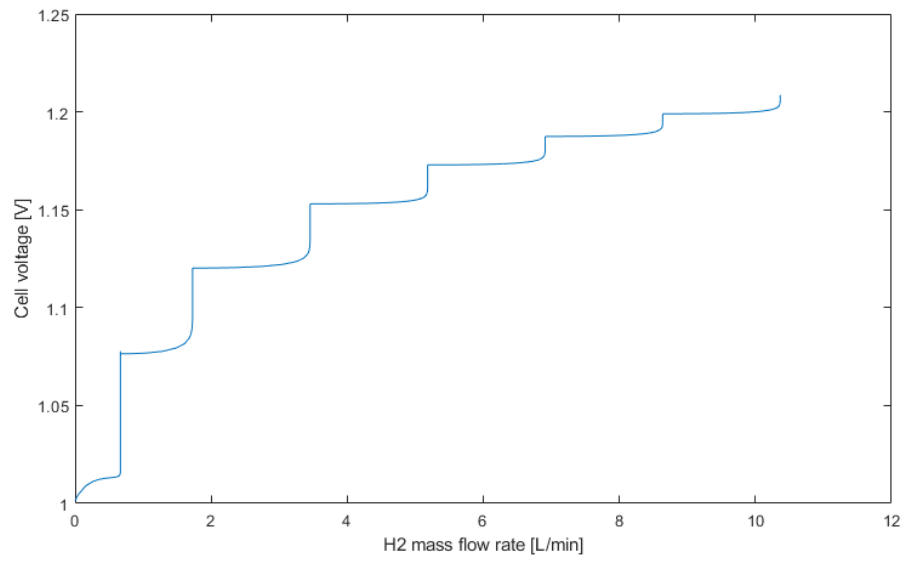
ETSEIB

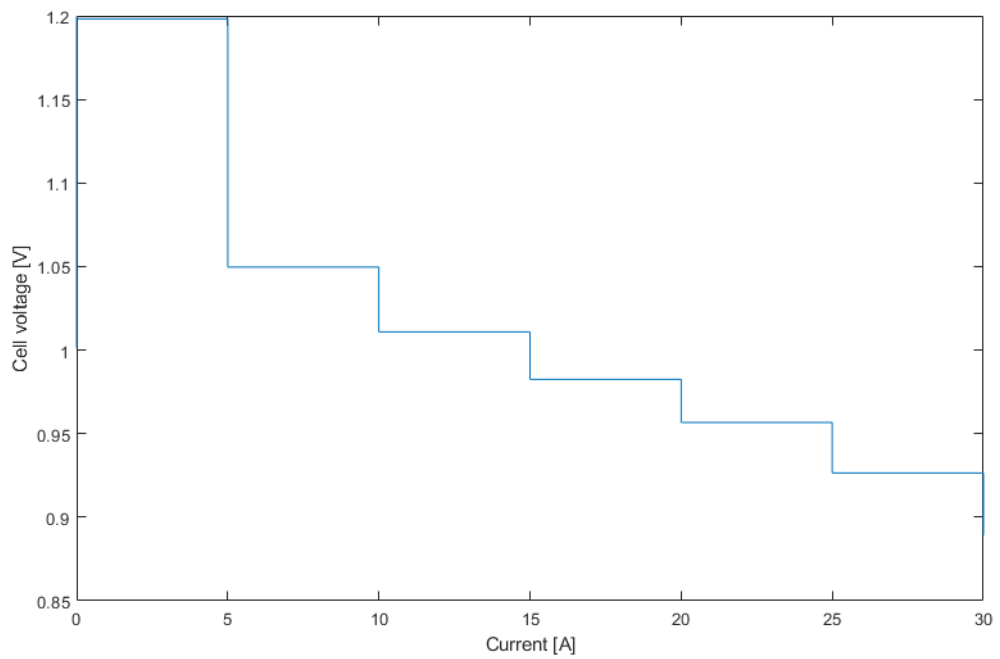Figure 5. Nernst voltage dependence on H2 partial pressure with no current demand

Figure 6. Nernst voltage dependence on current demand, maintaining constant mass flow rates of $H_2 = 7,8 \; L \cdot min^{-1}$ and $Air = 30 \; L \cdot min^{-1}$

2.4.3.   Activation polarization

Activation polarization can be defined as the overpotential (change of electrode potential) caused by overcoming the energy barrier of the slowest step of the electrochemical reaction. The reacting species require a certain activation energy to transfer the electrons to or from the electrode, which is obtained from a small subtraction of the total voltage produced by the fuel cell. These losses depend mostly on the electrochemical reaction, the materials and microstructure, reactant activity (therefore utilization), and on a smaller scale on current density.

For high temperature cells, this overpotential is smaller due to the activation energy needed being lower. This does not mean, however, that it is not relevant to the total voltage: as seen in Figure 4, its effect is most notable at low current densities, although it is present and considerable at all operating points.

Typically, the relation between current density (i) and activation overpotential (η_{act}) is defined by the *Butler-Volmer* equation, and calculated separately for anode and cathode:

$$i = i_o \cdot \left(e^{\frac{\alpha \cdot n \cdot F \cdot \eta_{act}}{RT}} - e^{-\frac{(1-\alpha) \cdot n \cdot F \cdot \eta_{act}}{RT}} \right) \qquad\qquad (15)$$

Where i_o refers to the exchange current density of anode or cathode, n is the number of exchanged electrons and α is the charge transfer coefficient, an indicator of the fraction of the electrostatic potential energy affecting the reduction rate in an electrode reaction, with the remaining fraction $(1-\alpha)$ affecting the corresponding oxidation rate.[14] It is also related to the symmetry of the activation energy barrier, for positive or negative overpotentials.

The exchange current density, i_o, can be determined using an empirical expression, based on the Arrhenius law. This law relates reaction rates to the temperature at which they take place. The expressions are as follows:

$$i_{o,A} = \gamma_A \cdot \left(\frac{P_{O_2}}{P_{ref}} \right)^{0,25} \cdot e^{\frac{-E_{act_A}}{RT}} \qquad\qquad (16)$$

$$i_{o,F} = \gamma_F \cdot \left(\frac{P_{H_2}}{P_{ref}} \right)^{1} \cdot \left(\frac{P_{H_2O}}{P_{ref}} \right)^{1} \cdot e^{\frac{-E_{act_F}}{RT}} \qquad\qquad (17)$$

Where γ_A and γ_F are, respectively, the phenomenological coefficients in the air and fuel electrodes. These coefficients are pre-exponential parameters that allow the adjustment of the

i_o values. The exponential constants on the pressure divisions are difficult to determine and are assumed as constant with the values shown in equations (16) and (17) based on the previous work in the model done in [15]. By working in *bar*, $P_{ref} = 1 \, bar$ and the equations simplify.

In low-density currents, where $e^{\frac{\alpha \cdot n \cdot F \cdot \eta_{act}}{RT}} \ll 1$ and $e^{-\frac{(1-\alpha) \cdot n \cdot F \cdot \eta_{act}}{RT}} \ll 1$, the *Butler-Volmer* equation can be simplified as follows:

$$i \approx i_o \cdot \frac{n \cdot F \cdot \eta_{act}}{RT} \qquad (18)$$

And the activation polarization isolated as:

$$\eta_{act} \approx \frac{RT}{n \cdot F} \cdot \frac{i}{i_o} \qquad (19)$$

In high-density currents, where $e^{\frac{\alpha \cdot n \cdot F \cdot \eta_{act}}{RT}} \gg 1$, the *Butler-Volmer* equation can be simplified into what is known as the *Tafel* equation, as follows:

$$\eta_{act} \approx \frac{RT}{\alpha \cdot n \cdot F} \cdot \ln(i) - \frac{RT}{\alpha \cdot n \cdot F} \cdot \ln(i_o) = \frac{RT}{\alpha \cdot n \cdot F} \cdot \ln\left(\frac{i}{i_o}\right) \qquad (20)$$

Therefore, the total activation polarization (sum of anode and cathode polarizations) according to the *Tafel* equation is:

$$\eta_{act} = \frac{RT}{4 \cdot \alpha_A \cdot F} \cdot \ln\left(\frac{i}{i_{o,C}}\right) + \frac{RT}{2 \cdot \alpha_F \cdot F} \cdot \ln\left(\frac{i}{i_{o,F}}\right) \qquad (21)$$

Where α_A and $i_{o,A}$ refer to the air electrode, while α_F and $i_{o,F}$ refer to the fuel electrode.

But this means that η_{act} would have to be calculated differently depending on the current density, and the transition between both expressions can be difficult. Generally, the *Tafel* equation is a good approximation when $i > 4 \cdot i_o$, and for lower current densities it presents too much error, as well as being unusable when $i < i_o$. For this reason, various authors have proposed a general expression for the calculation of the activation polarization[16], usable at all current densities:

$$\eta_{act} = \frac{RT}{4 \cdot \alpha_A \cdot F} \cdot \sinh^{-1}\left(\frac{i}{2 \cdot i_{o,A}}\right) + \frac{RT}{2 \cdot \alpha_F \cdot F} \cdot \sinh^{-1}\left(\frac{i}{2 \cdot i_{o,F}}\right) \qquad (22)$$

2.4.4. Ohmic polarization

The materials present in the RSOC present a certain resistance to the flow of electrons through the interconnector, as well as the flow of ions through the electrolyte, known as the Ohmic resistance. Since this potential loss follows Ohm's law, it is proportional to current density, and thus linear. It depends on the different materials characteristics, temperature, and geometry.

$$\eta_\Omega = i \cdot R \qquad (23)$$

Where R is the total resistance of the solid oxide cell stack. This resistance can be calculated as a sum of the resistivity of the different elements multiplied by their geometric qualities:

$$R = l_{el} \cdot \rho_{el} + l_c \cdot \rho_c + l_a \cdot \rho_a + R_{contact} \qquad (24)$$

Being:

- l_x the width of the electrolyte, cathode, and anode electrodes in *cm*.
- ρ_x the resistivity of the electrolyte, cathode, and anode electrodes in *Ω·cm*.
- $R_{contact}$ a resistance product of the contact between the different elements.

To express the resistance in a way that is compatible with current density instead of total current, the actual value obtained is known as *Area Specific Resistance (ASR)*, expressed in *Ω·cm²*. A typical way to obtain this value is by performing an impedance spectroscopy on the stack, like the one seen in Figure 7. Dielectric spectroscopy (DS) or impedance spectroscopy, also known as electrochemical impedance spectroscopy, is frequently used to study the response of a sample subjected to an applied electric field of fixed or changing frequency. DS describes the dielectric properties of a material as a function of frequency. In DS, the radio and microwave frequency regions of the electromagnetic spectrum have been successfully made to interact with materials, to study the behaviour of molecules. DS is a universal and powerful tool to study soft matter, whose principle is mainly to determine the frequency-dependent complex permittivity of the material. It provides information on molecular dynamics as well as on important material parameters such as the static dielectric permittivity (ε) and DC electrical conductivity (σ). [17]

This way, equation (23) can be expressed as a function of ASR, in the form:

ETSEIB

$$\eta_\Omega = j \cdot ASR \qquad (25)$$

Where j refers to the current density in $A \cdot cm^{-2}$.
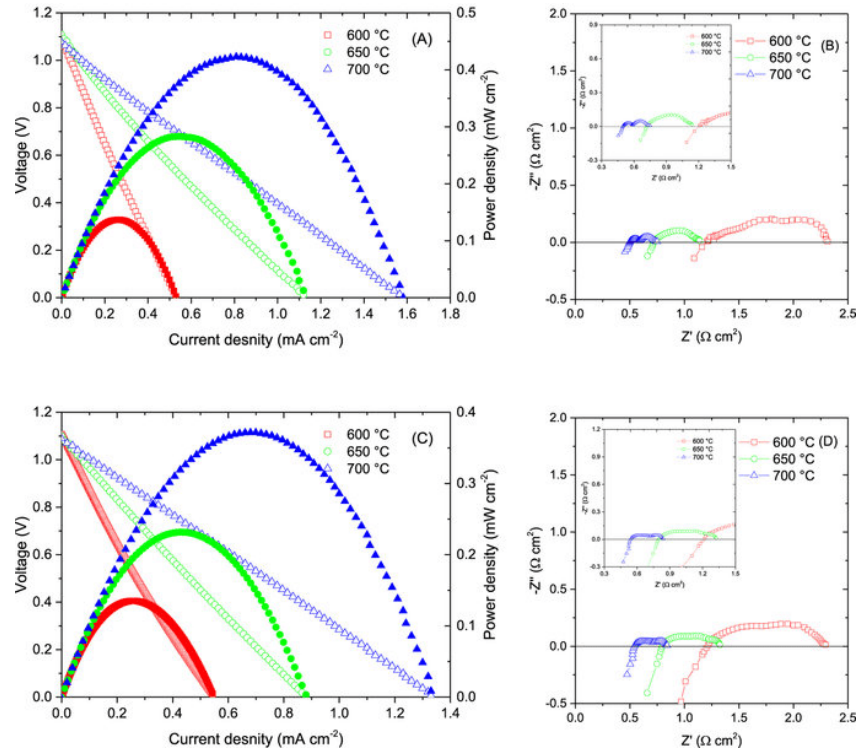

Figure 7. Example of a fuel cell impedance spectroscopy, from [18].

2.4.5.   Concentration polarization

Mass transport polarization, diffusion polarization, or concentration polarization are different names for losses associated to the change of concentration of reactants at the surface of the electrode when the reaction is taking place, typically at a high rate. Partial pressure of gases is crucial in the determination of the voltage, as seen previously, and when reactants are consumed at a great rate, the diffusion of gases towards the surface of the electrode might not be fast enough to ensure proper concentrations. Therefore, this polarization depends strongly on current density, reactant activity, and electrode characteristics.

In the case of the system operating in fuel cell mode, the hydrogen will be distributed through the porous anode at a certain rate, and the physical characteristics of it (thickness, pore density, porosity, tortuosity) play a key role in the diffusion of the gas. Since the electrochemical reaction takes place in the Triple-Phase Boundary (TPB) (Figure 8), very specific points where electrode, electrolyte and reactant gas are all present, the gas, in this case hydrogen, must be replenished at a rate fast enough to not hinder the reaction. For high current densities, the rate of replenishment must be very high, and cannot be achieved, resulting in a loss of partial pressure of reactants in the TPB points, and the loss of performance. The same holds true for the cathode, where oxygen is being reduced in the cathode's TPB, and oxygen ions flow through the electrolyte.
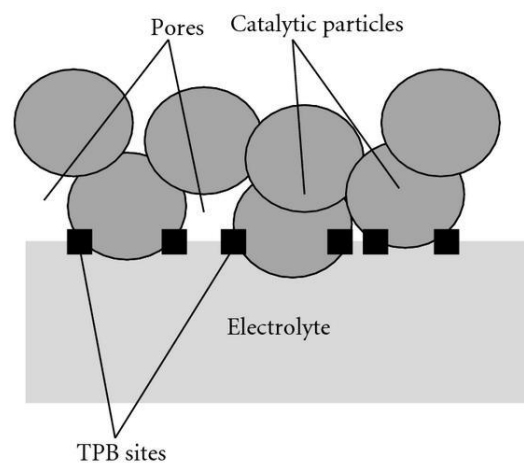

Figure 8. Simple visualization of TPB locations. From [19]

ETSEIB

To calculate mass transport polarization, the following equations can be derived from the Nernst equation, to represent the voltage drop as a function of the difference between each reactant gas' partial pressure, and the partial pressure in the TPB.[20]

$$\eta_{conc,A} = \frac{RT}{2F} \cdot \ln\left(\frac{p_{H_2} \cdot p_{H_2O,TPB}}{p_{H_2,TPB} \cdot p_{H_2O}}\right) \tag{26}$$

$$\eta_{conc,C} = \frac{RT}{4F} \cdot \ln\left(\frac{p_{O_2}}{p_{O_2,TPB}}\right) \tag{27}$$

Where $\eta_{conc,A}$ and $\eta_{conc,C}$ are the concentration losses in the anode and cathode, respectively. p_X are the known partial pressures of hydrogen, water, and oxygen.

$$\eta_{conc} = \eta_{conc,A} + \eta_{conc,C} \tag{28}$$

To determine the partial pressures for each gas in the TPB, Fick's law is applied and linear concentration gradients as a function of current density are assumed. Thus, the anode TPB partial pressures are calculated as:

$$p_{H_2,TPB} = p_{H_2} - \frac{RT \cdot L_A}{2F \cdot D_{H_2}^{eff}} \cdot i \tag{29}$$

$$p_{H_2O,TPB} = p_{H_2O} - \frac{RT \cdot L_A}{2F \cdot D_{H_2O}^{eff}} \cdot i \tag{30}$$

And the cathode TPB partial pressure is calculated as:

$$p_{O_2,TPB} = p_{O_2} - \left(\frac{P - p_{O_2}}{P}\right)\frac{RT \cdot L_C}{4F \cdot D_{O_2}^{eff}} \cdot i \tag{31}$$

Where L_{el} are the thickness of the anode and cathode in *cm*, P is the atmospheric pressure in *bar*, and D_i^{eff} is the effective molecular diffusion coefficient, unknown, describing how fast the gas can flow through the porous material, and measured in *$cm^2 \cdot s^{-1}$*.

Fick's law, applied in porous media, describes the effective diffusion coefficient as a function of porosity ε, tortuosity τ, and binary diffusivity coefficient D_{ij}, as per equation (32). More details on the calculations of the binary diffusivity coefficient, related to this work, can be found in [15].

$$D_i^{eff} = \frac{\varepsilon}{\tau} \cdot D_{ij} \qquad\qquad (\,32\,)$$

Due to the material properties of the RSOC, Knudsen diffusion must be considered. Knudsen diffusion considers the collision of particles with the pore walls. Essentially, it states that if the pore diameter is smaller than the mean free path of the diffusing gas molecules and the density of the gas is low, the gas molecules collide with the pore walls more frequently than with each other. [21]

$$D_{iK} = \frac{d_p}{3} \cdot \sqrt{\frac{8RT}{\pi M_i}} \qquad\qquad (\,33\,)$$

Where d_p is the mean pore diameter of the porous media in *cm*, and M_i is the molecular weight of the gas species, in *g·mol*[1]. Generally, Knudsen diffusion will be most relevant when the pore diameter is small, and the gas pressure is low. By considering both diffusion mechanisms, the total effective diffusion coefficient is:

$$D_i^{eff} = \frac{\varepsilon}{\tau} \cdot \frac{D_{ij} \cdot D_{iK}}{D_{ij} + D_{iK}} \qquad\qquad (\,34\,)$$

ETSEIB

2.4.6. Losses balance

After explaining all the polarizations that contribute to the real output power a RSOC will produce or consume, depending on the mode of operation, we can finally give the expression of voltage as a function of current. For a RSOC, the total stack voltage balance will include the losses by adding or subtracting them to the Nernst voltage, depending on if it is operating in SOEC or SOFC mode, respectively.

$$\begin{cases} V_{SOFC}(i) = E - \eta_{act} - \eta_{\Omega} - \eta_{conc}, & i > 0 \\ V_{SOEC}(i) = E + \eta_{act} + \eta_{\Omega} + \eta_{conc}, & i < 0 \end{cases} \qquad (35)$$

Considering power output as positive, so current will have positive values, and power consumption as negative, so current will have negative values. As seen in Figure 9, the negative values of current J correspond to SOEC mode, and the positive values correspond to SOFC mode.
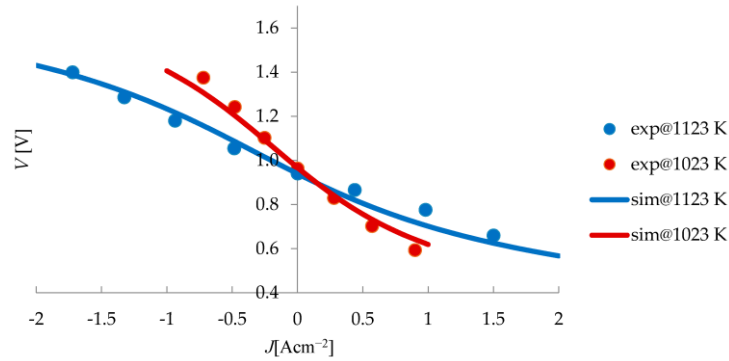

Figure 9. RSOC total single-cell potentials at different temperatures. From [22].

2.5. Thermodynamic balance of a RSOC

As seen previously, stack temperature affects many aspects of the RSOC performance, in either operation mode, as most electrochemical equations include temperature because the gases' characteristics heavily depend on it. For this reason, it is imperative to have an accurate thermodynamics balance that includes all relevant phenomena.

The contemplated phenomena in the thermodynamic balance are the following:

- The heat produced or consumed due to the electrochemical reaction.
- Convection losses to the gas mass flows.
- Heat loss to the environment.

Depending on the operation mode of the RSOC, heat will be produced or consumed by the electrochemical reaction. In the case of SOFC operation mode, the reaction is exothermic, while in SOEC operation mode, the reaction is endothermic. For this reason, in a well-isolated RSOC with little heat loss to the environment, some form of cooling will be required when operating as a fuel cell. A typical way to achieve the necessary cooling is by managing the air flow into the stack[23], which is the proposed solution in this work and is explained later. In the case of electrolysis, the oven will carry out the necessary heating to counteract the endothermic nature of the reaction.

The heat produced or consumed by the electrochemical reaction will be determined by the difference between the total energy and the RSOC stack energy. Assuming all non-reversible potential differential in the form of thermal energy, and that the reaction always takes place at a constant temperature of T = 1023 K, from equation (8) we can easily determine:

$$T\Delta S = Q = \Delta G - \Delta H \qquad\qquad (36)$$

Where Q is the heat produced or consumed by the electrochemical reaction in *Joules*. Therefore, the power in *Watts* can be calculated in the form:

$$\dot{Q}_{r,cell} = \Delta H \cdot j - V \cdot i \qquad\qquad (37)$$

Where $j = \frac{i}{2F}$ is the rate at which the reaction takes place, with the units $\frac{C}{s \cdot \frac{C}{mol}} = mol \cdot s^{-1}$.

So, it becomes:

$$\dot{Q}_{r,total} = LHV \cdot \frac{N \cdot i}{2F} - V \cdot N \cdot i \qquad (38)$$

LHV being the lower heating value of hydrogen, determined as 247.86 $kJ \cdot mol^{-1}$ for an operating temperature of 750ºC [24]. This is used instead of the high heating value (HHV) because the reaction results in steam and not liquid water. N is the number of cells, V is the voltage of a single cell and assumed equal for all cells, and i is the current being drawn or applied in A, which is positive for SOFC operation mode and negative in SOEC mode, making the reaction exothermic or endothermic, respectively.

Convection losses due to the gases mass flows entering the stack at a lower temperature than the operating temperature must be considered and added to the thermodynamic balance. To calculate the amount of heat absorbed by the gases flowing through the stack, it is considered that the reaction always takes place at the operating temperature, and the heat absorbed will be equal to the power needed to bring the gases to the operating temperature. Therefore:

$$\dot{Q}_{conv,i} = \dot{Q}_i^{T_{stack}} - \dot{Q}_i^{T_{gas,in}} \qquad (39)$$

$$\dot{Q}_i^{T_{gas,in}} = Cp_i^{T_{in}} \cdot \dot{m}_i \cdot T_i^{T_{in}} \qquad (40)$$

$$\dot{Q}_i^{T_{stack}} = Cp_i^{T_{stack}} \cdot \dot{m}_i \cdot T_i^{T_{stack}} \qquad (41)$$

Where, for a gas i, $\dot{Q}_{conv,i}$ is the heat needed to bring the gases to the operating temperature in $kJ \cdot s^{-1}$. Cp_i^T is the specific heat of the gas at each temperature in $kJ \cdot (kg \cdot K)^{-1}$ and $\dot{m}_i$ the mass flow rate in $kg \cdot s^{-1}$.

Finally, heat losses to the environment are calculated as follows:

$$\dot{Q}_{env} = K_{oven} \cdot S_{oven} \cdot (T_{stack} - T_{env}) \qquad (42)$$

Being K_{oven} the heat loss coefficient of the oven in $W \cdot m^{-2} \cdot K$ and S_{oven} the oven surface in m^2.

Finally, the oven will provide heat directly in W, to control the stack temperature.

Hence, the heat balance is as follows:

$$\dot{Q} = \dot{Q}_{r,total} - \sum_i \dot{Q}_{conv,i} - \dot{Q}_{env} + \dot{Q}_{oven} \qquad (43)$$

3. Programming of the experimental station

The completion of experiments and measurement of real data in SOFC and SOEC operating modes was the key to the full development of this work. A series of experiments were programmed to be performed in late 2020 and/or early 2021. The data obtained during these experiments contributed to the parameter estimation for the MATLAB/Simulink model, as well as provide useful information for the prototype that will be built in the context of the HyBCN project.

This station is in IREC's facilities, and during the development of this thesis was used by IREC and IRI. All the special equipment required was made available by both organisations, and the instrument tuning and programming in LabVIEW was carried out by the author, with the previous help of another IRI student and other IRI researchers.

In this section, the balance of plant (BOP) of the system will be explained, followed by the equipment used in the experimental station. Then, the LabVIEW program will be presented, showing its main features and user interface, and finally the experiments made.

3.1. Description of the experimental station

This RSOC experimental station has all the needed equipment to operate and measure data from a reversible solid oxide cell. All the relevant information for understanding it is explained in this chapter. In Figure 10 a front view of the experimental station is presented, and most of its relevant components are highlighted.

In essence, the station must be able to operate while controlling stack current, temperature, and gas mass flow rates. All the equipment described aims to fulfil this goal, and the program allows the user to operate this equipment for the completion of the experiments.
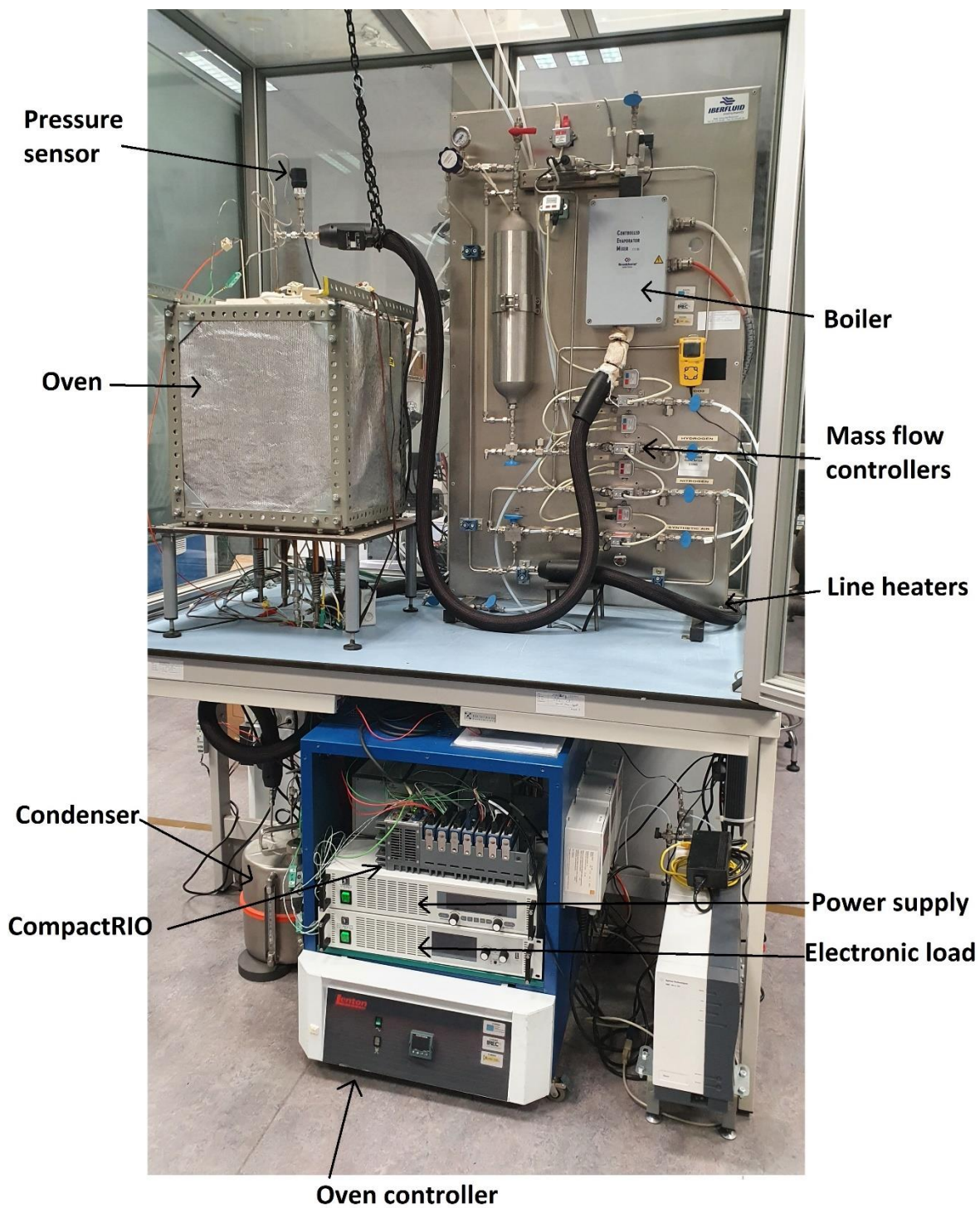
ETSEIB

Pressure sensor

Oven

Boiler

Mass flow controllers

Line heaters

Condenser

CompactRIO

Power supply

Electronic load

Oven controller

Figure 10. Experimental station.

3.1.1.   Balance of plant (BOP)

The balance of plant (BOP) is an engineering term which refers to the various supporting and auxiliary components in a system, other than the generating unit itself. They provide the support needed to ensure the plant can run safely and efficiently. It is important to understand the BOP of the experimental station since the programming must be made with the objective of controlling its components, ensuring the correct operation of the RSOC.

The IREC station has, other than the stack, a laboratory oven, mass flow controllers, a boiler to produce steam at a certain temperature, line heaters to make the gas flows enter the stack at a higher temperature and a condenser to condense water before releasing hydrogen to the atmosphere, avoiding condensation in the extractor.

A simple diagram of the mechanical BOP is seen in Figure 11. Note that the air out line is not connected directly to the stack. This is intentional, because the stack has an open cathode where air flows out of the stack into the oven cavity and is collected through the "air out" tube and directed to the atmosphere.
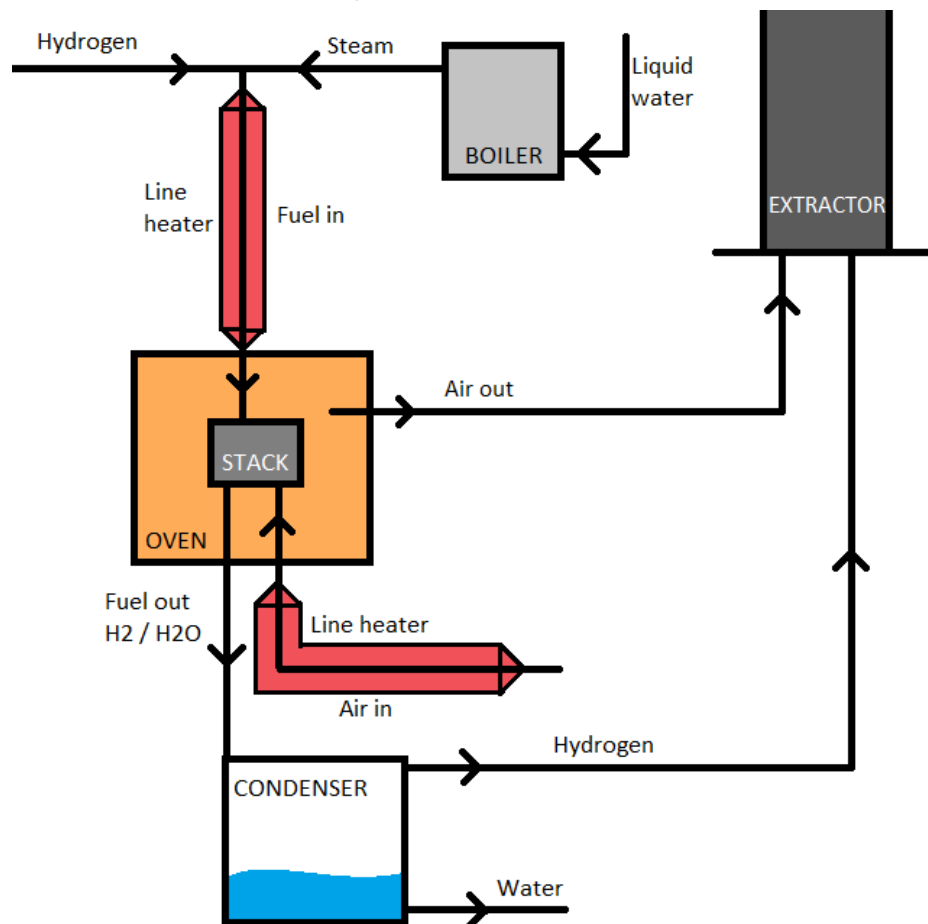

Figure 11. BOP diagram of the experimental station

The boiler evaporates water into steam at the designated temperature (typically 200ºC). Then, it is mixed with hydrogen and fed into the anode.

The line heaters ensure that the gases do not enter the stack at ambient temperature, which could be dangerous for the cells (big temperature differentials) as well as decrease the performance of the RSOC.

The stack used during the experiments has an open cathode, so the air exiting the stack is dispersed in the oven cavity and taken out by the extractor. Meanwhile, the fuel exiting the stack is taken to a condenser, where water is condensed, and hydrogen gas is taken out by the extractor.

3.1.2.   Instrumentation

The complete equipment setup includes the following devices:
- Stack
- Oven
- CompactRIO
  o Mass flow controllers
  o NI Modules
  o Pressure and temperature sensors
- Boiler
- Line heaters
- Condenser
- Power supply
- Electronic load
- Ethernet switch
- Personal Computer

For the measurement of the following variables within the specified ranges:

Measurement	Number	Range
Stack voltage	1	0 V to 50 V
Stack current	1	0 A to 70 A
Cell voltage	7	0 V to 50 V
Temperature	8	0 ºC to 1000 ºC
Pressure	3	0 bar to 400 mbar

Table 3. Required measurements and ranges for the experimental station.

ETSEIB

3.1.2.1. Stack (SOFCMAN Energy Technology)

The 30-cell standard SOFC stack module produced by SOFCMAN is composed of anode-supported cells with Ni-YSZ interconnects (or bipolar plates) and sealing materials.
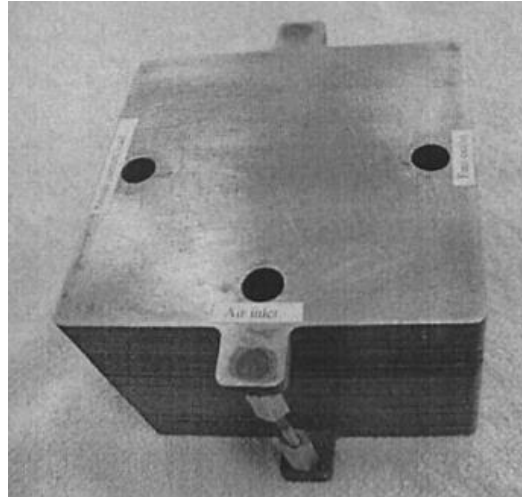

Figure 12.SOFCMAN stack

3.1.2.2. Oven (Lenton AWF 12/12) and temperature controller (Eurotherm 3216)

The oven is used to control the temperature of the stack, typically 750ºC or 800ºC. The Lenton AWF 12/12 laboratory oven has the following specifications:

Model	Maximum temperature [ºC]	Maximum continuous temperature [ºC]	Time to temperature [minutes]	Internal dimensions [mm] h x w x d	External dimensions [mm] h x w x d	Chamber capacity [L]	Maximum power [kW]	Net weight [kg]
AWF 12/12	1200	1150	80	200 x 200 x 300	700 x 555 x 615	12	2.75	54

Table 4. Oven characteristics

Its power is controlled by the Eurotherm 3126, a PID that reads and follows the oven temperature setpoint. It can vary the oven temperature at different speeds, using its "RAMP" mode, which will be used in the context of solid oxide fuel cells due to their high sensibility to fast temperature changes.

The oven has been modified to have access on the top and the bottom, allowing the gas tubes to enter the stack, as well as measuring instruments. This has significantly reduced its insulation capabilities, but it was necessary to access to the stack for experimental purposes.

Figure 13. Lenton oven in its original state

3.1.2.3. CompactRIO 9035

The CompactRIO (also shortened as cRIO) is an embedded controller used for advanced control and monitoring applications made by National Instruments. CompactRIO systems provide high-performance processing capabilities, sensor specific conditioned I/O, and a closely integrated software toolchain that make them ideal for Industrial Internet of Things, monitoring, and control applications. The real-time processor offers reliable, predictable behaviour, while the FPGA excels at smaller tasks that require high-speed logic and precise timing [25]. The CompactRIO 9035 has 8 module slots used for inputs/outputs.

Figure 14. CompactRIO 9035

Mass flow controllers (Bronkhorst F-110C)

The mass flow meters, as their name implies, are used for measuring the flow rate of a fluid through a tube. A controller allows the control of this mass flow rate. The same model is used, with different configurations, to control the flow of hydrogen gas, steam, synthetic air, nitrogen, and carbon monoxide, for a total of 5 mass flow controllers.

Figure 15. Bronkhorst F-110C mass flow controller

NI Modules

- **1x NI-9206 32-Channel, 16-bit Analog Input for Fuel cells**

This module has 16 differential analog inputs (32 channels) with four programmable input ranges of ±200 mV, ±1 V, ±5 V, and ±10 V. Its maximum sampling rate is 250 kS·s^{-1}.[25]

Figure 16. NI-9206 module

This module was intended for measuring single-cell voltages, but its limitation to ±10 V made it impossible for the studied experimental system. Instead, it was used for measuring the 3 pressures (fuel in, fuel out, air in), and two extra temperatures with type K thermocouples. These two extra temperatures were not measured with the specialised NI-9211 because a total of 9 thermocouples were used during the measurements, and the NI-9211 only allowed for 8 measurements. Also, the thermocouples were in contact with conductive materials, and that made its direct measurement impossible for the dedicated module, so they were measured with the NI-9206.

- **2x NI-9211 24-bit Thermocouple Input**

The NI 9211 thermocouple input module for use with CompactDAQ and NI CompactRIO chassis includes a 24-bit delta-sigma analog-to-digital converter, anti-aliasing filters, open-thermocouple detection, and cold-junction compensation for high-accuracy thermocouple measurements. It allows the measurement of 4 thermocouples, and, by using two, 8 temperatures were measured during the experiments.

Figure 17. NI-9211 module

- **1x NI-9870 4-Port RS232 Serial**

The NI-9870 adds RS232 serial ports to CompactRIO systems. The serial ports are accessed directly from the FPGA to offer you flexibility in communicating with serial devices. The module has individual buffers on every port that save FPGA space and simplify programming. The NI-9870 supports standard start bit, stop bit, and handshaking settings. It uses an external power to provide maximum compatibility and reliability under all serial port conditions.

ETSEIB

This module will be used to communicate with the system's devices such as the oven, power supply, electronic load, and mass flow controllers.

Figure 18. NI-9870 module

- **1x NI-9221 8-Ch 12-bit Analog Input**

The NI 9221 is an analog input module for CompactDAQ and CompactRIO systems. It provides eight channels of ±60 V input with 800 kS·s⁻¹ sample rate. This module will be used to measure the absolute voltages of cells at different points of the stack, in groups of 6 (Cells 1,7,13,18,24,30). This leaves two inputs free, which were used for measuring individual cell voltages in cells 19 and 25. This is the alternative that was chosen instead of using the module 9206, the voltage range of which was too small. Its tolerance, with a voltage range of 120V and 12 bits resolution, is of 0.03V.

Figure 19. NI-9221 module

Pressure sensors

- **3x Wika A10**

The pressure transmitter Wika A10 is a device able to convert pressure into an electrical signal, via the deformation of a strain gauge, changing its resistance depending on the applied pressure and, thus, the voltage signal. These sensors will be used to measure the following gas mass flow pressures: fuel inlet, fuel outlet, and air inlet.

Figure 20. Wika A10 pressure sensor

Temperature sensors

- **9x OMEGACLAD^{TM} XL thermocouple**

A thermocouple is an electrical device consisting of two dissimilar metals bonded to each other, typically by welding. The bimetallic junction develops a small voltage that varies with temperature. [26]

Figure 21. OMEGACLAD^{TM} XL thermocouple

As seen in Figure 22, five thermocouples are placed in different spots within the oven chamber to have a good understanding of how good the temperature regulation is, and if the temperature gradients are very relevant. Since the stack has an open cathode, the temperature at the exit of the cathode electrode is measured with the *T+cat* thermocouple. A sixth thermocouple was placed at the top, next to the oven's thermocouple which it uses for controlling the temperature, to have a secondary, more reliable measurement of that temperature. The three remaining thermocouples measured fuel inlet, fuel outlet and air inlet temperatures, respectively.
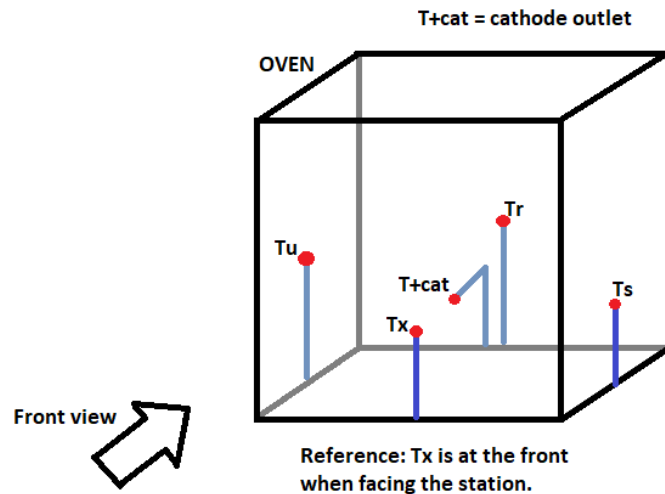

Figure 22. Diagram showing positions of oven thermocouples

3.1.2.4. Boiler (Bronkhorst™ CEM Evaporator W-303B)

The Controlled Evaporation and Mixing Evaporator W-303B is suited for precise vapour flow delivery, composed by mixing up to 1200 $g \cdot h^{-1}$ H_2O with max. 100 $ln \cdot min^{-1}$ of carrier gas at operating pressures between vacuum and 100 bar. The temperature-controlled mixing device is used in combination with a (thermal or Coriolis) liquid flow meter and an MFC for carrier gas, together forming a Controlled Evaporation and Mixing (CEM) System.

Figure 23. CEM Evaporator W-303B

In the case of the experimental station, the carrier gas is steam, since we have a liquid water deposit, and it must be evaporated before entering the RSOC stack. Typically, it was set to a target temperature of 200ºC.

3.1.2.5. Line heaters

The purpose of line heaters is to avoid the gases entering the stack at ambient temperature, which would introduce a lot of thermal stress to the stack when increasing the mass flow rate of any gas. They also ensure the steam from the boiler does not condense before entering the stack. Typically, they were set at a target temperature of 200ºC. They can be seen highlighted in Figure 10.

ETSEIB

3.1.2.6. Condenser

The purpose of the condenser is to receive all the fuel mass flow exiting the stack. The composition of this mass flow will be rich in water when operating in SOFC mode, and rich in hydrogen when operating in SOEC mode, but both components will be present at any given time. To avoid condensation of water in the gas channel that leads hydrogen gas to the atmosphere through the extractor, which could impede the free circulation of gas, water is condensed and accumulated in the condenser before hydrogen is sent out to the atmosphere. It can be seen highlighted in Figure 10. It is made of stainless steel and has a volume of approximately 10L.

3.1.2.7. Power supply (EA PS 9080-120 2U)

A power supply is an electrical device that supplies electric power to an electrical load. The primary function of a power supply is to convert electric current from a source to the correct voltage, current, and frequency to power the load. As a result, power supplies are sometimes referred to as electric power converters. A programmable power supply (PPS) is one that allows remote control of its operation through an analog input or digital interface such as RS232 or GPIB. Controlled properties may include voltage, current, and in the case of AC output power supplies, frequency.[27]

This device will provide power to the RSOC when operating in SOEC mode. It is an exception, as it is the only device other than the electronic load that is controlled directly by the PC, instead of the CompactRIO. The reason for this is that drivers found for these devices only worked if executed by the PC, and not by the CompactRIO. Unfortunately, this limited the rate at which communication with these devices could be made to about 400ms. This communication was established using an ethernet switch and Modbus TCP protocol.

This model has a microprocessor that acts as a controller, enabling fast measurement and display of values.

Voltage	0..80V
Current	0..120A
Power	0..3000W

Table 5. Power supply characteristics

Figure 24. EA PS 9080-120 2U

3.1.2.8. Electronic load (EA EL 9080 B HP)

A programmable load is a type of test equipment or instrument which emulates DC or AC resistance loads normally required to perform functional tests of batteries, power supplies or solar cells. By virtue of being programmable, tests like load regulation, battery discharge curve measurement and transient tests can be fully automated and load changes for these tests can be made without introducing switching transient that might change the measurement or operation of the power source under test.[28]

This device will absorb power from the RSOC when operating in SOFC mode. It is the only device other than the power supply that is controlled directly by the PC, instead of the CompactRIO. The communication was also established using an ethernet switch and Modbus TCP protocol, and the same limitations that the power supply has apply for the electronic load.

Voltage	0..80V
Current	0..85A
Power	0..1200W

Table 6. Electronic load characteristics

Figure 25. EA EL 9080 B HP

ETSEIB

3.1.3. Communications

Not only it is important to have all necessary devices, within the correct operational ranges, for the development of a successful experimental station. It is necessary to establish a series of communication protocols for a bidirectional communication with the experimental equipment.

A typical communication architecture is the master-slave model, in which a device is in control of the others. In this case, the computer will be the master, directly controlling the CompactRIO, the power supply and the electronic load. At the same time, the CompactRIO will be the master to the oven controller and the MFCs.
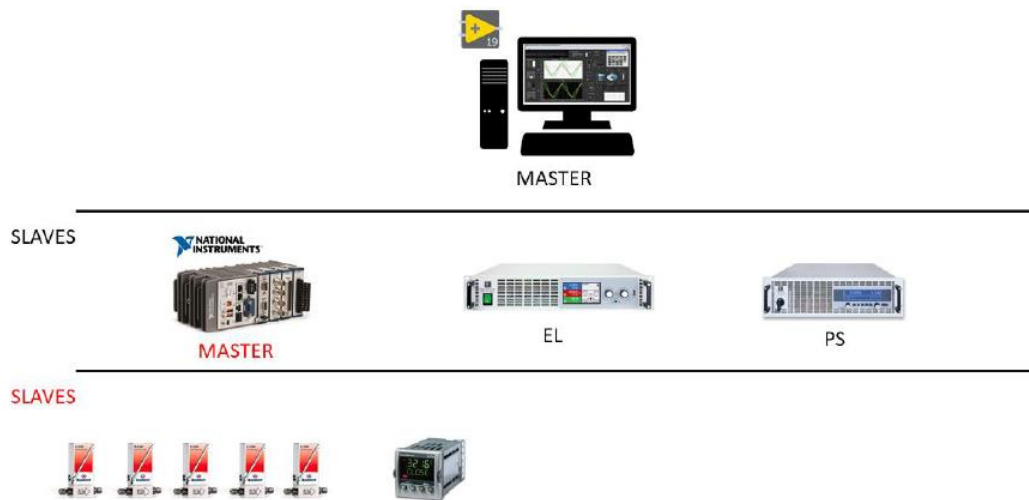

Figure 26. Master-slave structure in the experimental station, taken from [15]*.*

All the devices that only send measurement information and do not need to be controlled are wired to the CompactRIO or its modules, as seen in Figure 27.

To communicate with its slaves (CompactRIO, EL, PS), the PC uses a Modbus TCP protocol via an ethernet switch. This is a Modbus variant used for communications over TCP/IP networks, connecting over port 502. Thus, the IP addresses of these devices are:

- CompactRIO: 10.0.0.2
- Electronic Load: 10.0.0.3
- Power Supply: 10.0.0.4

On the other hand, the CompactRIO uses a Modbus RTU (Remote Terminal Unit) communications protocol to communicate with its slaves. Modbus RTU is an open serial

protocol derived from the Master/Slave architecture originally developed by Modicon (now Schneider Electric). It is a widely accepted serial level protocol due to its ease of use and reliability. Modbus RTU is widely used within Building Management Systems (BMS) and Industrial Automation Systems (IAS). This protocol primarily uses an RS-232 or RS-485 serial interfaces for communications and is supported every commercial SCADA, HMI, OPC Server and data acquisition software program in the marketplace. This makes it very easy to integrate Modbus compatible equipment into new or existing monitoring and control applications [29].

The MFCs are all controlled through a same communication port the VISA resource name of which is "ASRL3::INSTR". NI-VISA is an API that provides a programming interface to control Ethernet/LXI, GPIB, serial, USB, PXI, and VXI instruments in NI application development environments like LabVIEW, LabVIEW NXG, LabWindows/CVI, and Measurement Studio. The API is installed through the NI-VISA driver. VISA stands for Virtual Instrument Software Architecture.[25]

Within this port, each MFC has an individual node assigned, which can be called to control each one separately. The node numbers are:

- Node 1: Water mass flow controller.
- Node 2: Hydrogen mass flow controller.
- Node 3: Nitrogen mass flow controller.
- Node 4: Air mass flow controller.
- Node 5: CO_2 mass flow controller (unused).

The communication with the oven controller is established with the communication port "ASRL4::INSTR", and the LabVIEW program directly writes the values needed in the registers of interest with Modbus drivers, in order to be able to control the oven temperature ramping problem. This allows the user to choose a target temperature, a velocity ($°C \cdot min^{-1}$) for ramping, and a dwelling time in hours, during which the oven will remain at the target temperature before turning off. The maximum value for dwelling time is 99 hours, but if the oven must remain at the same temperature for longer, the "Pause" button in the LabVIEW front panel can be activated to remain at the working temperature indefinitely.
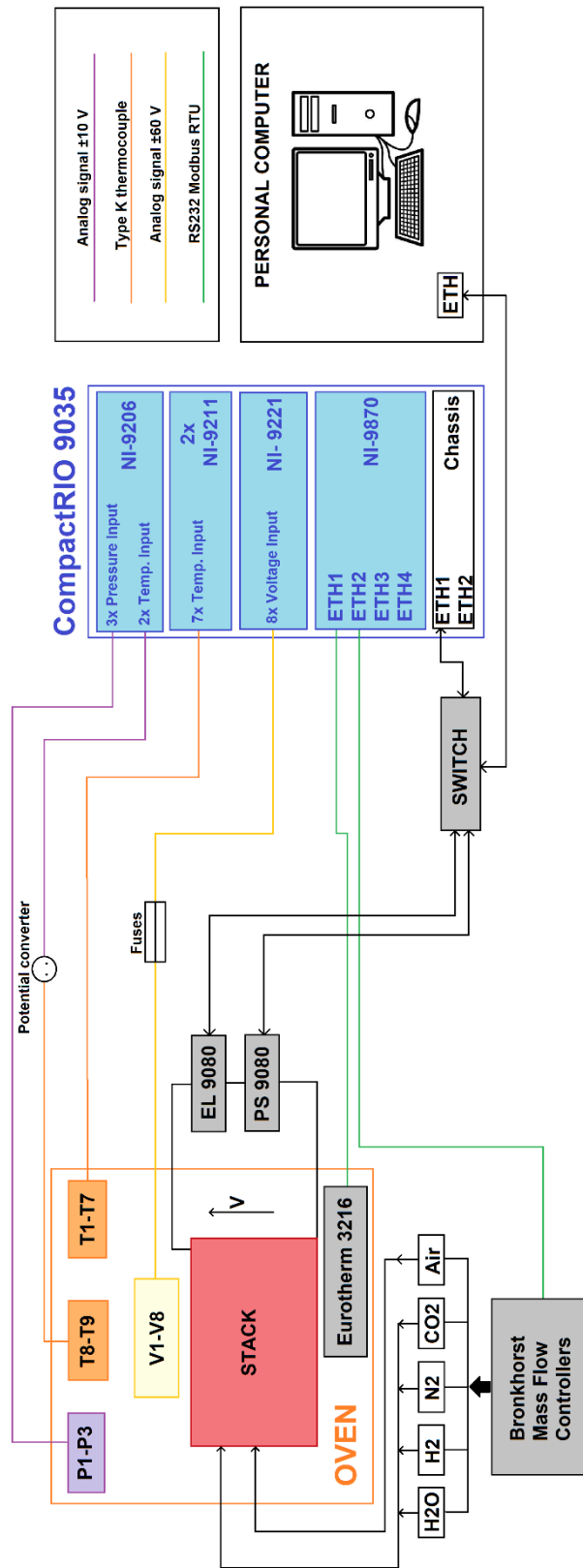
Figure 27. Communications diagram

3.2. Program and user interface

A LabVIEW program, using the communications interface described previously, must be able to control the experimental station and all its essential components. The main objective of this program is to be able to automatically perform the set of experiments described below. In all cases, the power control is galvanostatic (current control). Two main types of experiments are described:

- Polarization curve: For static analysis of performance and efficiency, capturing data about voltage, current, gas compositions, pressures, and temperatures in SOFC and SOEC operation modes.
- Sweep: For dynamic analysis of performance, as well as reversibility, with a fast current ramping capturing data about voltage, current, gas compositions, pressures, and temperatures in SOFC, SOEC and reversible operation modes.

The LabVIEW program presented in [15], although quite complex, still presented some problems and failed to meet some necessary requirements before carrying out the set of experiments agreed between IREC and IRI. While essentially remaining the same, the polishing of the program to ensure its safety, practicality, overall performance, and the achievement of all experimental requirements implied a thorough revision.

Firstly, the program encountered some internal errors which caused it to crash or behave unexpectedly very often. This was the first thing addressed in this work, as it was important to have a reliable program when operating the RSOC stack. Secondly, communications with the instruments were revised and, in the case of the oven, created. All instruments, including the thermocouples, pressure sensors, mass flow controllers, etc. were double-checked to ensure the correct measurement of data and their compatibility with CRIO modules. New information tabs like "Massflow Charts", "Temperature Charts" and "Pressure Charts" were added, and others were modified to more easily present information to the user. A safety protocol was added and is explained in section 3.2.2. Two data recording subVI were programmed to ensure the acquisition of all relevant data.

A typical fuel cell can work during thousands of hours, but the RSOC stack used in this work degraded rapidly. Early degradation for RSOC can be attributed to the important mechanical stresses and its brittle ceramic components[30], resulting in broken cells due to thermal stress or other problems. Due to this rapid degradation of the fuel cell stack, not all the

experiments that were programmed were carried out. Nevertheless, as presented later this chapter, a lot of experimental data was obtained during the 2 weeks before the stack performance was too poor to continue operating the RSOC.

3.2.1.   General interface

The general interface of the program includes all relevant aspects for manual operation of the RSOC station. On the left-hand side, current, gas mass flow rates, and oven setpoint can be manipulated. Total voltage, cell groups voltages, temperatures and pressures can be visualised. The extra tabs "Voltage/Current charts", "Massflow charts", "Temperature charts", and "Pressure charts" were added to allow the user to visualise changes more easily for those measurements.

While the main program is running, a recording is set to save all measured data every 1 second. This will help have a general idea of how the RSOC has reached operating temperature, which can take up to 12 hours from ambient temperature and monitor what the tasks the operator has been executing, without using much disk space.

While an experiment is undergoing, a faster recording SubVI is enabled, recording at a rate of 200ms. When the experiment ends, it automatically saves all data in a *.csv* file, along with a screenshot of the V-I graph, and another one with the time-current and time-voltage graphs, useful for quickly checking how the experiment developed.

An emergency LED on the top-right is ready to indicate if the safety mode has been engaged, and it will be maintained until the reset button under it is pressed. Safety mode is explained below.

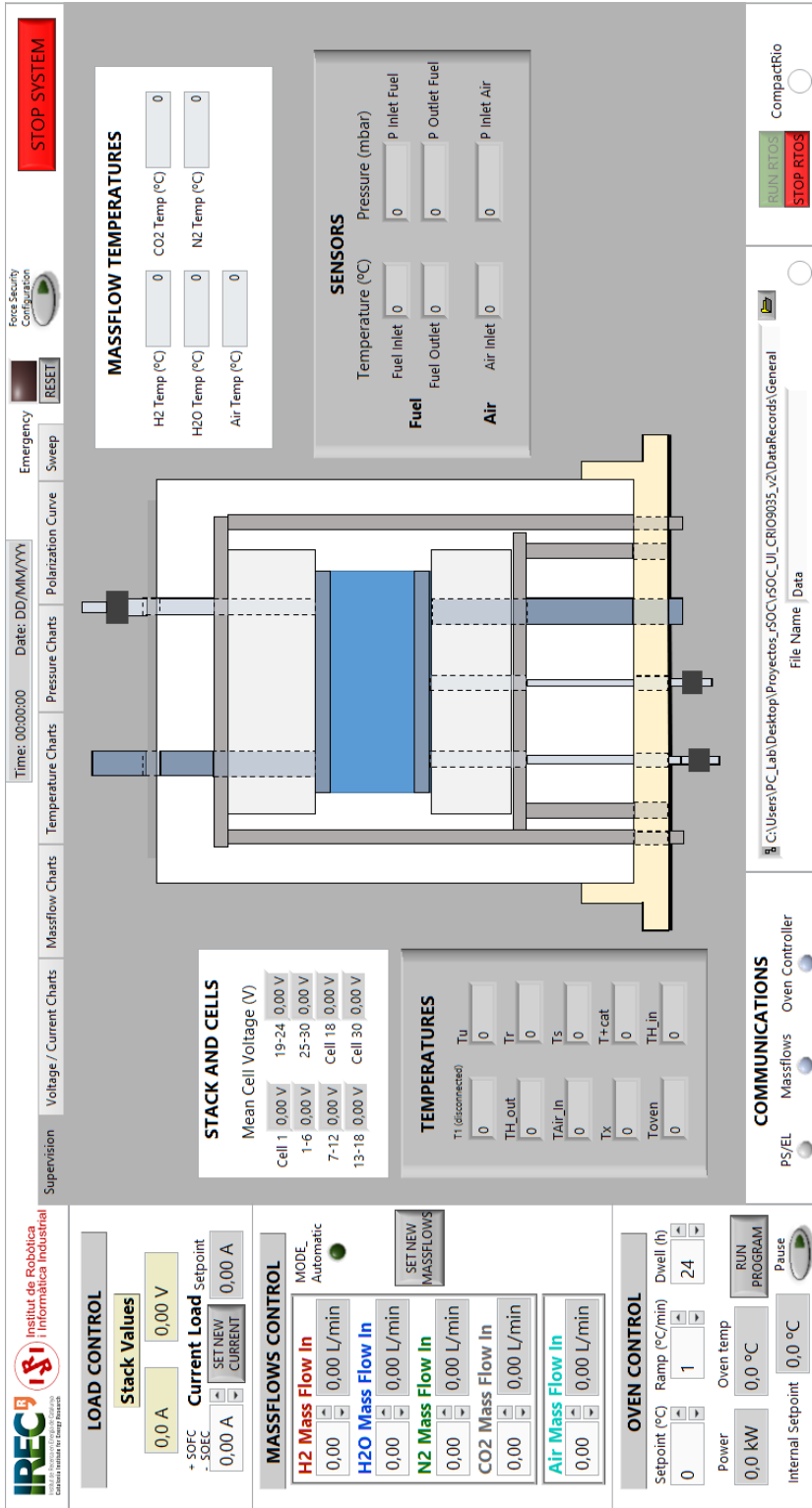The LabVIEW project containing all the VIs and SubVIs programmed can be found in Annex 2.

Figure 28. LabVIEW Front Panel.

3.2.2. Safety

A safety SubVI running within the CompactRIO was developed, which constantly checks if any of the following unwanted conditions occur while the program is running:

- RSOC voltage is below 0,6 V/cell or over 1,5 V/cell.
- Air, H_2 or N_2 mass flow rate setpoint is not achieved for 10 seconds or more.
- H_2O (g) mass flow rate setpoint is not achieved for 30 seconds or more.
- Chamber temperature does not change at a rate over $5^oC \cdot min^{-1}$.

If any of the listed problems happens, safety mode is engaged automatically to avoid any possibility of operating under dangerous conditions for any long period of time. Safety mode performs the actions listed below:

- Current is set to 0 A.
- Gas mass flow rates are set to security levels:
    - H_2 MF = 0,5 $L \cdot min^{-1}$
    - H_2O MF = 0 $L \cdot min^{-1}$
    - N_2 MF = 5 $L \cdot min^{-1}$
    - Air MF unchanged or set to 3 L/min if lower.
- All undergoing experiments are terminated.
- The program ignores all current and mass flow rate setpoints manually entered.
- The red "Emergency" LED is turned on.
- A message is displayed on screen indicating the reason for the emergency (voltage, mass flow rate, or temperature issue).
- An e-mail notification is sent to certain people indicating the reason for the emergency (voltage, mass flow rate, or temperature issue).

The reason why the air mass flow rate is unchanged is because it is not dangerous to the components, and a big change in air mass flow (e.g., from 15 $L \cdot min^{-1}$ to 5 $L \cdot min^{-1}$) would result in a dramatic increase in air inlet temperature to the fuel cell stack, due to the slower movement of the gas in the channel, which would induce a considerable thermal stress to the RSOC stack.

To exit security mode, the user must click the "Reset" button under the red LED in the front panel UI, as seen in Figure 28. Then, everything can be controlled manually by the user again.

A "Force security configuration" button was added in case the user wants to stop all undergoing experiments or enter security mode for any reason.

ETSEIB

3.2.3. Polarization curve experiment

A polarization curve displays the voltage output of the fuel cell for a given current density loading. Polarization curves can be obtained with an electronic load, which draws a fixed current from the fuel cell and measures the fuel cell output voltage. When the current (load) on a fuel cell is changed, the fuel cell heat and water balance change, and it may take time to reach a new equilibrium point. During testing, a designated period should be used to allow the fuel cell to reach the new equilibrium. The establishment of an equilibrium period varies depending upon whether the fuel cell load has been increased or decreased. Relevant test data can be obtained from the fuel cell by adjusting the load. Typically, the load is programmed to increase or decrease by a certain step-size.[31]

A polarization curve experiment may last various hours, as several minutes must be spent at each current setpoint to allow the RSOC to reach steady state. Analysing these stationary operation points is the goal, since it brings knowledge about the characterisation of the studied stack, allowing to check for the most efficient combination of gas mass flow rates for a certain power demand. For this reason, it is typical to perform polarization curves with changing mass flow rates for every operating point. These mass flow rates are calculated as a fuel or reactant utilization percentage, referring to how much of the total flow rate is reacting. The program automatically calculates the total mass flow rate for each current point in the following way:

$$\dot{m}_i = \frac{\dot{m}_i^r}{FU_i} \qquad\qquad (\,44\,)$$

Where $\dot{m}_i$ is the reacting gas mass flow in $kg{\cdot}s^{-1}$, $\dot{m}_i^r$ is the reacted mass flow of the reacting gas in $kg{\cdot}s^{-1}$, which is hydrogen in SOFC mode and steam in SOEC mode, and FU_i is the fuel utilization, between 40% (0,4) and 80% (0,8).

$$\dot{m}_i^r = N \cdot \frac{i}{2F} \cdot M_i \qquad\qquad (\,45\,)$$

Where N is the number of cells, i the current in A, and M_i the molar mass of the gas.

ETSEIB

In the case of fuel composition being different than 100% reacting gas (e.g., water is added to the fuel mass flow in SOFC mode, or hydrogen is added to the fuel mass flow in SOEC mode), the mass flow rate of the other gas in the fuel mix must be calculated. The user can choose molar fraction percentage for the other gas species in the fuel mixture, which is steam for SOFC mode and hydrogen for SOEC mode.

$$\dot{m}_k = \frac{\dot{m}_i \cdot MF_k}{MF_i} \qquad (46)$$

Where MF_k is the mass fraction of gas k, and MF_i is the mass fraction of gas i. For any specified fuel gas mixture, $MF_k + MF_i = 1$.

$$MF_i = \frac{M_i \cdot FC_i}{M_i \cdot FC_i + M_k \cdot FC_k} \qquad (47)$$

Where M_x is each gases' molar mass and FC_x is each gases' molar fuel composition, and $FC_i + FC_k = 1$. For SOFC mode, in most experiments $FC_{H_2} = 1$. In SOEC mode, an example of fuel composition is $FC_{H_2O} = 0,9$ and $FC_{H_2} = 0,1$, which would result in:

$$MF_{H_2} = \frac{M_{H_2} \cdot FC_{H_2}}{M_{H_2} \cdot FC_{H_2} + M_{H_2O} \cdot FC_{H_2O}} = \frac{0,002 \cdot 0,1}{0,002 \cdot 0,1 + 0,018 \cdot 0,9} = 0,0122 \qquad (48)$$

The polarization curve tab allows the user to start an experiment of this type. When the program is prompted to start the programming of the options, the sweep experiment tab is disabled, to avoid incompatibilities.

The mode selection allows choosing between SOFC and SOEC modes, and one-way or round-trip current profiles. Depending on the mode chosen, the current profile will be positive or negative, and the gas mass flow rate options might be different.

To choose the current profile, the maximum current must be chosen, and the number of steps will determine the height of each current step. An additional option is to set an "start point" that will be reached from 0 A in steps of 0,2 A, as seen in Figure 29. The purpose of this feature is to allow for more data at lower currents, which could result in a better understanding of activation losses.
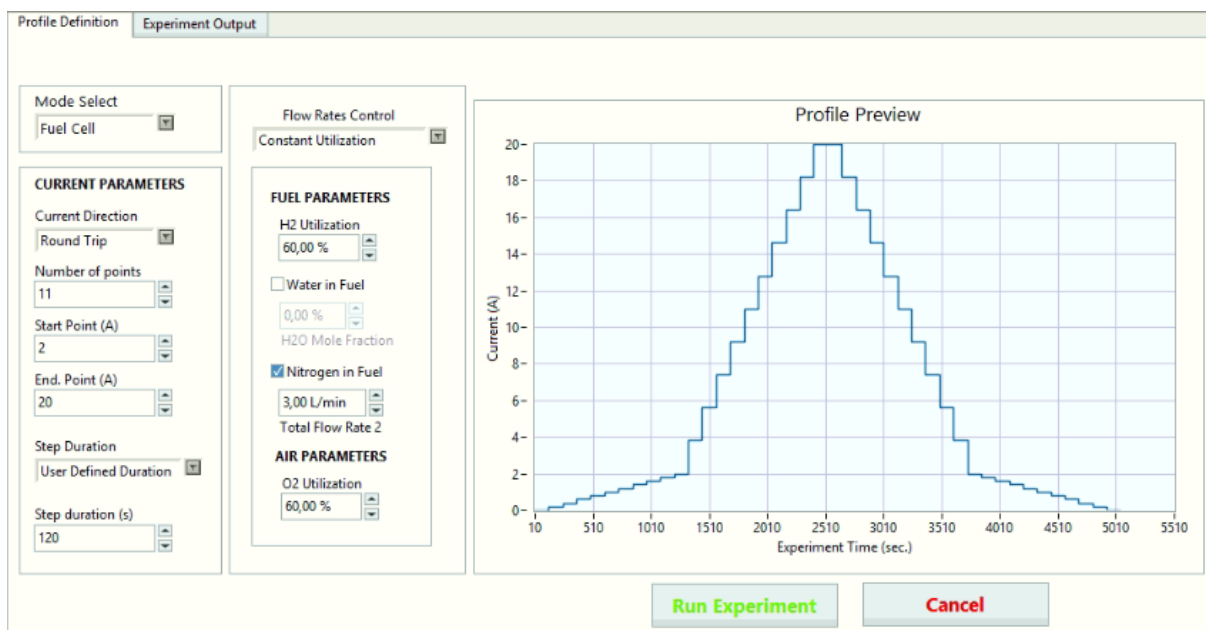
Figure 29. Polarization curve experiment screen in LabVIEW

All the polarization curve experiments performed with a new RSOC stack installed in the experimental station are listed in Table 7 and Table 8. The number and conditions of the experiments were decided with the intention of having a complete characterisation of the stack. All experimental data can be found in Annex 1.

Exp. Number	Current: (Max A)- Pol. Curve (# steps, 1-2 ways)	Hydrogen: FU (%) Flux (L·min⁻¹)	Air: FU (%) (L·min⁻¹)	Water anode: Molar fraction (%)	Nitrogen anode: flux (L·min⁻¹)	Temp. (ºC)	Date
Exp. 1	p.curve (18A, 12, 2-w)	60%	60%	0%	Variable QTotal = 3	750	19/02
Exp. 2	p.curve (18A, 12, 2-w)	80%	60%	0%	Variable QTotal = 3	750	19/02
Exp. 3	p.curve (20A, 13, 2-w)	40%	60%	0%	Variable QTotal = 3	750	23/02
Exp. 4	p.curve (18A, 13, 2-w)	60%	80%	0%	Variable QTotal = 3	750	23/02
Exp. 5	p.curve (18A, 12, 2-w)	60%	60%	0%	Constant Q = 3	750	23/02
Exp. 6	p.curve (14A, 13, 2-w)	60%	60%	10%	Constant Q = 3	750	24/02
Exp. 7	p.curve (16A, 11, 2-w)	60%	60%	0%	Variable QTotal = 3	800	25/02

Exp. Number	Current: (Max A)- Pol. Curve (# steps, 1-2 ways)	Hydrogen: FU (%) Flux (L·min⁻¹)	Air: FU (%) (L·min⁻¹)	Water anode: Molar fraction (%)	Nitrogen anode: flux (L·min⁻¹)	Temp. (ºC)	Date
Exp. 8	p.curve (14A, 11, 2-w)	80%	60%	0%	Variable QTotal = 3	800	25/02
Exp. 9	p.curve (20A, 13, 2-w)	40%	60%	0%	Variable QTotal = 3	800	25/02
Exp. 10	p.curve (16A, 12, 2-w)	60%	80%	0%	Variable QTotal = 3L	800	01/03
Exp. 11	p.curve (14A, 11, 2-w)	60%	60%	0%	Constant Q = 3	800	01/03
Exp. 12	p.curve (13A, 11, 2-w)	60%	60%	10%	Constant Q = 3	800	02/03

Table 7. SOFC polarization curve experiments performed

An example of an automatically generated image for a polarization curve experiment in LabVIEW can be seen in Figure 30.
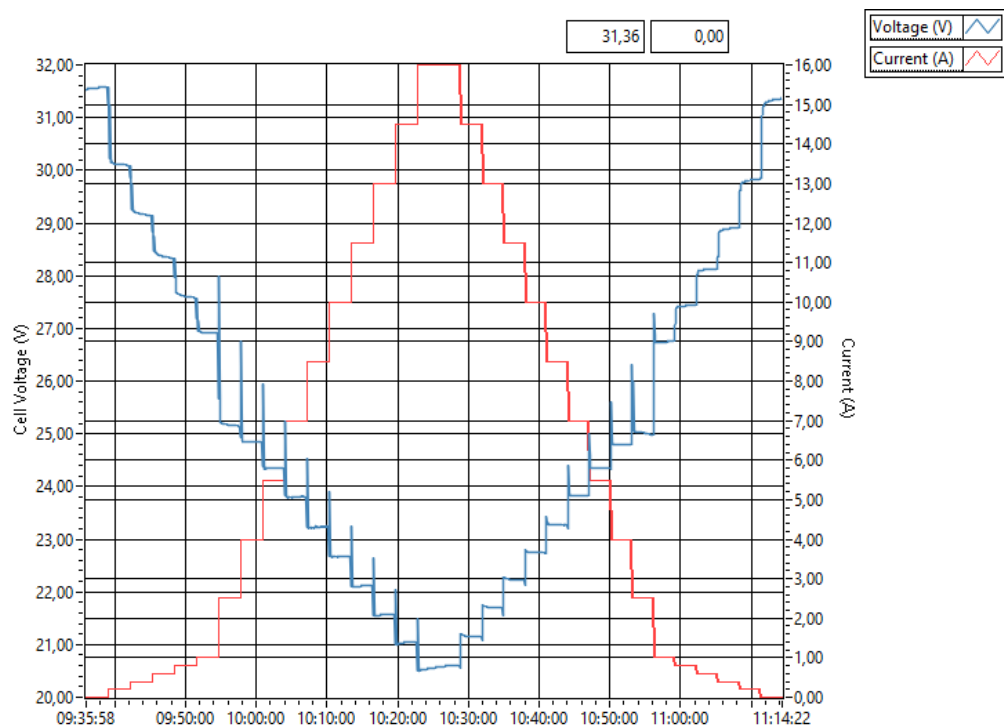

Figure 30. Polarization curve SOFC experiment 7

It can be appreciated that the maximum current reached was 16 A, for a voltage of approximately 20,5 V, for a total power of approximately 330 W. The performance of the studied RSOC stack was poor compared to other 30-cell RSOC stacks, which should reach 21 V when the current demand is close to 30A, for a total power of over 500 W.

Exp. Number	Current: (Max A)- Pol. Curve (# steps, 1-2 ways)	Water Vapor: RU (%)- flux (L·min⁻¹)	Air flux (L·min⁻¹)	Hydrogen in anode (molar fraction %)	Nitrogen anode: flux (L·min⁻¹)	Temp. (ºC)	Date
Exp. 1	p.curve (24A, 12, 2-w)	RU=60	10	10%	Variable QTotal=3,5	750	22/02
Exp. 2	p.curve (24A, 12, 2-w)	RU=80	10	10%	Constant 3	750	22/02
Exp. 3	p.curve (24A, 12, 2-w)	RU=40	10	10%	Constant 3	750	23/02
Exp. 4	p.curve (24A, 12, 2-w)	RU=60	10	30%	Constant 3	750	24/02
Exp. 5	p.curve (22A, 11, 2-w)	RU=60	10	50%	Constant 3	750	24/02
Exp. 6	p.curve (22A, 11, 2-w)	RU=60	10	10%	Constant 3	800	25/02 02/03
Exp. 7	p.curve (18A, 10, 2-w)	RU=80	10	10%	Constant 3	800	02/03
Exp. 8	p.curve (20A, 11, 2-w)	RU=40	10	10%	Constant 3	800	02/03

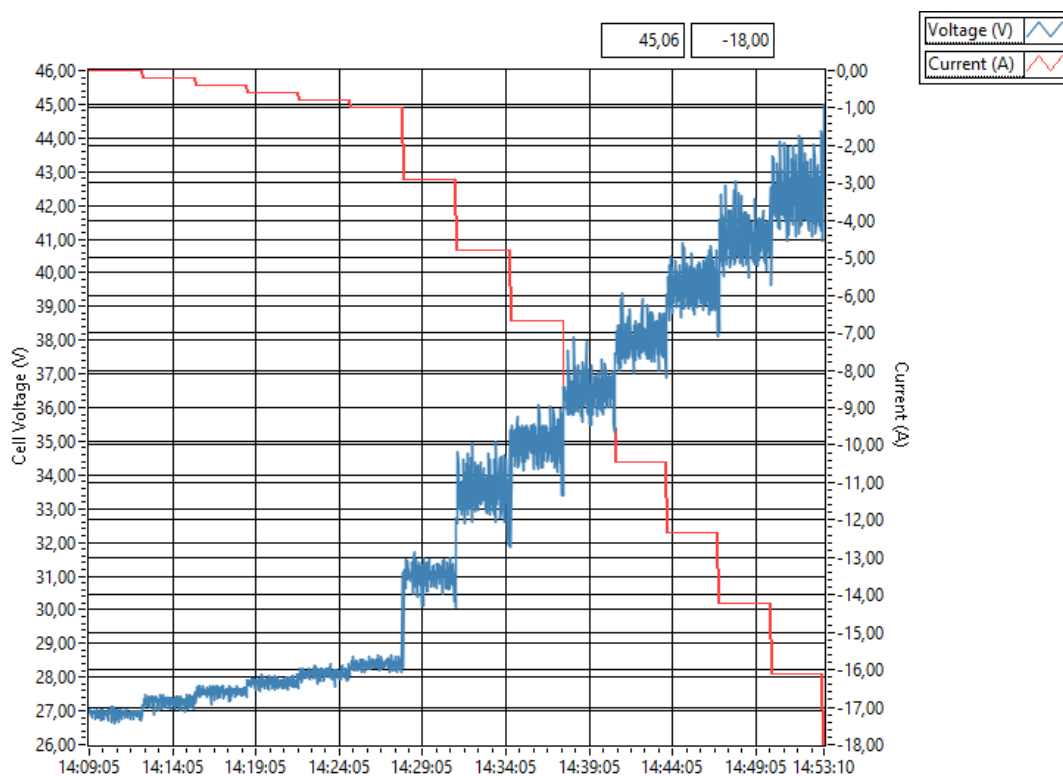*Table 8. SOEC polarization curve experiments performed*

Figure 31. Polarization curve SOEC experiment 7

As seen in Figure 31, the experiment was suddenly terminated when the total voltage reached 45 V. This is a security measure, as voltages over 1,5V/cell can be dangerous to the RSOC components. To complete an experiment in these conditions, a current profile with a lower maximum current should be chosen.

Programmatically, the pseudo-code of the polarization curve is as follows:

Algorithm 1 → Polarization Curve experiment

```
Program PolCurve(ExpOptions)

For N in NumSteps Do
     If MassFlowRates == Constant Then
          Set MassFlowSP = Gas Mass Flow
     Else
          Set MassFlowSP = MassFlowController(CurrentSteps[N])
     EndIf

     If CurrentSteps[N] > CurrentSteps[N-1] Then
          Wait until (MassFlowRead == MassFlowSP)
     EndIf

     Set Current = CurrentSteps[N]

     Wait for (StepDuration)
EndFor

EndProgram
```

The reason the program only waits until the mass flow rates have reached their setpoint if CurrentSteps[N] > CurrentSteps[N-1] is because if reducing the current the stack would operate at very high fuel utilizations (FU) while waiting for the mass flow rates to reach their new lower setpoint. In SOFC mode, operating at a higher than intended FU could result in a rapid decrease in voltage, unexpectedly ending the experiment if the decrease is enough to make the program engage safety mode.

3.2.4. Current sweep experiment

A current sweep takes a maximum of a few minutes to perform, and its goal is to test the dynamic response of the RSOC system. Unlike the polarization curve, in a current sweep the mass flow rates, temperature, and other operating conditions will be constant. As previously mentioned, the current sweep will be tested in SOFC, SOEC and reversible operation modes. The reversible operation mode is simply a current sweep with constant mass flow rates of 50% hydrogen and 50% steam, where the current will be positive for SOFC mode and negative for SOEC mode, as seen in Figure 32.

In this set of experiments, a fast ramping of 40 A/min was applied, reaching the limiting voltage, and then ramping back down to 0 A. The limiting voltage is the minimum or maximum voltage (SOFC or SOEC operation mode) that the user wants to reach. It is typically a security measure, as demanding too much power from the RSOC could be dangerous to its components, resulting in a faster degradation. In SOFC operation mode, this security voltage is typically of 0,6-0,7 V/cell, which totals 18-21 V for a stack with 30 cells. In SOEC operation mode, the security voltage is of 1,3-1,4 V/cell, totalling 39-42V.
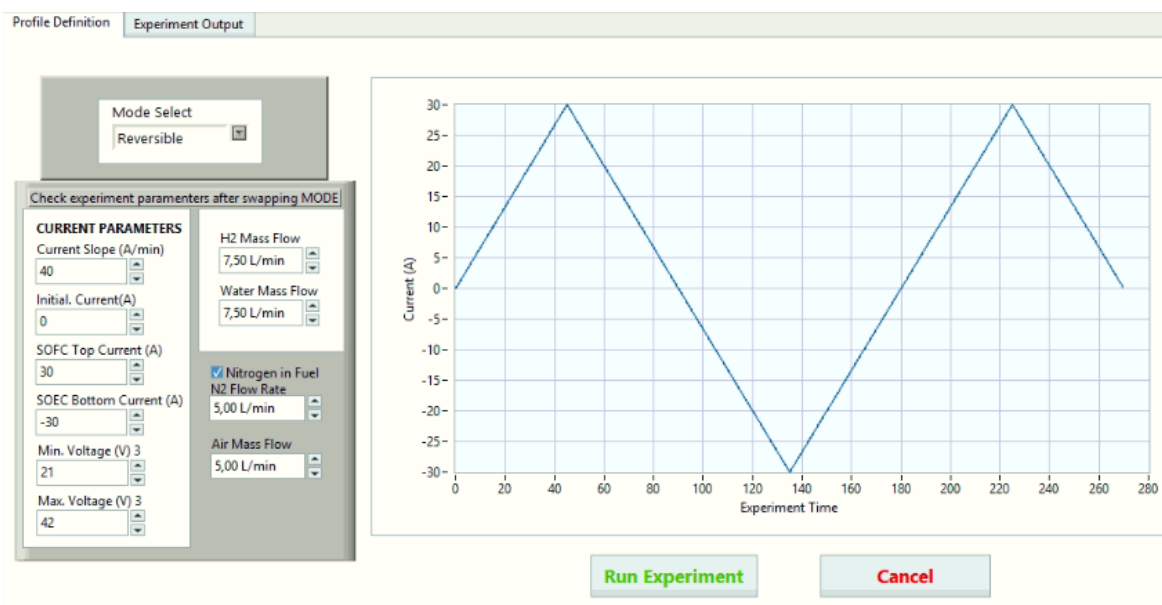

Figure 32. Sweep experiment screen in LabVIEW.

In reversible mode, the current goes up to "SOFC Top Current", then down to "SOEC Bottom Current", back up to "SOFC Top Current" and then to 0 A: The reason for this is that it was determined that it could be of interest to have data on the transition from positive to negative current values, and from negative to positive current values.

Top and bottom currents are selected, as well as minimum and maximum total voltage values. During the experiment, when either is reached (e.g., in SOFC mode, at 20 A, the voltage is already at 21 V) the current profile will change the direction it is going, to avoid stressing the stack.

All the current sweep experiments performed with a new RSOC stack installed in the experimental station are listed in Table 9, Table 10 and Table 11. The number and conditions of the experiments were decided with the intention of having a complete characterisation of the stack. All experimental data can be found in Annex 1.

Experiment Number	Current: sweep (A/s), one-two way	Hydrogen flow (L·min⁻¹)	Air flow (L·min⁻¹)	Water flow (L·min⁻¹)	Nitrogen anode flow (L·min⁻¹)	Temp. (ºC)	Date
Exp. 1	40 A/min, 2-w	12	26 L/min	0	0	750	18/02
Exp. 2	40 A/min, 2-w	10	26 L/min	0	0	750	18/02
Exp. 3	40 A/min, 2-w	8	26 L/min	0	0	750	18/02
Exp. 4	40 A/min, 2-w	10	26 L/min	0	0.8 L/min	750	18/02
Exp. 5	40 A/min, 2-w	10	26 L/min	0	1.6 L/min	750	18/02
Exp. 6	40 A/min, 2-w	10	26 L/min	0	4 L/min	750	18/02
Exp. 7	40 A/min, 2-w	10	26 L/min	1	0	750	18/02
Exp. 8	40 A/min, 2-w	10	26 L/min	1.6	0	750	18/02
Exp. 9	40 A/min, 2-w	10	26 L/min	4	0	750	18/02
Exp. 10	40 A/min, 2-w	10	28 L/min	0	0	750	18/02
Exp. 11	40 A/min, 2-w	10	20 L/min	0	0	750	24/02
Exp. 12	40 A/min, 2-w	12	26 L/min	0	0	800	01/03
Exp. 13	40 A/min, 2-w	10	26 L/min	0	0	800	01/03
Exp. 14	40 A/min, 2-w	8	26 L/min	0	0	800	01/03
Exp. 15	40 A/min, 2-w	10	26 L/min	0	0.8 L/min	800	01/03
Exp. 16	40 A/min, 2-w	10	26 L/min	0	1.6 L/min	800	01/03
Exp. 17	40 A/min, 2-w	10	26 L/min	0	4 L/min	800	01/03
Exp. 18	40 A/min, 2-w	10	26 L/min	1	0	800	01/03
Exp. 19	40 A/min, 2-w	10	26 L/min	2	0	800	01/03
Exp. 20	40 A/min, 2-w	10	26 L/min	4	0	800	01/03
Exp. 21	40 A/min, 2-w	10	28 L/min	0	0	800	01/03
Exp. 22	40 A/min, 2-w	10	20 L/min	0	0	800	01/03
Exp. 23	40 A/min, 2-w	10	15 L/min	0	0	800	01/03
Exp. 24	40 A/min, 2-w	10	30 L/min	0	0	800	01/03

Table 9. SOFC current sweep experiments performed.

ETSEIB

Experiment Number	Current: sweep (A/s), one-two way	Water flow (L·min⁻¹)	Air flow (L·min⁻¹)	Hydrogen flow (% (L·min⁻¹))	Nitrogen anode flow (L·min⁻¹)	Temp. (ºC)	Date
Exp. 1	40 A/min, 2-w	10	26	10% (1,1)	0	750	18/02
Exp. 2	40 A/min, 2-w	10	26	10% (1,1)	2	750	18/02
Exp. 3	40 A/min, 2-w	8	26	10% (0.88)	2	750	18/02
Exp. 4	40 A/min, 2-w	6	26	10% (0.67)	2	750	18/02
Exp. 5	40 A/min, 2-w	10	26	30% (4,26)	2	750	18/02
Exp. 6	40 A/min, 2-w	8	26	30% (3,42)	2	750	18/02
Exp. 7	40 A/min, 2-w	6	26	30% (2,57)	2	750	18/02
Exp. 8	40 A/min, 2-w	10	26	50% (10)	2	750	18/02
Exp. 9	40 A/min, 2-w	8	26	50% (8)	2	750	18/02
Exp. 10	40 A/min, 2-w	6	26	50% (6)	2	750	18/02
Exp. 11	40 A/min, 2-w	12	26	10% (1,33)	2	750	18/02
Exp. 12	40 A/min, 2-w	15	26	10% (1,66)	2	750	18/02
Exp. 13	40 A/min, 2-w	10	26	10% (1,1)	0	800	01/03
Exp. 14	40 A/min, 2-w	10	26	10% (1,1)	2	800	01/03
Exp. 15	40 A/min, 2-w	8	26	10% (0.88)	2	800	01/03
Exp. 16	40 A/min, 2-w	6	26	10% (0.67)	2	800	01/03
Exp. 17	40 A/min, 2-w	10	26	30% (4,26)	2	800	01/03
Exp. 18	40 A/min, 2-w	8	26	30% (3,42)	2	800	01/03
Exp. 19	40 A/min, 2-w	6	26	30% (2,57)	2	800	01/03
Exp. 20	40 A/min, 2-w	10	26	50% (10)	2	800	01/03
Exp. 21	40 A/min, 2-w	8	26	50% (8)	2	800	01/03
Exp. 22	40 A/min, 2-w	6	26	50% (6)	2	800	01/03
Exp. 23	40 A/min, 2-w	12	26	10% (1,33)	2	800	01/03
Exp. 24	40 A/min, 2-w	15	26	10% (1,66)	2	800	01/03

Table 10. SOEC current sweep experiments performed.

Experiment Number	Current: sweep (A/s), one-two way	Water flow (L·min⁻¹)	Hydrogen flow (L·min⁻¹)	Air flow (L·min⁻¹)	Nitrogen anode flow (L·min⁻¹)	Temp. (ºC)	Date
Exp. 1	Sweep 2-w	10,45	10,45	26	2	750	18/02
Exp. 2	Sweep 2-w	8,36	12,54	26	2	750	18/02
Exp. 3	Sweep 2-w	10,45	10,45	26	2	800	01/03
Exp. 4	Sweep 2-w	8,36	12,54	26	2	800	01/03
Exp. 5	Sweep 2-w	12,54	8,36	26	2	800	01/03

Table 11. Reversible current sweep experiments performed.

The pseudocode for the current sweep experiment is as follows:

Algorithm 2 → Current sweep experiment

```
Program Current_Sweep(ExpOptions)

Set MassFlowSP = Gas Mass Flow
Wait until (MassFlowRead == Gas Mass Flow)

For N in NumPoints Do
    Set Current = CurrentPoints[N]

    If Voltage <= VoltageLimitMin or Voltage >=
    VoltageLimitMax
        Skip N until CurrentPoints[N] == Current
    EndIf

    Wait 200 ms

EndFor

EndProgram
```

If the voltage limit has been reached, it starts returning to 0 A and, if it is already reducing the current, it stays as is.

This allows the user to set a high maximum current, intending to reach it during the experiment, but if the voltage limit is reached before the maximum current, the program will behave as intended and not allow the voltage to reach dangerous values (too high or too low), which could endanger the RSOC components.

ETSEIB

4. Modelling and control of the RSOC system

This chapter will first explain the Simulink model, introducing the new elements added to the model to accurately simulate the prototype in the context of the HyBCN project.

After, an attempt to fit the simulation results to the experimental data will be performed, using global optimization techniques to find suitable parameters.

4.1. Previous models

The first model related to the current one was made in November 2016, based on the work of Y. Zhu et. al. [32], using a SOFC model provided by Mathworks in the Simulink programming environment. The model was extended with the polarization losses calculations, related to the electrochemical reaction. This dynamic model set the way forward for posterior versions.

In a later iteration of the model, made in 2017, the stack model was divided into three different volumes to better represent gas behaviour inside of it. These volumes are the Inlet Manifold, corresponding to the air inlet in the cathode; Fuel Cell Stack; and Outlet Manifold, corresponding to the air outlet in the cathode. Gas properties are more accurately calculated in each volume, representing their dynamics.

The same year, the model was furtherly improved in the scope of the REFER project, still including the electrochemical and thermodynamic model of a SOFC cell, as well as two possibilities of system control (oven power and air flow, for thermal balance). More parameters were added and all of them were polished, as well as feeding more information to the model such as the open circuit voltage calculation, dry air cathode input, new operating temperature (750ºC) and the possibility of steam in fuel mixture.

In addition, experimental data from a SOFC station in IREC was available, and allowed manifold constants, valve constants, electrochemical parameters, and thermal parameters in the model to be more accurate in representing the real SOFC stack. This stack was provided by the manufacturer SOFCMAN Energy Technology, as is the one used during the experiments in the context of this work.

The model, in its previous iteration before this work, included the electrochemical balance, the calculation of partial pressures in the gas channels, inlet and outlet manifold dynamics, thermodynamics balance, simple mass flow rate control blocks and a representation of the oven power controller by a PID.

Some of these calculations have not been modified, as is the case of the manifolds and gas channel partial pressures calculations. For the detailed description of the unchanged subsystems, refer to previous works such as [3] and [15]. Others have been modified to try to represent the real RSOC better, as is the case of the thermodynamics balance and oven controller, which will be described. The boiler and heat exchangers have been incorporated to represent the prototype that is to be built within the context of the HyBCN project, and finally the electrochemical balance has been improved with physical data and parameter estimation based on experimental data.

4.2. Reversible Solid Oxide Cell model

The RSOC model integrates all elements that play a part in the stack itself. This includes the manifolds model, the mass flow channels model, the electrochemical model, and the thermodynamic balance, as seen in Figure 33. Other aspects in the BOP such as controllers and auxiliary equipment will be explained later.

This part of the model has been developed over the years by the Automatic Control group, as described previously. Therefore, sections 0 and 4.2.2 will be presented, but not thoroughly explained. On the other hand, sections 4.2.3 and 0 require a more detailed description since they play a bigger role in this work's context.

ETSEIB
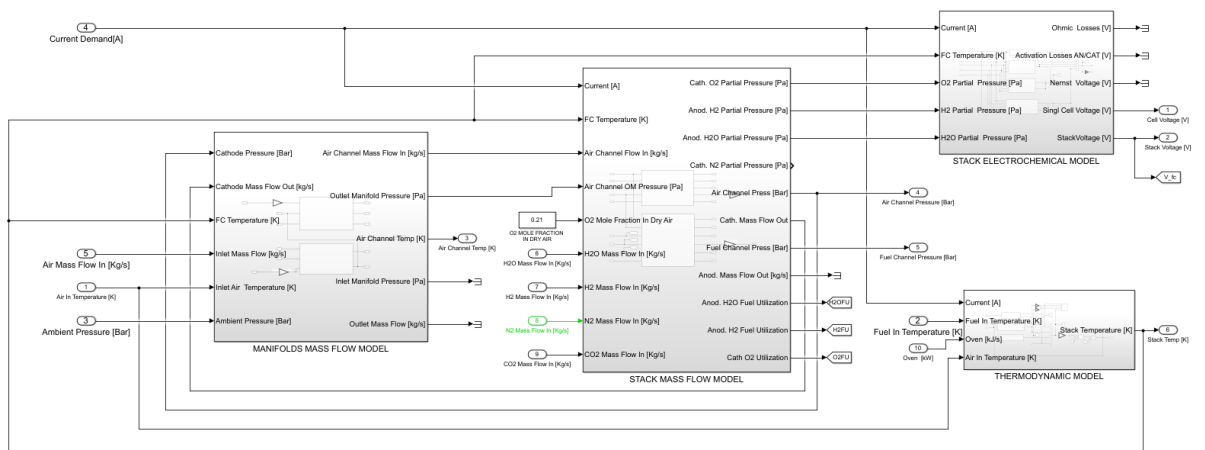
Figure 33. RSOC dynamic model.

4.2.1. Inlet and outlet manifolds

The manifolds model attempts to model the dynamics of the air mass flow channel. They simulate a volume before the cathode's entrance and after the cathode's exit where the air gas has its distinguished partial pressure and flow rate, which influences the dynamics of the cathode. This was adapted from [33], and all details of this block are given in [3].
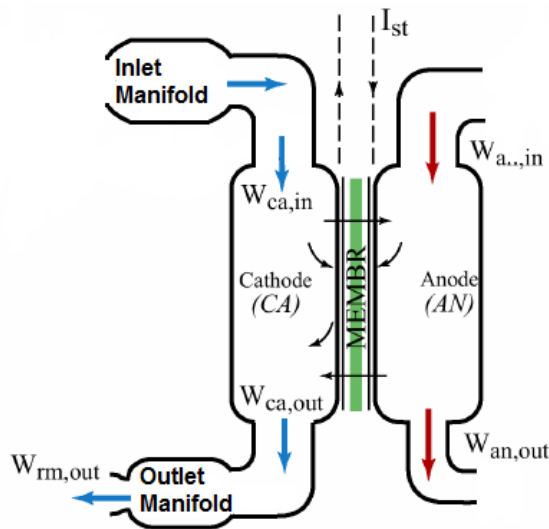

Figure 34. Manifolds diagram

Parameter	Value	Units
K_{IM}	$5 \cdot 10^{-8}$	$kg \cdot (Pa \cdot s)^{-1}$
K_{OM}	$3{,}35 \cdot 10^{-8}$	$kg \cdot (Pa \cdot s)^{-1}$
V_{IM}	$0{,}02$	m^3
V_{OM}	$0{,}005$	m^3

Table 12. Manifold parameters

Where K_{IM}, K_{OM} are the inlet and outlet manifolds valve constants respectively, and V_{IM} and V_{OM} are the volumes.
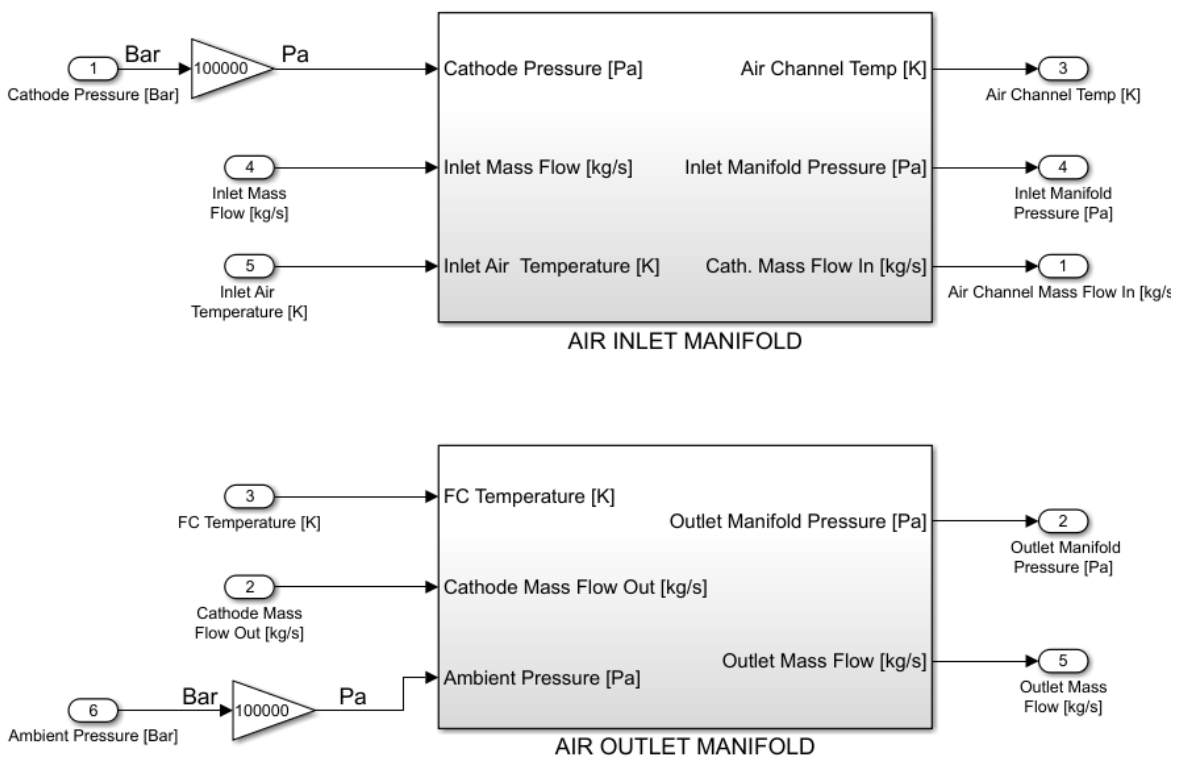
Figure 35. Manifolds model inputs and outputs.

4.2.2. Mass flows model

The stack mass flows model is a subsystem distinguishing the anode and cathode sides, where the partial pressure of each gas is calculated, necessary for the calculation of the electrochemical reaction.

Essentially, each channel has a volume, and the reacting gases are added or removed from the total balance, which yields new masses in each volume. The amount of reacting gas is calculated as explained in Equation (45).

Therefore, the balance of mass is as follows:

$$\frac{\partial m_i}{\partial t} = \dot{m}_i^{in} - \dot{m}_i^{r} - \dot{m}_i^{out} \qquad (49)$$

This allows for the calculation of partial pressures using the ideal gases law, in the form:

$$p_i = \dot{m}_i \cdot \frac{RT}{M_i \cdot V_{ch}} \qquad (50)$$

Where V_{ch} is the anode or cathode channel volume, in m^3.

In the anode, H_2, H_2O and N_2 gases are present, and their mass flow rates can be controlled independently, while in the cathode a single dry air mass flow controller is present, and dry air is 21% O_2 and 79% N_2.

Finally, the parameters in this model are:

Parameter	Value	Units
K_{AN}	$1{,}5 \cdot 10^{-8}$	$kg \cdot (Pa \cdot s)^{-1}$
K_{CA}	$9{,}385 \cdot 10^{-9}$	$kg \cdot (Pa \cdot s)^{-1}$
V_{AN}	0,005	m^3
V_{CA}	0,01	m^3

Table 13. Electrode parameters

Where K_{AN}, K_{CA} are the inlet and outlet manifolds valve constants respectively, and V_{AN} and V_{CA} are the volumes.

An example of the calculation of partial pressures for each gas can be seen in the case of O_2 in the cathode in Figure 36.
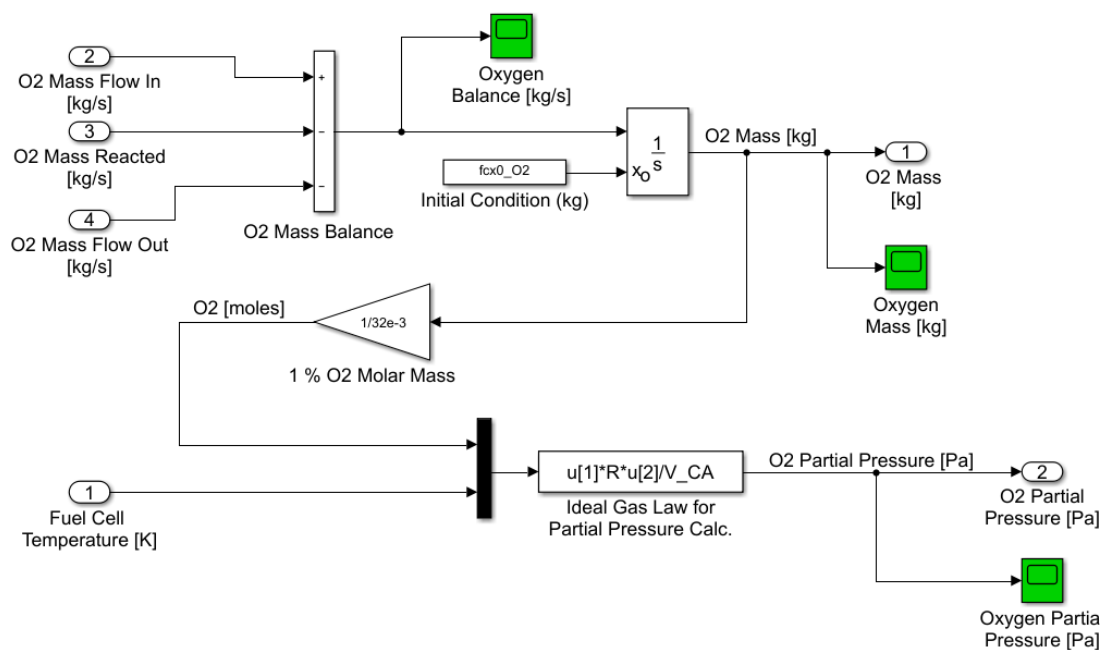
Figure 36. O$_2$ Partial Pressure calculation.

4.2.3. Electrochemical model

➢ **Nernst Voltage**

The Nernst voltage is determined as per Equation (14), but since E_0 (reversible voltage) is dependent on temperature, it is determined through linear regression of the free Gibbs energy values at different temperatures seen in Table 2, in the form:

$$E_0 = 1{,}2708 + 2{,}738 \cdot 10^{-4} \cdot T_{stack} \qquad (51)$$

Where T_{stack} is the stack temperature determined by the thermodynamics balance in *K.*
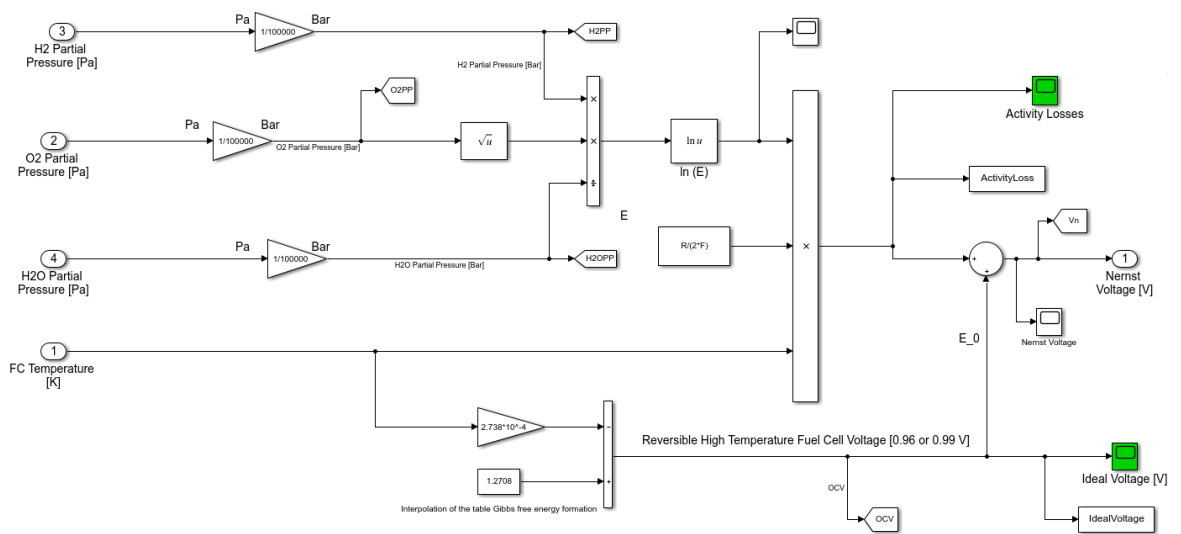
Figure 37. Nernst voltage calculation in Simulink model

➢ **Ohmic polarization**

Equation (25) is implemented, where the area is known, and is equal to 63 cm^2, and ASR is a parameter dependent on temperature. Previously, its value was set to 0,165 $\Omega \cdot cm^{-2}$ at 750ºC, but as explained in section 5, with the available experimental data a new value of 0,7252 $\Omega \cdot cm^{-2}$ at 750ºC has been determined in this work.
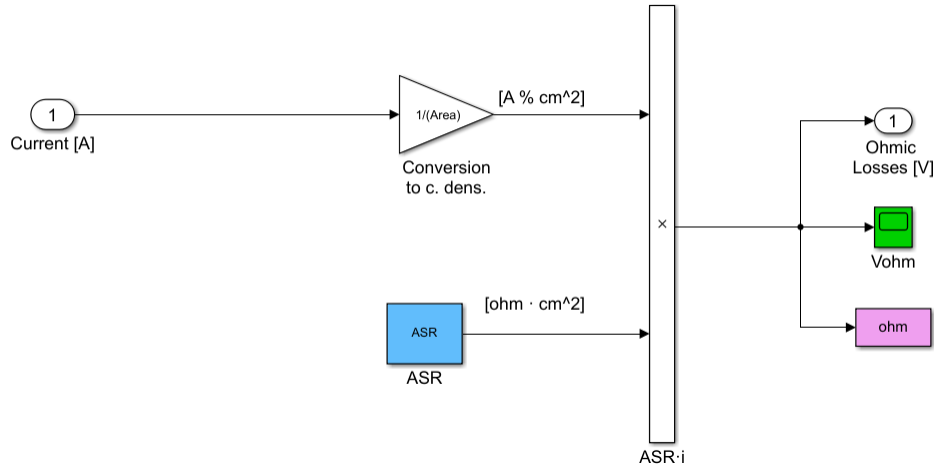
Figure 38. Ohmic polarization calculation in Simulink model

➢ **Activation polarization**

For each electrode, the $i_{o,el}$ and $\eta_{act,el}$ calculations are implemented in Simulink blocks, as Equations (16), (17) and (22). In previous works, the phenomenological coefficients γ_{el} were extracted from the literature, but thanks to the experimental data obtained, they were estimated as parameters, as seen in section 5.

The implementation of the equations in the Simulink model can be seen in Figure 39, Figure 40 and Figure 41. The parameters in this calculation are:

Parameter	Value	Units
E_{actAN}	100000	$kJ \cdot mol^{-1}$
E_{actCA}	120000	$kJ \cdot mol^{-1}$
α_{AN}	0,5	-
α_{CA}	0,5	-
γ_{AN}	*Parameter estimation*	$A \cdot cm^{-2}$
γ_{CA}	*Parameter estimation*	$A \cdot cm^{-2}$

Table 14. Activation polarization parameters
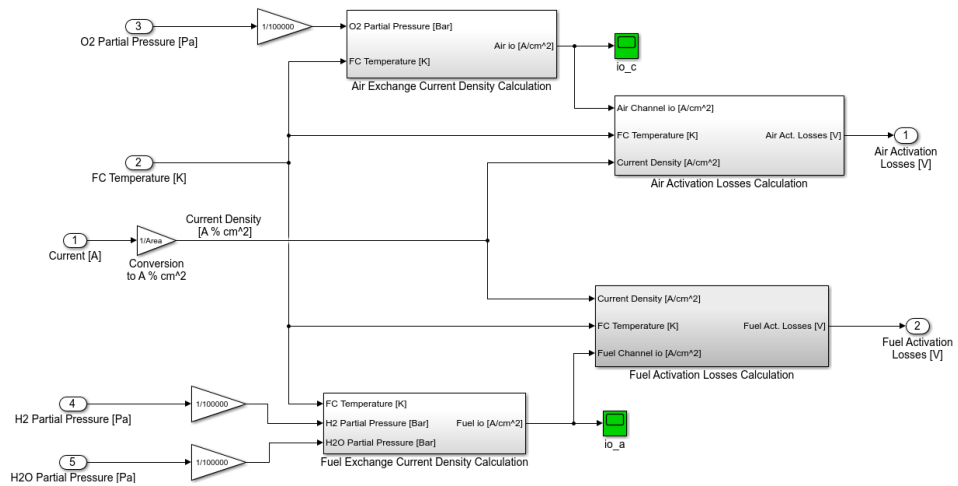
Figure 39. Activation losses calculation in Simulink
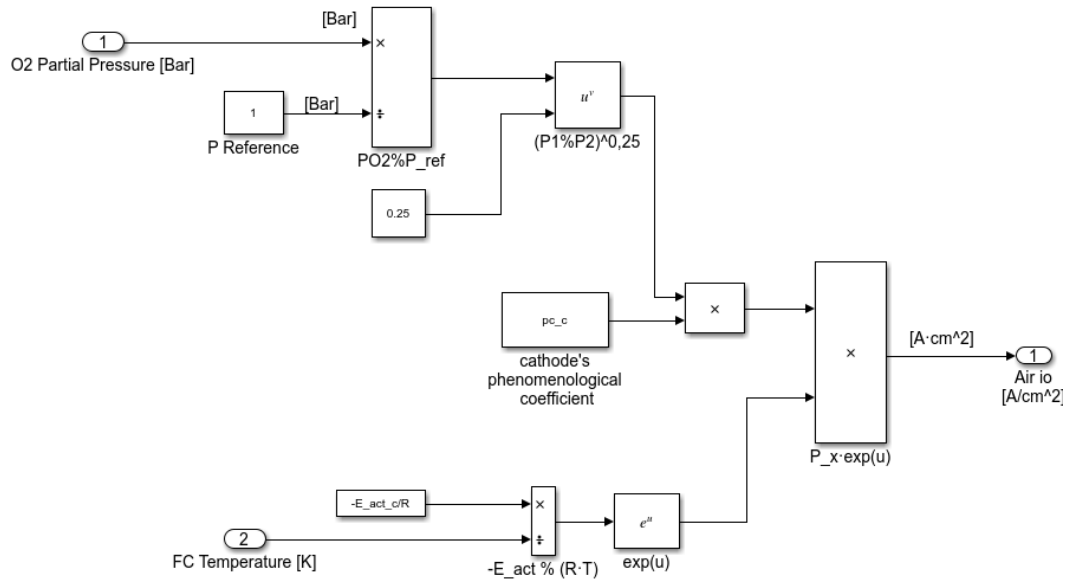
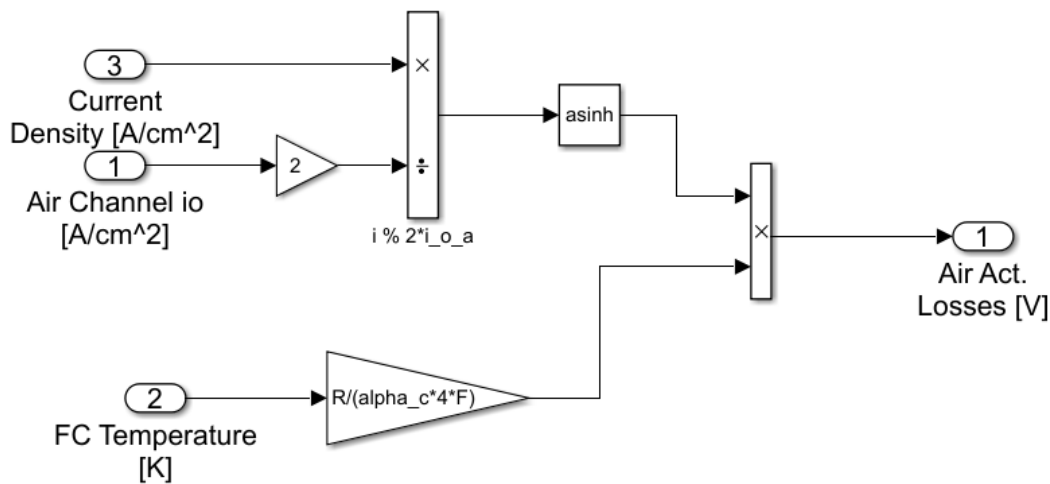*Figure 40. Air Exchange Current Density Calculation block*

Figure 41. Air Activation Losses Calculation block

➢ **Concentration polarization**

The concentration losses are also implemented with the equations presented in 2.4.5, with the exception that the details in the determination D_i^{eff} are not modelled, and instead in the previous work its value was determined beforehand. In section 5, τ_A and τ_C are determined with the use of experimental data and optimization methods.

The parameters are the following:

Parameter	Value	Units
ρ_{AN}	0,38	*cm*
ρ_{CA}	0,014	*cm*
ε_A	17%	-
ε_C	34%	-
τ_A	*Parameter estimation*	-
τ_C	*Parameter estimation*	-

Table 15. Concentration polarization parameters

Where ρ_{EL} is the thickness of each electrode and is a known value of the RSOC stack being studied and ε_{EL} is the porosity of each electrode, as seen in Figure 42.
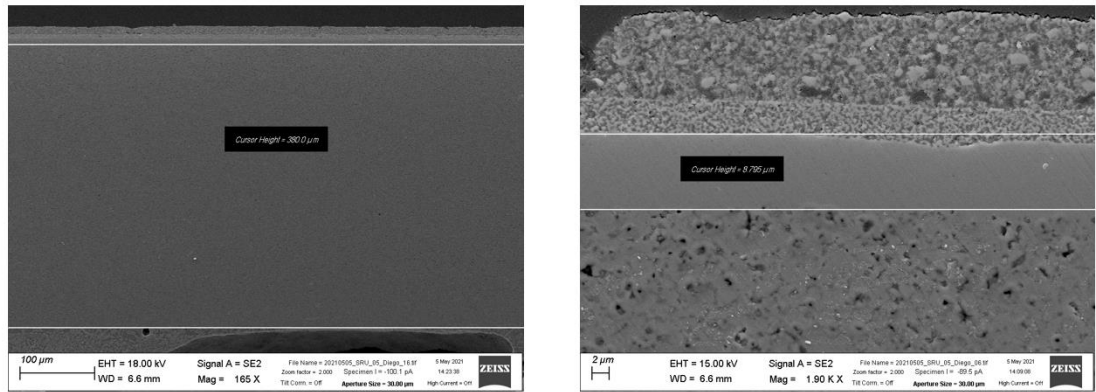
- Anode thickness: 380 µm
- Electrolyte thickness: 9 µm
- Cathode thickness: 4 µm of CGO barrier layer + 10 µm of LSCF-CGO (in their cell description they say the LSCF-CGO thickness is 25 µm).

Figure 42. Electrode and electrolyte thickness determination by IREC

The implementation of Equations (26), (27), (29), (30), (31) in the Simulink model is done in the Concentration Losses Calculation block.
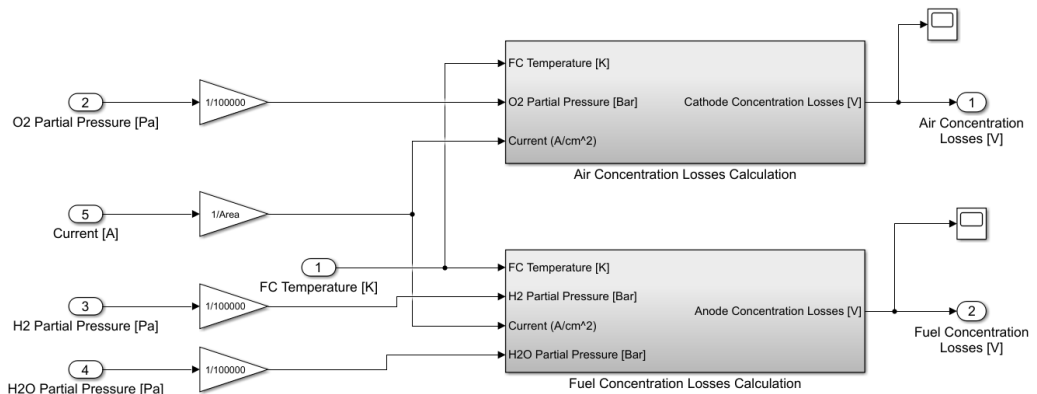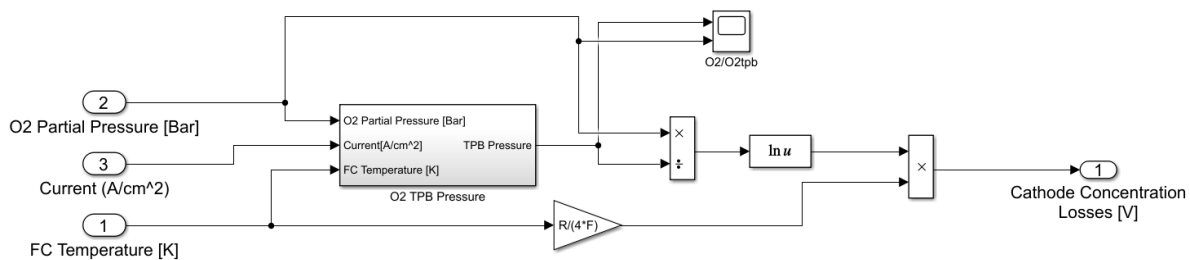

Figure 43. Concentration Losses Calculation block

Figure 44. Air Concentration Losses Calculation block
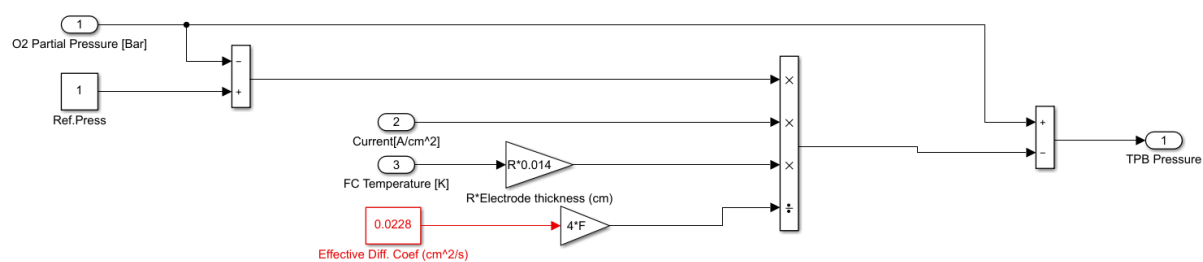
Figure 45. O$_2$ TPB Pressure block

4.2.4. Thermodynamic balance model

The thermodynamic balance is extremely important, as gases' properties are dependent on temperature, resulting in big changes in RSOC performance. The total heat balance is calculated as shown in Equation (43), and $\dot{Q}_{r,total}$, $\dot{Q}_{conv}$ and $\dot{Q}_{env}$ are determined by Equations (38), (41) and (42) respectively.
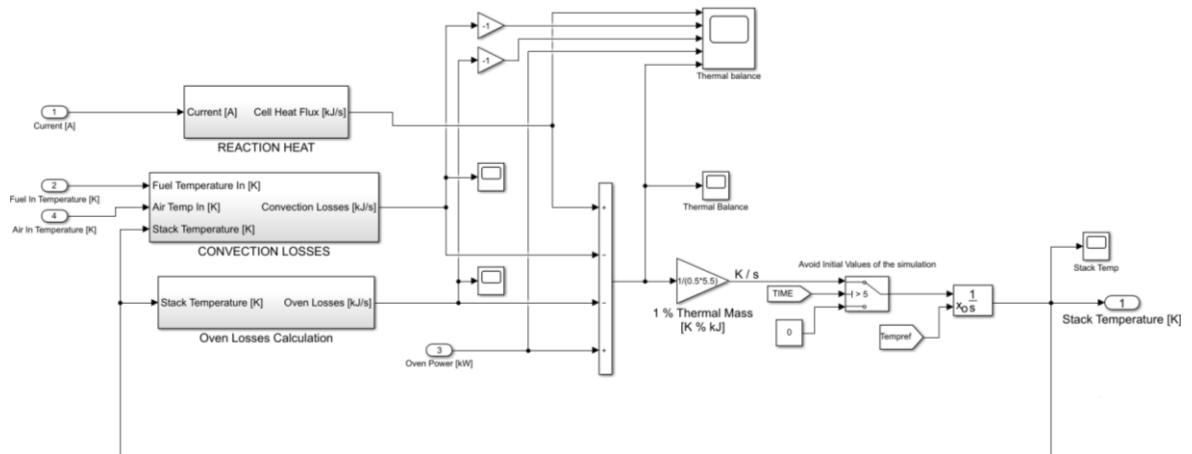

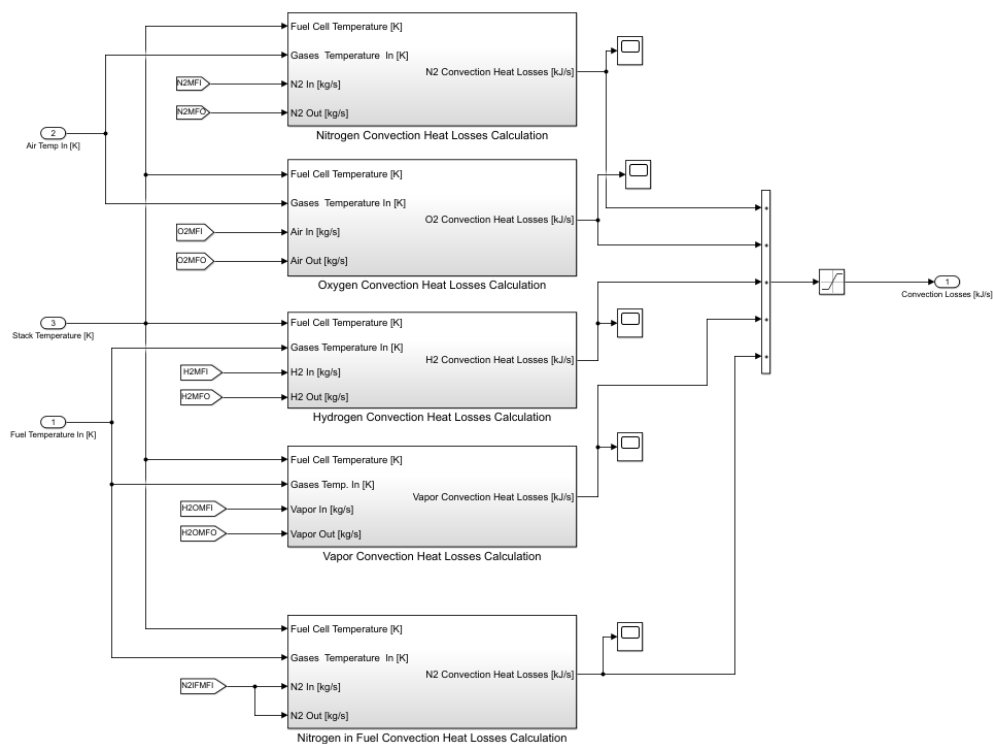*Figure 46. Thermodynamic Balance block*
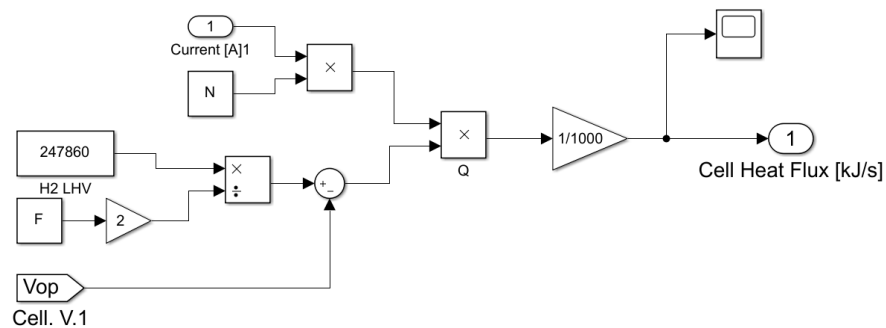
Figure 47. Reaction Heat block

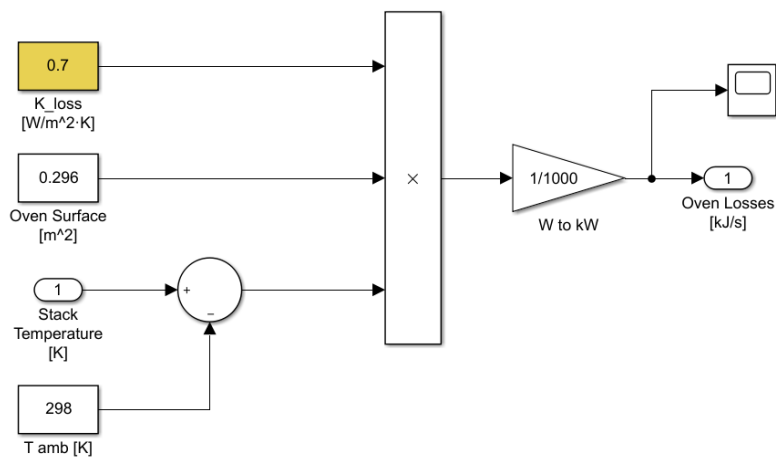*Figure 48. Convection Losses block*

Figure 49. Oven Losses Calculation block

The resulting thermal balance can be seen in Figure 75.

4.3. Balance of plant modelling

To reliably represent the real system, more elements in the balance of plant (BOP) were added to the model. The following physical auxiliary equipment was modelled: fuel mixer (or boiler), and two heat exchangers, for the fuel and air gas channels. On the other hand, a global efficiency calculation was added, as it is relevant to the results and expectations from the real system that is to be built.

The condenser, which will be installed in the prototype after the fuel outlet and will condense water to separate it from green hydrogen, has not been modelled. An initial approach was made, but after some consideration it was decided that it was not of much relevance, and eventually left out of the model. The reasoning was that, after the fuel heat exchanger, a tube approximately 50 cm long would take the fuel to the condenser, in which most water will already condensate or reduce its temperature significantly. Therefore, no refrigeration would be needed in the condenser, which means that modelling this auxiliary device would bring no relevant information to the completion of the prototype.

The BOP of the prototype, which was modelled, can be seen in Figure 50. Its main difference with the experimental station is that it has no line heaters, and it uses heat exchangers, which should improve efficiency significantly.
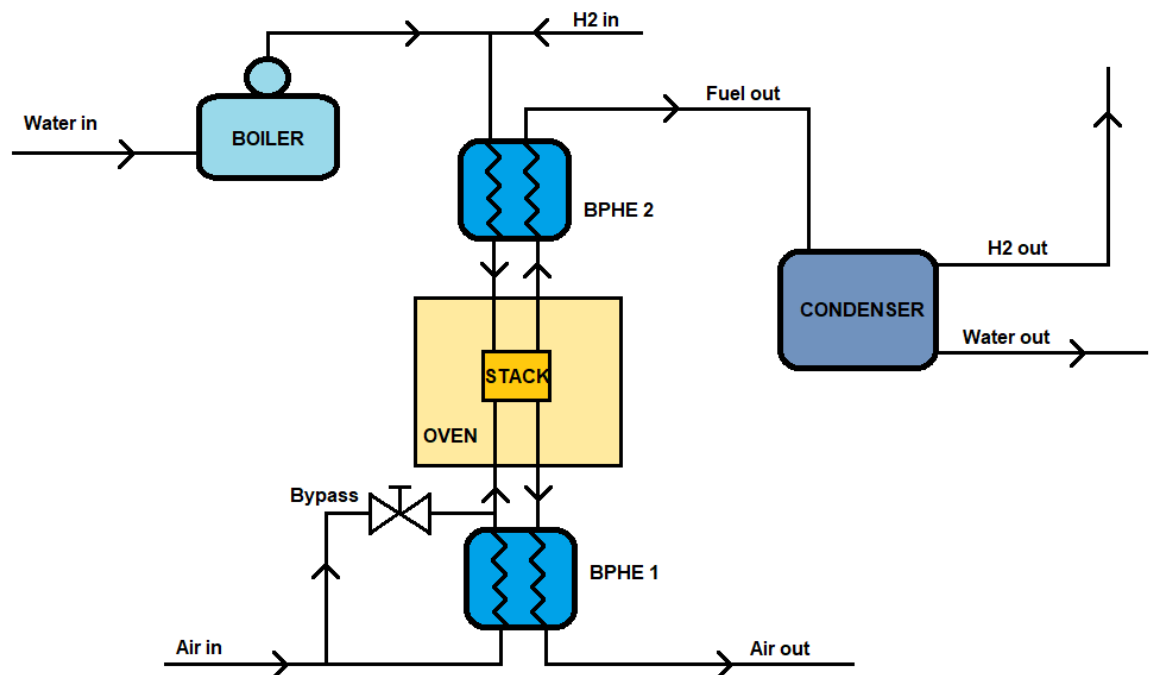

Figure 50. BOP of HyBCN prototype

The air bypass is a common way to control the refrigeration of the stack, which will be needed in SOFC operating mode because of its exothermic nature. It is dependent on stack temperature and controlled by the air mass flow controller, explained in section 4.4.1.

4.3.1.   Boiler (water evaporator)

The boiler or evaporator is an auxiliary device that evaporates water to steam and brings it to a certain temperature, as indicated by its setpoint.

$$q_{ev} = \dot{m} \cdot \left(\dot{Cp_l} \cdot (T_{ev} - T_{amb}) + \lambda \right) \tag{52}$$

$$q_{sh} = \dot{m} \cdot \dot{Cp_g} \cdot (T_{final} - T_{evap}) \tag{53}$$

$$q_{boiler} = q_{ev} + q_{sh} \tag{54}$$

Where $\dot{m}$ is the water mass flow in $kg{\cdot}s^{-1}$, $\lambda = 2257{,}92 \, kJ/kg$ is the enthalpy of vaporization at 1 *bar*, and $\dot{Cp_l} = 4{,}18 \, kJ \cdot (kg \cdot K)^{-1}$ and $\dot{Cp_g} = 2 \, kJ \cdot (kg \cdot K)^{-1}$ are the specific heats of liquid water and steam, respectively. $T_{amb} = 293K$, $T_{ev} = 373K$ for the system at a constant pressure of 1 *bar*, and $T_{final} = 473K$ is the setpoint temperature of the boiler and set to 200ºC.

Since all the needed variables are known, and the temperature setpoint T_{final} is chosen, the determined heating power q_{boiler} is the relevant variable, since it will participate in the calculation of global efficiency as shown in section 4.3.3.
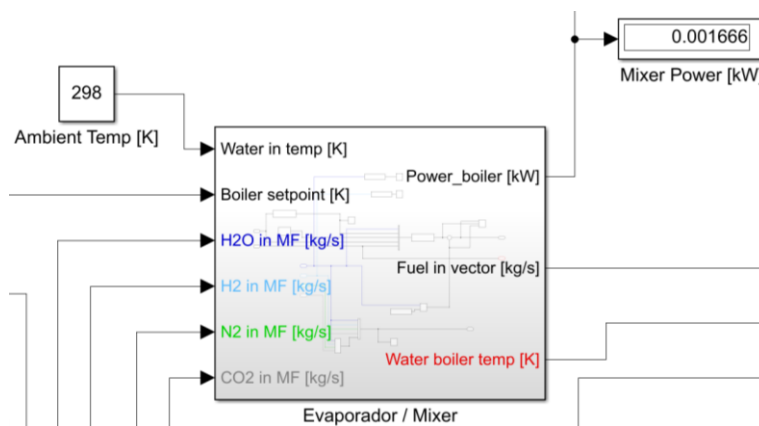

Figure 51. Boiler block

4.3.2.   Heat exchangers

To improve efficiency of the RSOC system, heat exchangers play a big role in the conservation of heat within the system. Brazed plate heat exchangers (BPHE) are compact, highly efficient, and durable liquid-to-liquid, gas-to-liquid, or gas-to-gas heat exchangers. These heat exchangers are constructed from stacked plates brazed together that are typically corrugated to add surface area and more heat transfer. BPHE's efficient counterflow design allows 90% of the material to be used for heat transfer. These heat exchangers can be up to 80-90% smaller than a conventional shell-and-tube design. The brazed plate construction offers a rugged, efficient, and long-lasting heat exchanger that withstands demanding environments.[34]

As seen in Figure 50, recuperative BPHEs in the system are air-air and fuel-fuel. Therefore, air exiting the RSOC at operating temperature (e.g., 750ºC) will heat up the air entering, and fuel exiting the RSOC at operating temperature will heat up the fuel entering. Since the BPHEs will be placed as close as possible to the stack, and in a chamber next to the oven, the gases exiting the stack are assumed to enter the exchangers at operating temperature, and no heat losses to the environment are considered in the model. This will not be true in the real system, but it should give a reasonable approximation, given only small heat losses to the environment are expected.

A very accurate model of the dynamics inside the heat exchanger is not needed since the main goal of the modelling of the auxiliary components is to get an estimate global efficiency. To calculate the temperature of cold and hot side gases at the exit of each heat exchanger, the Number of Transfer Units (NTU) method is used. This method is useful to calculate the rate of heat transfer in heat exchangers (especially counter-current exchangers) when there is insufficient information to calculate the Log-Mean Temperature Difference (LMTD), which requires knowing at least one of the output temperatures. In heat exchanger analysis, if the fluid inlet and outlet temperatures are specified or can be determined by simple energy balance, the LMTD method can be used; but when these temperatures are not available the NTU (Effectiveness) method is used. The effectiveness-NTU method is very useful for all the flow arrangements, besides parallel flow and counterflow ones.[35] A diagram of a counter-current heat exchanger is shown in Figure 52.

NTU uses the general expressions for the calculation of transferred heat:

$$q = U \cdot S \cdot \Delta T \qquad (55)$$

$$q = \dot{m} \cdot \dot{C}p \cdot \Delta T \qquad (56)$$

Where q is the heat transfer rate in *kW*, U is the overall heat transfer coefficient in *kW·(m²·K)⁻¹*, S is the heat transfer area in *m²*, ΔT is the temperature difference between inlet and outlet in *K*, and $\dot{m}$ is the mass flow rate in *kg·s⁻¹*.
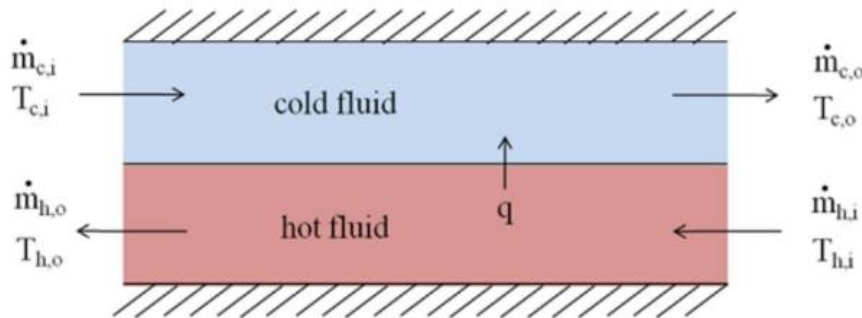

Figure 52. Counter-current heat exchanger diagram

The NTU method is based on calculating the heat capacity rates (mass flow rate multiplied by specific heat) of the hot and cold sides (C_h and C_c), and naming the smaller one C_{min}, as shown:

$$C_{min} = \min\,(\dot{m}_c \cdot \dot{C}p_c, \dot{m}_h \cdot \dot{C}p_h) \qquad (57)$$

Which allows for the calculation of the maximum possible heat transferred in the heat exchanger (q_{max}), considering the fluid with the lower capacity rate and assuming infinite area of exchange:

$$q_{max} = C_{min} \cdot (T_h^{in} - T_c^{in}) \qquad (58)$$

The heat capacity ratio C_r is defined as follows:

$$C_r = \frac{C_{min}}{C_{max}} \qquad (59)$$

The effectiveness ε is the ratio between the actual heat transfer rate and the maximum heat transfer rate, a dimensionless coefficient between 0 and 1:

$$\varepsilon = \frac{q}{q_{max}} \qquad (60)$$

The Number of Transfer Units, NTU, for a heat exchanger is calculated in the form:

$$NTU = \frac{U \cdot A}{C_{min}} \qquad (61)$$

And, for counter-current flow, effectiveness is then calculated using NTU and C_r:

$$\varepsilon = \frac{1 - e^{(-NTU \cdot (1 - C_r))}}{1 - C_r \cdot e^{(-NTU \cdot (1 - C_r))}} \qquad (62)$$

This allows to calculate the heat transfer rate q by isolating q in Equation (60), therefore allowing the calculation of the outlet temperature for both cold and hot sides isolating T_{side}^{out} from the temperature difference term in Equation (56).

The manufacturer, Kaori Heat Treatment Co., provided information on the necessary known parameters:

Parameter	Value	Units
U	0,012694	$kW \cdot (m^2 \cdot K)^{-1}$
A_{HE1}	0,304	m^2
A_{HE2}	0,187	m^2

Table 16. Heat exchangers parameters

The mass flow rates in the cold and hot sides are known. The entering mass flow rates are determined by the controllers, and the reacting gases are calculated as explained in section 714.2.2, using Equation (45). Since it is assumed no heat losses to the environment take place, the inlet temperature of the gas exiting the stack is known to be the stack operating temperature.

Gases entering the heat exchanger are at ambient temperature, except for steam, which is at the boiler's setpoint temperature (e.g., 200ºC) because it has been evaporated by the boiler, as explained previously. This means that the temperature of the fuel mixture must be calculated, in the form:

$$T_{c,2}^{in} = \frac{T_{H_2} \cdot \dot{m}_{H_2} \cdot \dot{C}p_{H_2} + T_{N_2} \cdot \dot{m}_{N_2} \cdot \dot{C}p_{N_2} + T_{H_2O} \cdot \dot{m}_{H_2O} \cdot \dot{C}p_{H_2O}}{\dot{m}_{H_2} \cdot \dot{C}p_{H_2} + \dot{m}_{N_2} \cdot \dot{C}p_{N_2} + \dot{m}_{H_2O} \cdot \dot{C}p_{H_2O}} \qquad (63)$$

Where T_i is the temperature of gas i in *K*, $\dot{m}_i$ the mass flow rate of gas i in *kg/s*, and Cp_i is the specific heat of each gas in the mixture in *kJ·(kg·K)⁻¹*. $T_{c,2}^{in}$ refers to the inlet temperature of the cold side of BPHE 2 (fuel-fuel heat exchanger).

The specific heat ($\dot{C}p$) of each individual gas is known, and the total $\dot{C}p$ of fuel mixture $\dot{C}p_{mix}$ is calculated based on the mass fraction of every gas in the fuel and T_{mix}, as follows:

$$\dot{C}p_{mix} = \sum \dot{C}p_i \cdot w_i \qquad (64)$$

Where $\dot{C}p_i$ is the specific heat at T_{mix} of each gas in the mixture in *kJ·(kg·K)⁻¹* and w_i is the mass fraction of each gas in the mixture (between 0 and 1).

On the other hand, at the exit of BPHE 1 (air-air heat exchanger), the bypass mass flow rate is mixed with the heat exchanger mass flow rate before entering the stack. As previously explained, the reason for the existence of the bypass is to allow cooling of the stack via convection of air mass flow when the thermodynamics balance requires it (SOFC mode). Thus, the final temperature of air is calculated as:

$$T_1^{final} = \frac{T_{c,1}^{out} \cdot \dot{m}_{air,HE} \cdot \dot{C}p_{air} + T_{amb} \cdot \dot{m}_{air,Bypass} \cdot \dot{C}p_{air}}{\dot{m}_{air,HE} \cdot \dot{C}p_{air} + \dot{m}_{air,Bypass} \cdot \dot{C}p_{air}} \qquad (65)$$

Where $T_{c,1}^{out}$ is the outlet temperature of the cold side of BPHE 1 (the heated air entering the stack), $\dot{m}_{air,x}$ is the mass flow rate of air either each channel, and T_{amb} is the ambient temperature of 293 *K*.
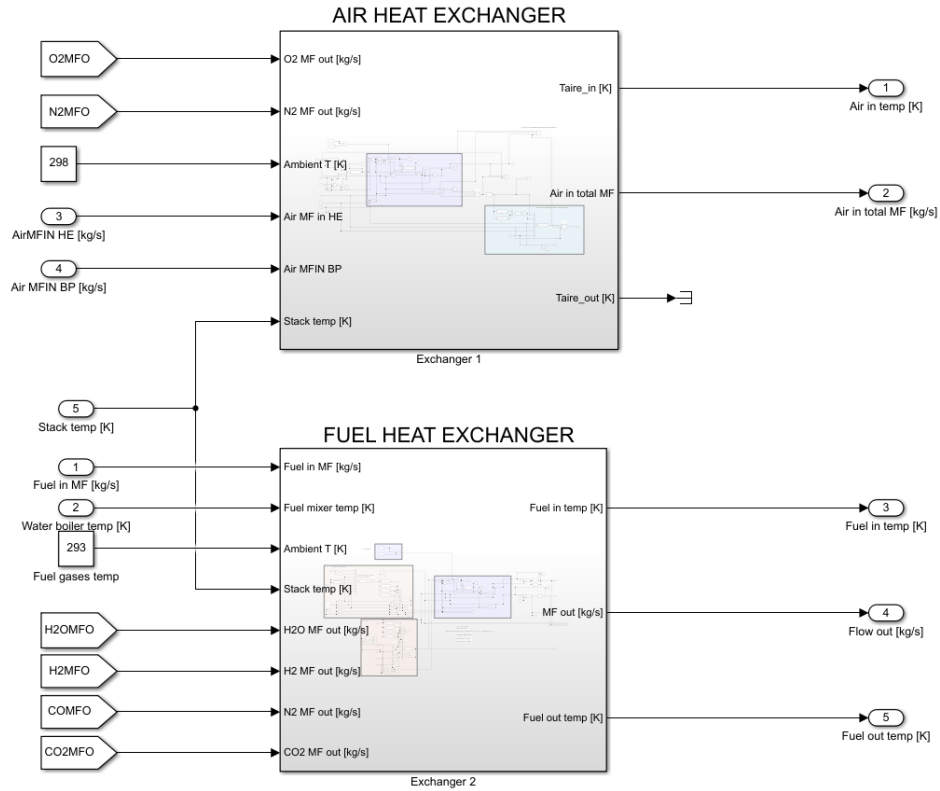
ETSEIB

Figure 53. Heat exchanger blocks

4.3.3.   Efficiency calculation

The global efficiency calculation is a very relevant aspect to the BOP. In either fuel cell or electrolyser operation modes, maximum efficiency is desired for all operating points, and the operating points with the highest efficiency are of notable interest. The general efficiency equation is:

$$\eta = \frac{P_{out}}{P_{in}} \qquad\qquad (66)$$

In SOFC operating mode, the output energy is simply the electrical power. In SOEC operating mode, the output energy is the generated hydrogen's heating power $\dot{Q}_{H_2}^{out}$, defined as its mass flow rate multiplicated by its high heating value (285,84 kJ·mol⁻¹). For each operating mode, SOFC and SOEC, the efficiency calculation will be different, since the output (useful) energy and input (consumed) energy is different, as shown:

$$\begin{cases} \eta_{SOFC}(i) = \dfrac{i \cdot V}{\dot{Q}_{H_2}^{in} - \dot{Q}_{H_2}^{out} + q_{boiler} + P_{oven}}, & i \geq 0 \\[3mm] \eta_{SOEC}(i) = \dfrac{\dot{Q}_{H_2}^{out} - \dot{Q}_{H_2}^{in}}{|i| \cdot V + q_{boiler} + P_{oven}}, & i < 0 \end{cases} \qquad (67)$$

Where i is the stack current in A, V is the stack voltage in V, $\dot{Q}_{H_2}^{in}$ is the heating power of the hydrogen sent into the stack, while $\dot{Q}_{H_2}^{out}$ is the heating power of H_2 exiting the stack, which is essentially the same as comparing the H_2 mass flow rate at the fuel inlet and outlet. In SOFC mode, when $\dot{m}_{H_2}^{out} < \dot{m}_{H_2}^{in}$ because H_2 is consumed in the reaction, the difference is in the denominator. In SOEC mode, when $\dot{m}_{H_2}^{out} > \dot{m}_{H_2}^{in}$ and the useful energy is the H_2 generated, it is on the numerator.

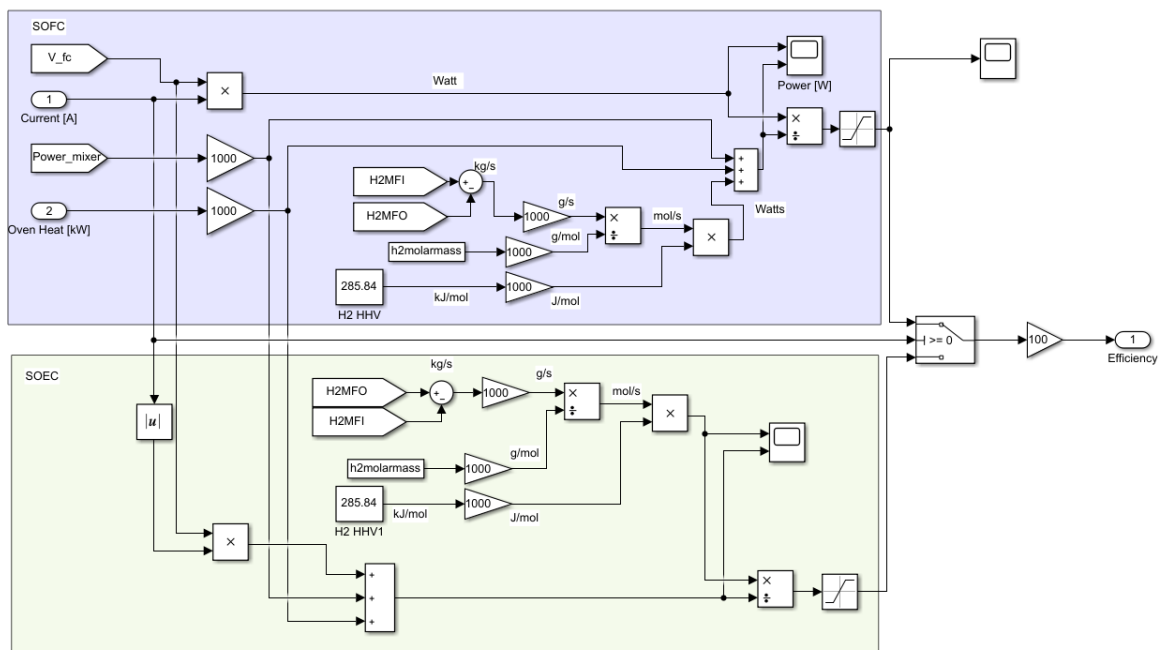The formula, to give a result closer to the one expected in the prototype, assumes hydrogen recirculation.

Figure 54. Efficiency calculation block

4.4. Reversible Solid Oxide Cell controllers

The model is not complete with the design of controllers to ensure the correct and efficient performance of the RSOC. There are two main aspects that are critical to the operation of a RSOC: gas mass flow rates (hence its partial pressures) and temperature. The control system must adapt to different current profiles and operating conditions. For this reason, the following controllers were designed:

- Air Mass Flow Rate and Bypass Refrigeration Controller
- Fuel Mass Flow Rate Controller
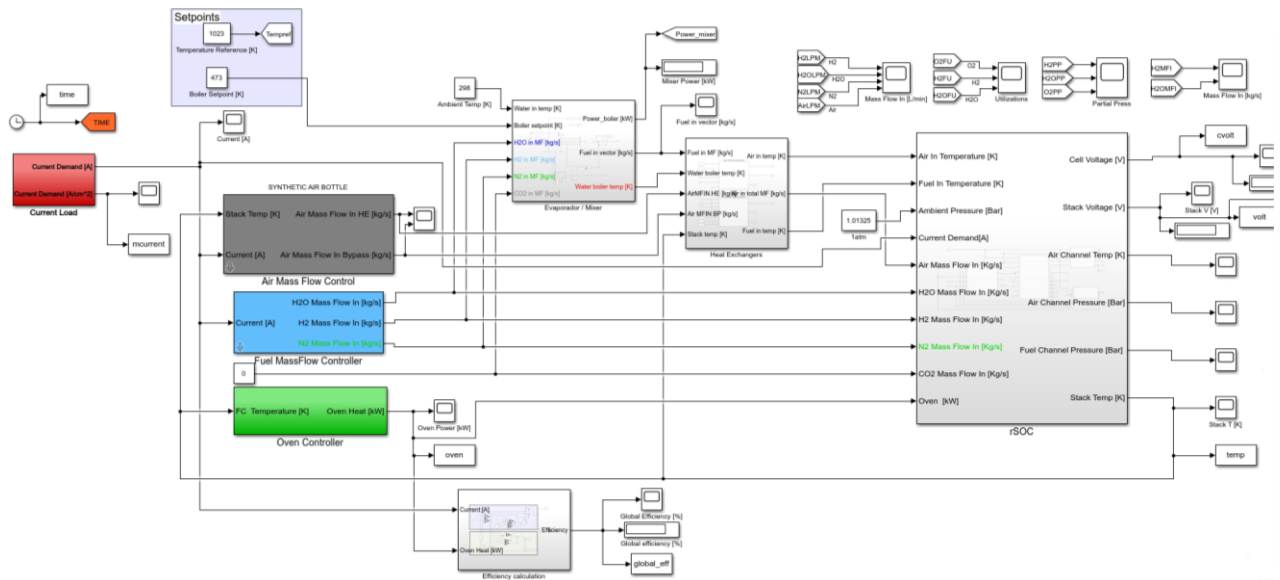- Oven Power Controller

Figure 55. Full RSOC and Controllers Model in Simulink

4.4.1. Air Mass Flow Rate and Bypass Refrigeration Controller

This controller is responsible of controlling the air mass flow rate entering the RSOC stack, and it has two parts. Firstly, it controls the total mass flow of air that must enter the stack at a given point (Air Mass Flow Rate Control). Secondly, it controls how much air must go through the heat exchanger, and how much must go through the bypass (Refrigeration Control).
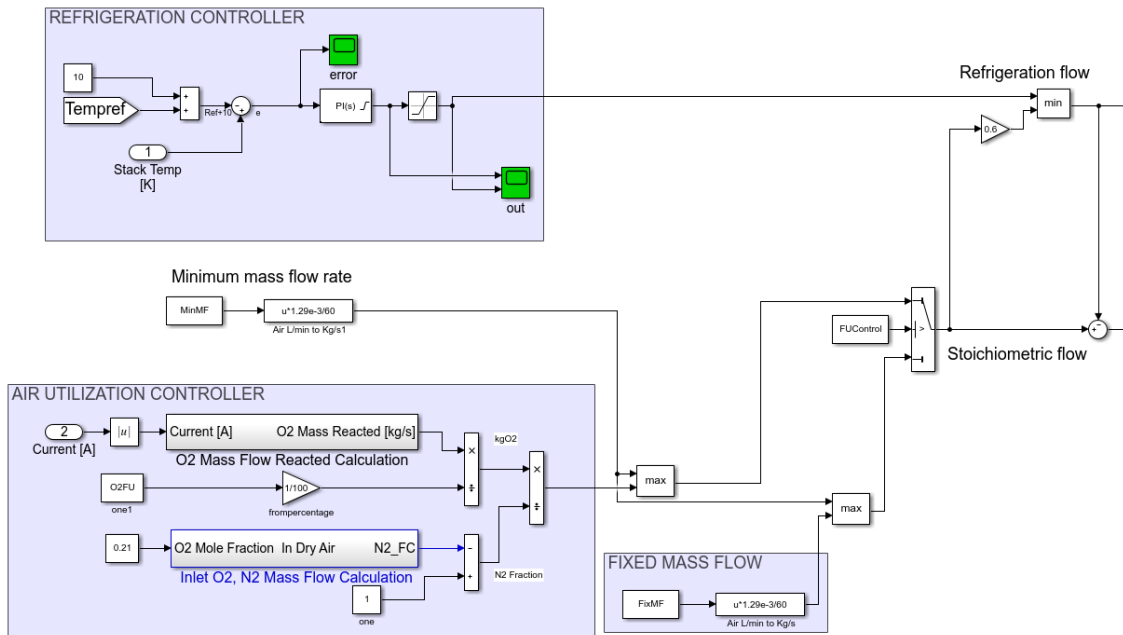

Figure 56. Air Mass Flow Controller block

4.4.1.1. Air Mass Flow Rate Control

The total mass flow of air that enters the stack has two possible configurations that the user can choose from. In both cases, the minimum air mass flow must be defined, and will be sent if the controller setpoint is lower. To make it easier for the user to define the controller mode and its setpoints, the user interface in Figure 57 is programmed. The full controller block can be seen in Figure 56. It has two outputs:

- Air mass flow rate in Bypass in $kg \cdot s^{-1}$
- Air mass flow rate in Heat Exchanger in $kg \cdot s^{-1}$

And two operating modes, ruled by the switch block "FUControl" seen in Figure 56.

- **Fixed mass flow rate mode**

Setting a constant flow rate for the full duration of the current profile is possible. This is useful, for example, when simulating sweep experiments, or when working on SOEC mode.

- **Oxygen utilization mode**

In the same fashion as fuel utilization explained in section 2.4.2, in SOFC mode oxygen is also consumed, and its utilization can be calculated. The feed-forward controller, when operating in this mode, calculates the reacted oxygen as per Equations (44) and (45), and then the total oxygen to satisfy the utilization set by the user and then sends the total air mass flow ($O_2 + N_2$) required.
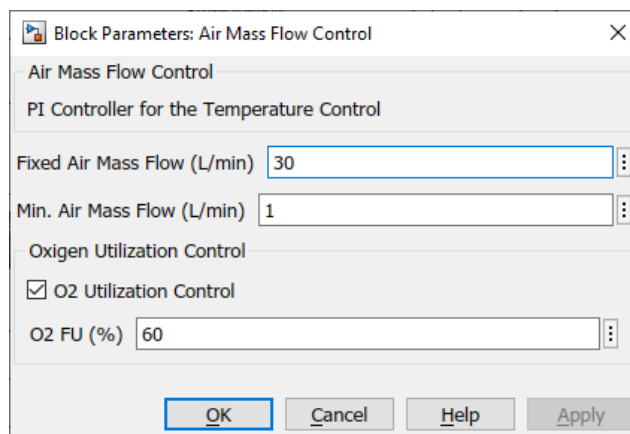
Figure 57. Air Mass Flow Controller configuration

4.4.1.2. Bypass Refrigeration Control

Temperature control is achieved by using two different PI controllers: the bypass refrigeration control and the oven heating control. They are independent of each other, so a solution to avoid opposing control actions had to be proposed. This was discussed with other HyBCN project members, since it is necessary to refrigerate the prototype that will be constructed.

Because the oven controller will work independently and will not communicate with the refrigeration controller, an important goal was to avoid both opposite controller actions happening at the same time, wasting energy. For this reason, the refrigeration controller follows a setpoint of *Reference Temperature + 10* as seen in Figure 55. The simulation of this controller action is shown in Figure 62, and an increase in the convection losses resulting from this control action can be seen in Figure 75.

In practice, this 10ºC hysteresis is not very meaningful for a RSOC station, and it simplified the construction and control loop definition enough to be justified. The values of the PI controller are kp = 8,472e-05 and ki = 2,68e-07. The controller will also never send over 60% of the total air mass flow to the bypass. This is because a minimum temperature of approximately 300ºC is needed for security, to avoid subjecting the RSOC stack to important thermal gradients, and therefore material stress. An example of refrigeration in SOFC mode for a current profile with 5A steps from 0A to 20A can be seen in Figure 70. There, refrigeration is required on the highest current operating points because the reaction heat is substantial enough to not be compensated by convection and ambient heat losses. When refrigerating, oven power is always 0 kW, as seen in Figure 74.

4.4.2. Fuel Mass Flow Rate Controller

It is important for this block to have different configurable options for fuel composition and mass flow rate, as it must be able to replicate the gas configurations used in all experiments for later comparison. It has three outputs:

- H_2 mass flow rate in *$kg \cdot s^{-1}$*
- H_2O mass flow rate in *$kg \cdot s^{-1}$*
- N_2 mass flow rate in *$kg \cdot s^{-1}$*

Like the Air Mass Flow Controller, it has two modes to be chosen for operation, ruled by a switch block:

- **Fixed mass flow rate mode**

The user can directly choose constant H_2 and H_2O mass flow rates, which will be the same for the whole simulation. This is useful for comparison with current sweep experiments which were performed with these conditions.

ETSEIB

- **Fuel utilization mode**

This feed-forward controller calculates the reacted gas mass flow based on the current input and based on the utilization setting chosen by the user, determines the needed fuel mass flow. In SOFC operating mode (positive current values), the reacting fuel is H_2 and, in SOEC operating mode (negative current values), the reacting fuel is H_2O.

Additionally, the fuel composition can be chosen (0 to 1) with $FC_{H2}+FC_{H2O} = 1$ at any given time. The needed calculations for this mode are done in the block shown in Figure 58.
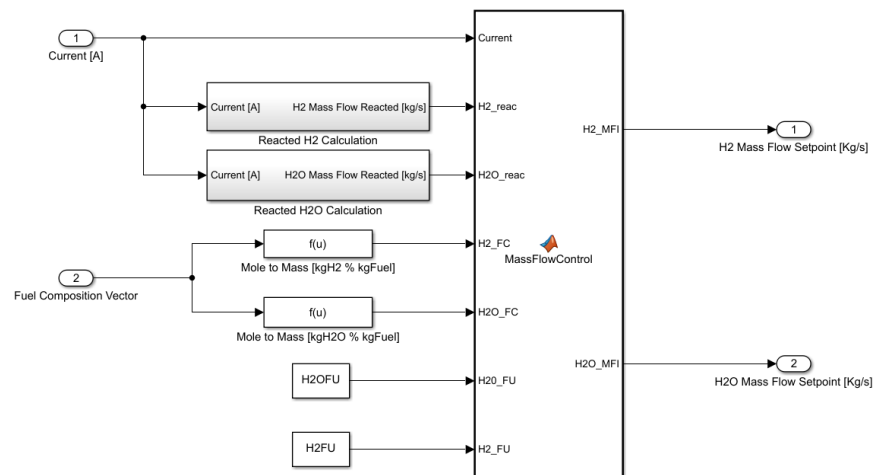

Figure 58. Fuel Utilization calculation block

To make it easier for the user to define the controller mode and its setpoints, the user interface in Figure 59 is programmed.
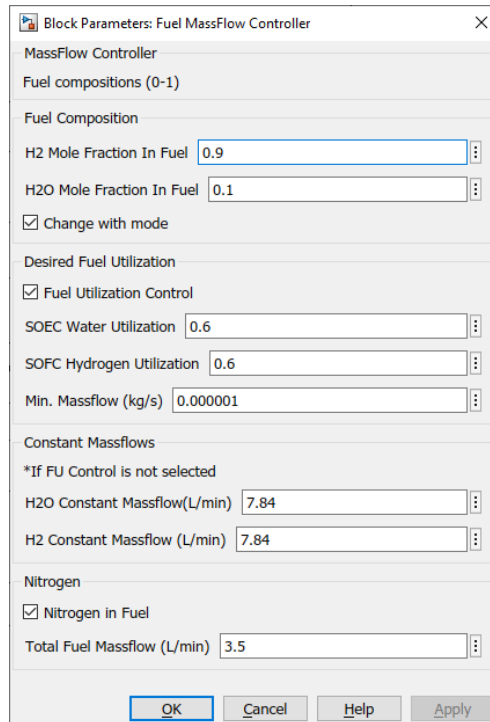

Figure 59. Fuel Mass Flow Controller configuration

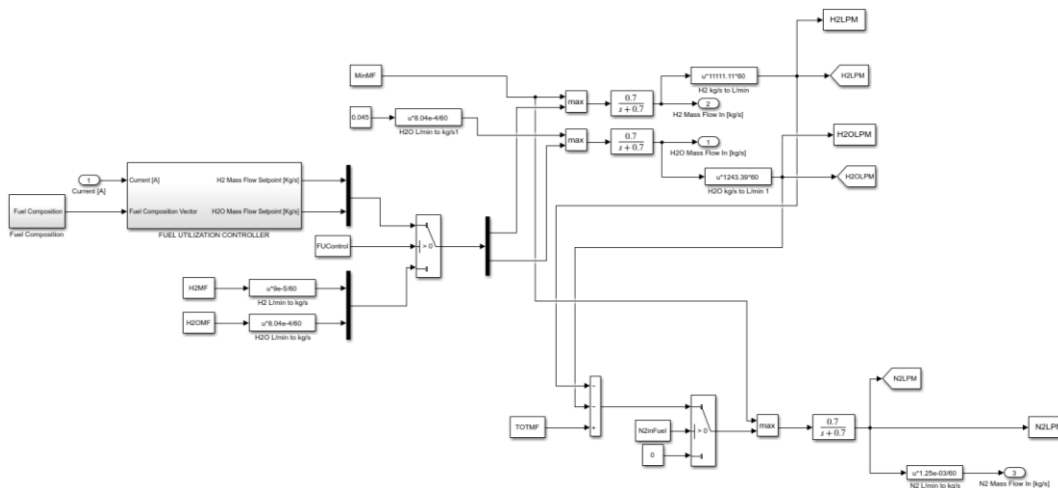And Figure 60 shows the general view of the controller block:

Figure 60. Fuel Mass Flow Controller block

4.4.3.   Oven Controller

In most operating points of the RSOC, heating will be required due to the heat losses to the environment and the convection losses from gas mass flow rates. The only exceptions to this statement are currents high enough in SOFC mode to produce enough reaction heat to compensate all the other heat losses.

As previously mentioned, the oven controller operates independently from the refrigeration controller, and only follows the temperature setpoint indicated by the user. Therefore, its control loop is simple, and the controller is a PI with the constants kp = 0,2 and ki = 0,001. The maximum power the oven can deliver is 2,75 kW, as described in the equipment section. Its implementation in Simulink is shown in Figure 61.
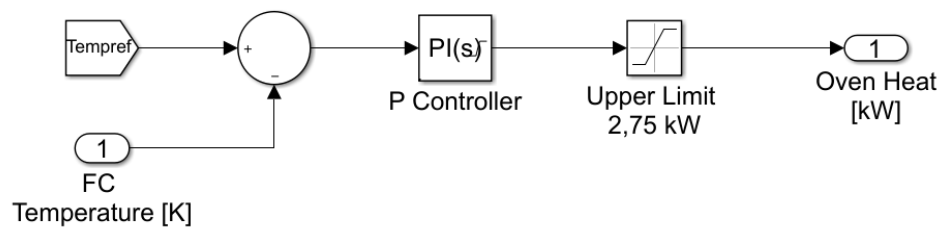

Figure 61. Oven Controller block

Figure 62 shows a simulation in both SOFC and SOEC operating modes. The oven and refrigeration perform the control of the stack temperature, allowing the 10ºC hysteresis when refrigeration is required. Additionally, the oven power and convection losses can be seen in Figure 75, alongside all the other elements affecting the thermal balance.
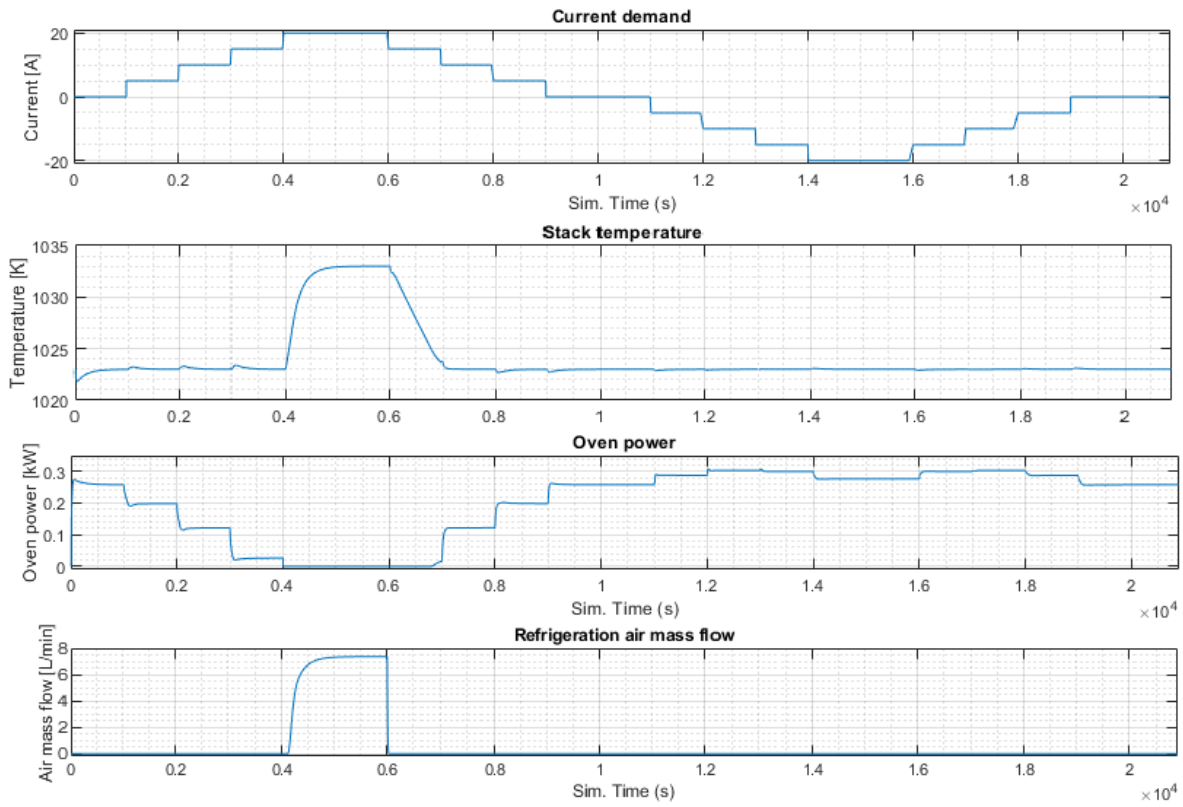
Figure 62. Temperature control in the Simulink RSOC model

5. Parameter estimation

Although the model includes all empirical and semi-empirical equations necessary to represent the real system in a simulation, in the old Simulink model some parameters remained unknown, and without the availability of experimental data, were taken from the literature. In this section, an attempt was made at comparing experimental data to simulation results, estimating the chosen model parameters.

Optimization is the mathematical selection of a best element, regarding to some criterion, from a set of available alternatives. Estimation theory is a branch of statistics that deals with estimating the values of parameters based on measured empirical data that has a random component. This section aims to use the experimental data obtained to estimate a series of parameters so the model can more accurately represent the real RSOC. Because the RSOC was observed to degrade rapidly, this work only contemplates experimental data from the first four days of operation.

To check for significant stack degradation, two current sweeps with the same operating conditions were performed every day (morning and evening). Figure 63 shows that on the afternoon of February 23rd and morning of February 24th the RSOC performed notably worse than average due to some currently unknown issue. This is most likely related to mechanical stress and cracking of materials. An image of a 30-cell RSOC stack with broken cells that was retrieved from the experimental station can be seen in Figure 64. This is not the stack that the experiments mentioned in this work were performed with.
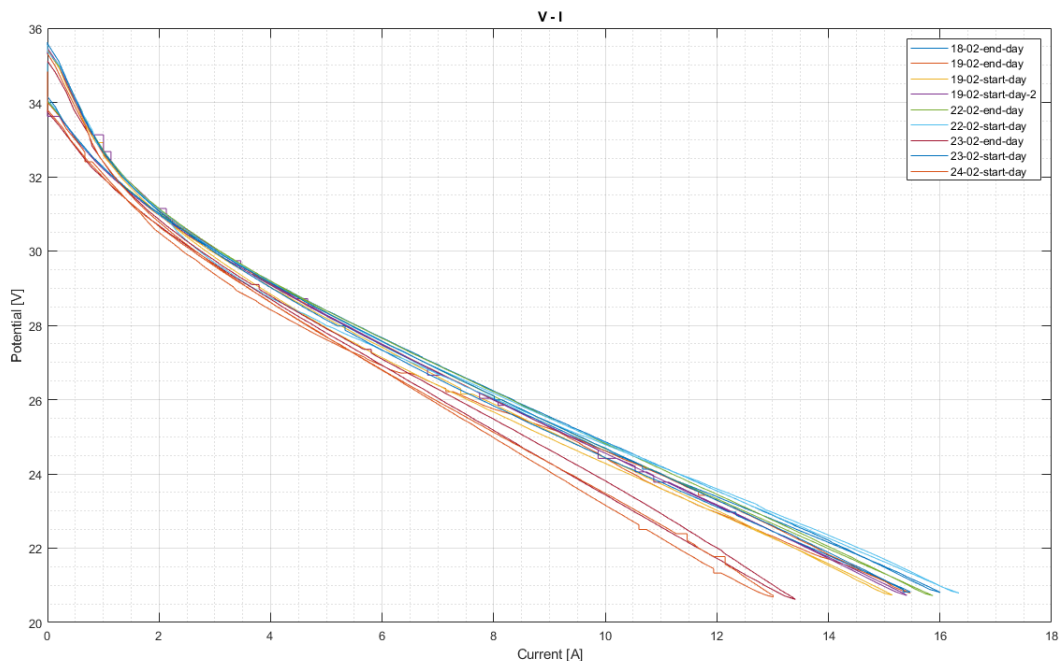

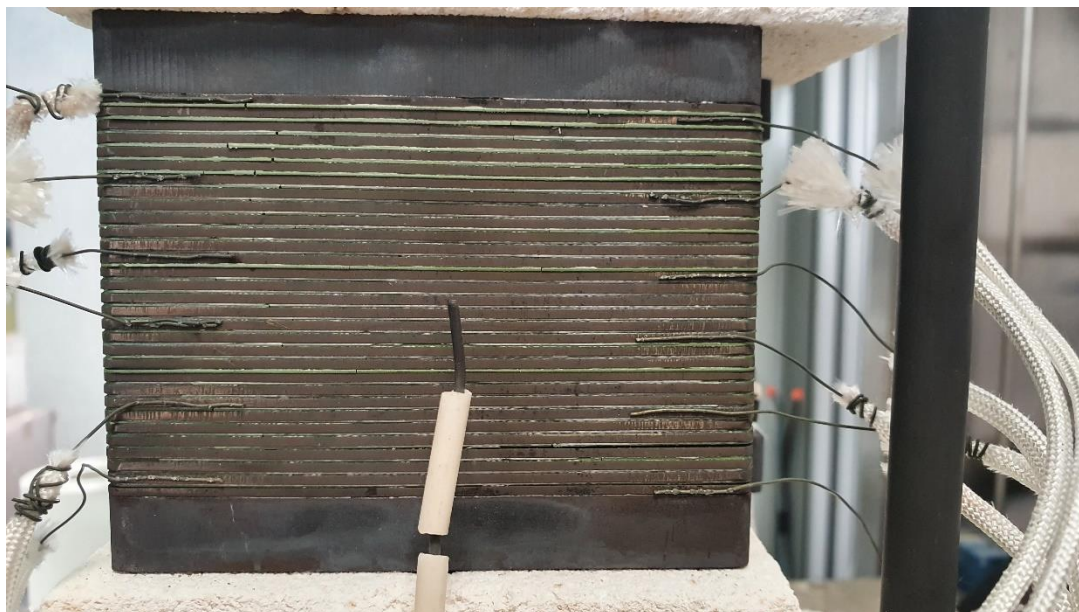*Figure 63. Current sweep "degradation control" experiments*

Figure 64. RSOC stack showing broken cell interconnects, a sign of degradation. Cables on individual cells were used to obtain additional voltage data.

In later works, all experimental data will be considered and the establishment of a relation between RSOC parameters and observed degradation will be attempted, but it is outside the scope of this work. The experiments performed between February 18th and February 23rd are shown in Table 7-8.

5.1. Problem formulation

The goal of optimization is to minimise or maximise an objective function. Since temperature remained practically constant during the studied experiments, it was decided to only compare experimental and simulated stack voltage, assuming a constant temperature throughout the experiment. The real system presents a certain hysteresis between the stack voltage when increasing current (e.g., from 0 *A* to 15 *A*) versus decreasing current (e.g., from 15 *A* to 0 *A*), but the zero-dimension model developed is not able to represent this phenomenon. For this reason, only the increasing current values were considered in the objective function, which is the following:

$$RMSE = \sqrt{\frac{\sum_{n=1}^{N}(\hat{v}_n - v_n)^2}{N}}$$

(68)

Where $RMSE$ is the Root Mean Square Error, $\hat{v}_n$ is the estimated voltage for a certain current setpoint I_n, v_n is the experimental voltage for a certain current setpoint I_n, and N is the total number of current points studied.

5.1.1. Parameters

The parameters estimated will modify the activation, ohmic and concentration polarizations, fitting the Current-Voltage curve to the experimental data. The parameters chosen are the following:

Parameter	Description	Equation	Old Value	Units
γ_A	Phenomenological coefficient (Anode)	(16)	600000	$A·cm^{-2}$
γ_C	Phenomenological coefficient (Cathode)	(17)	415500	$A·cm^{-2}$
ASR	Area-Specific Resistance	(25)	0,165	$\Omega·cm^2$
τ_A	Anode tortuosity	(34)	8,76	-
τ_C	Cathode tortuosity	(34)	13,47	-

Where old values are taken from the starting point of the model, explained in [15].

5.1.2. Particle Swarm Optimization

Particle swarm optimization (PSO) is a population-based optimization technique inspired by the motion of bird flocks and schooling fish. It is based on a simple mathematical model, developed by Kennedy and Eberhart in 1995. PSO shares many similarities with evolutionary computation techniques. The system is initialized with a population of random solutions (called "particles"), and the search for the optimal solution is performed by updating generations [36]. Each particle's movement is influenced by its local best known position but is also guided toward the best known positions in the search-space, which are updated as better positions are found by other particles[37]. This is expected to move the swarm toward the best solutions, and particles having a certain inertia that is reduced with each iteration, making it easier to converge on the best solution.

The programmed optimization algorithm initialized 30 particles (sets of 5 parameters) and distributed them in the search space between the upper and lower boundaries using the MATLAB function *unifrnd()*, also giving them a random initial velocity. Their objective function cost was analysed, and the local and global best positions were updated. Then, the particles moved iteratively according to the PSO algorithm, updating their cost every iteration, until they converge to a global solution. In Figure 65, it can be seen how a particle's current velocity,

personal best position and global best position influence its velocity vector calculation on a new iteration. The code used for this optimization can be found in Annex 3.

In order to evaluate the model at steady-state in each current point, the MATLAB function *trim()* is used, which returns the steady-state voltage output given a current input. Then, these voltage output values are evaluated in objective function (68).
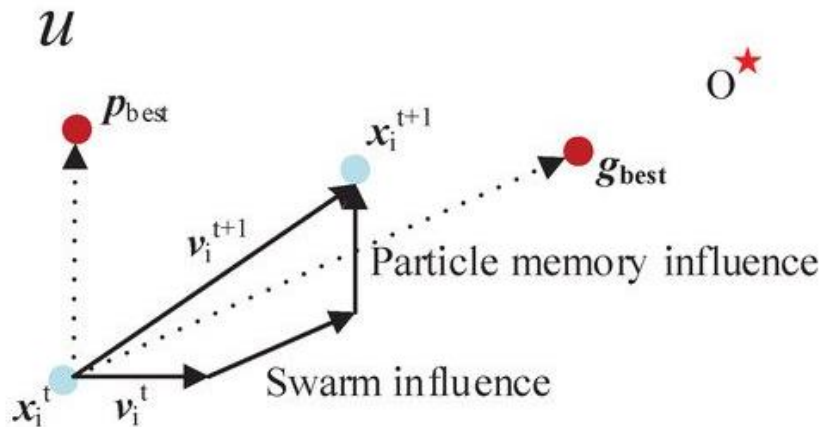
Figure 65. Example of particle velocity calculation in PSO algorithm [38]

5.2. Steady state estimation results

Steady-state estimation refers to the comparison of exclusively stationary operating points. This means a polarization curve with 10 steps will only compare 10 voltage values to the simulated values, for the same current inputs as the experiment. These voltage values were taken from the seconds before the next step, when the operating point was stable, and the voltage was constant. The experiments typically waited 3 minutes between current steps.

Experiments considered in this estimation are experiments 1-3 of Table 7 and experiments 1-3 of Table 8. They were all performed at 750ºC and in the early days of operation before degradation affected stack performance considerably. They are again listed below:

Exp. Number	Current: (Max A)- Pol. Curve (# steps, 1-2 ways)	Hydrogen: FU (%) Flux (L·min^{-1})	Air: FU (%) (L·min^{-1})	Water anode: Molar fraction (%)	Nitrogen anode: flux (L·min^{-1})	Temp. (ºC)	Date
Exp. 1 SOFC	p.curve (18A, 12, 2-w)	60%	60%	0%	Variable QTotal = 3	750	19/02
Exp. 2 SOFC	p.curve (18A, 12, 2-w)	80%	60%	0%	Variable QTotal = 3	750	19/02
Exp. 3 SOFC	p.curve (20A, 13, 2-w)	40%	60%	0%	Variable QTotal = 3	750	23/02

Exp. Number	Current: (Max A)- Pol. Curve (# steps, 1-2 ways)	Water Vapor: RU (%)- flux (L·min^{-1})	Air flux (L·min^{-1})	Hydrogen in anode (molar fraction %)	Nitrogen anode: flux (L·min^{-1})	Temp. (ºC)	Date
Exp. 1 SOEC	p.curve (24A, 12, 2-w)	RU=60	10	10%	Variable QTotal=3,5	750	22/02
Exp. 2 SOEC	p.curve (24A, 12, 2-w)	RU=80	10	10%	Constant 3	750	22/02
Exp. 3 SOEC	p.curve (24A, 12, 2-w)	RU=40	10	10%	Constant 3	750	23/02

5.2.1.   Area Specific Resistance (ASR) determination

Impedance spectroscopy, the usual method to determine electrical resistance in cells, was not available, so it was not possible to determine ASR before starting parameter estimation, and it remained an unknown parameter. It was decided that the first step was to analyse the two experiments at 40% Fuel Utilization in SOFC and SOEC modes (Experiment 3 in Table 7 and Experiment 3 in Table 8). Ohmic polarization is widely accepted as dominant in the linear range of the Current-Voltage graph because it is also a linear loss directly related to current density. Therefore, only the voltage outputs between 5 A and 18 A were considered.

Two optimizations were made for each experiment, to ensure the ASR value fell in similar ranges, and the final ASR value for the stack operating at 750ºC was established as the mean of the 4 obtained values.

Experiment	Mode	ASR
Experiment 3	SOFC	0,7149
Experiment 3	SOFC	0,7420
Experiment 3	SOEC	0,7456
Experiment 3	SOEC	0,6983
MEAN	**Both**	**0,7252**

Table 17. ASR determination

As seen in Table 17, the estimated ASR value at 750ºC for the characterised stack is 0.7252 $\Omega \cdot cm^2$.

5.2.2. Other parameters estimation

After determining the ASR value, it was set to its estimated value and unchanged because all experiments studied were performed at 750ºC. The PSO algorithm was then used to estimate the remaining four parameters: γ_A, γ_C, τ_A, τ_C.

- **SOFC experiments parameter estimation**

First, experiments 1-3 in Table 7 were considered at the same time, with the intention of estimating a set of parameters in SOFC mode for different operating conditions (60%, 80% and 40% fuel utilization, respectively). The algorithm was slow because it had to compile and simulate the steady-state voltage for every current point in every set of parameters. For an experiment with 18 current points and 30 particles (sets of parameters), it would have to simulate the model 540 times just to finish one iteration. For this reason, it was decided to do only 10 iterations but to run the optimization algorithm multiple times and assess the results. From four optimizations, the following results were obtained:

ETSEIB

Optimization	γ_A	γ_C	τ_A	τ_C	Cost
#1	$10^{6,253}$	$10^{8,304}$	3,095	4,977	0,4353
#2	$10^{6,270}$	$10^{8,570}$	6,185	5,027	0,4353
#3	$10^{6,243}$	$10^{7,666}$	4,886	4,786	0,4356
#4	$10^{6,263}$	10^{9}	1	5,180	0,4351

Table 18. Parameters estimated from SOFC Pol. Curve experiments

In Figure 66, the simulated voltage approximates the experimental results for the same set of parameters (from Optimization #1). It is not a perfect approximation, but it was found in the literature that it is typically difficult to simulate different operating conditions reliably with the same set of parameters. Still, it gives reasonably good results, and it can be improved with more data and optimization efforts in later works.
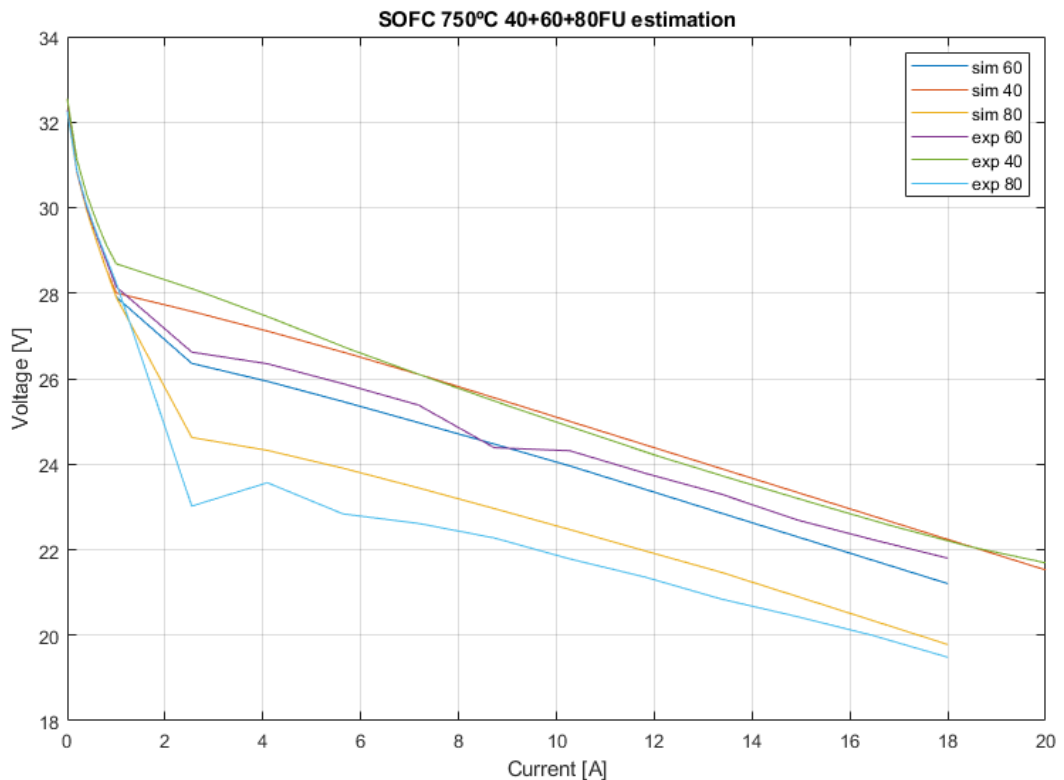

Figure 66. Experimental vs. Simulated Current-Voltage graph for SOFC experiments

- **SOFC + SOEC experiments parameter estimation**

    Like the previous case, the remaining four parameters were estimated but this time all six studied experiments were considered in the objective function. Three optimizations are shown, that resulted in the lowest cost:

Optimization	γ_A	γ_C	τ_A	τ_C	Cost
#1	$10^{6,347}$	$10^{6,740}$	6,799	12,085	0,5540
#2	$10^{6,349}$	$10^{6,968}$	5,168	12,065	0,5541
#3	$10^{6,341}$	$10^{6,726}$	7,357	12,005	0,5541

Table 19. Parameters estimated from SOFC+SOEC Pol. Curve experiments

    The three optimizations resulted in similar parameters, so it is possible to conclude that a global minimum was reached. It can be seen in Figure 67 that there is almost no difference in experimental voltage for SOEC mode between 40% utilization and 60% utilization. This is impossible for the model to reproduce, so a big part of the error comes from that phenomenon. In this case, the SOFC simulated voltage was closer to the experimental values for 80% FU, but worse for 60%, where the simulated curve is slightly below the experimental result. Therefore, it can be concluded that this estimation was relatively successful, as it can represent the different operational voltages in the characterised stack. In the future, more data will be considered, and new estimation methods will be tested.
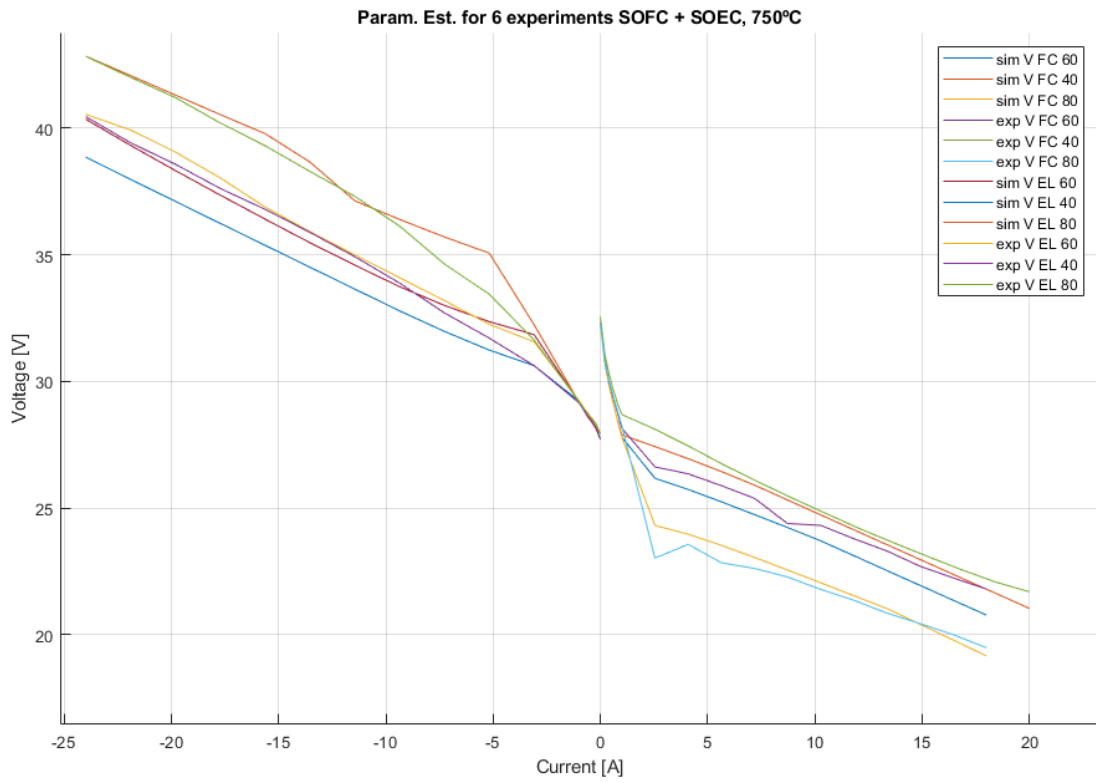
Figure 67. Experimental vs. Simulated Current-Voltage graph for SOFC+SOEC experiments

5.3. Simulation results

Even though the estimated parameters results roughly fit the small set of experimental data studied, the results are much closer to experimental data with the current version of the model than with the initial version, presented in the previous work [15]. As seen in Figure 68, a full simulation of a polarization curve with 60% Fuel Utilization round-trip from 0 A to 20 A in SOFC mode, and from 0 A to -20 A in SOEC mode was performed, and all the resulting relevant simulated data is presented here.
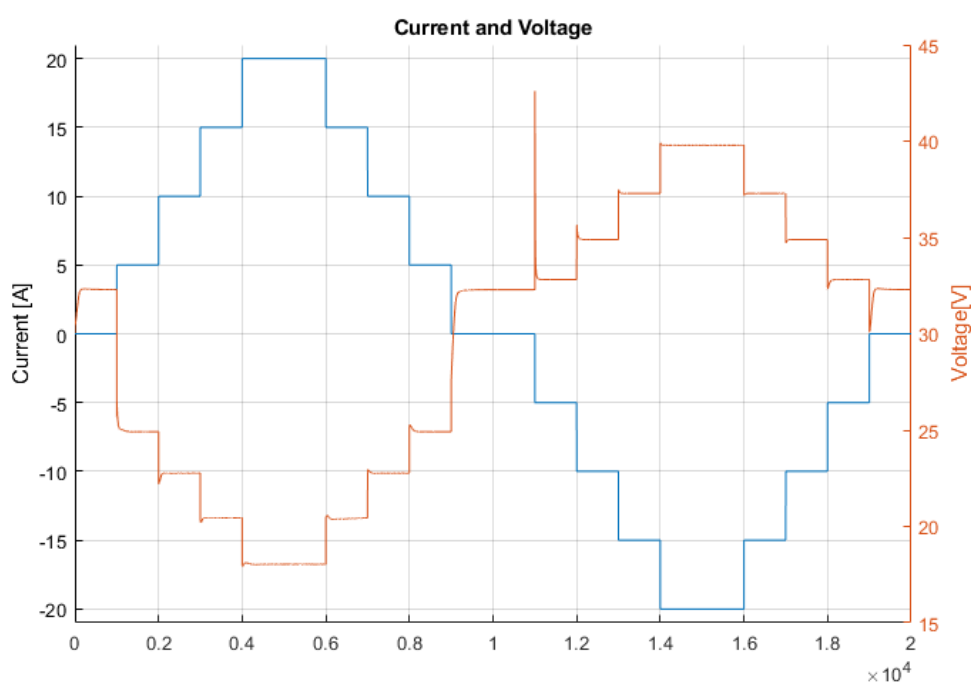

Figure 68. Current and voltage graphs against time

The mass flow rates, according to 60% Fuel Utilization in both modes and an air utilization of 60% for SOFC (irrelevant for SOEC) are shown in Figure 69.
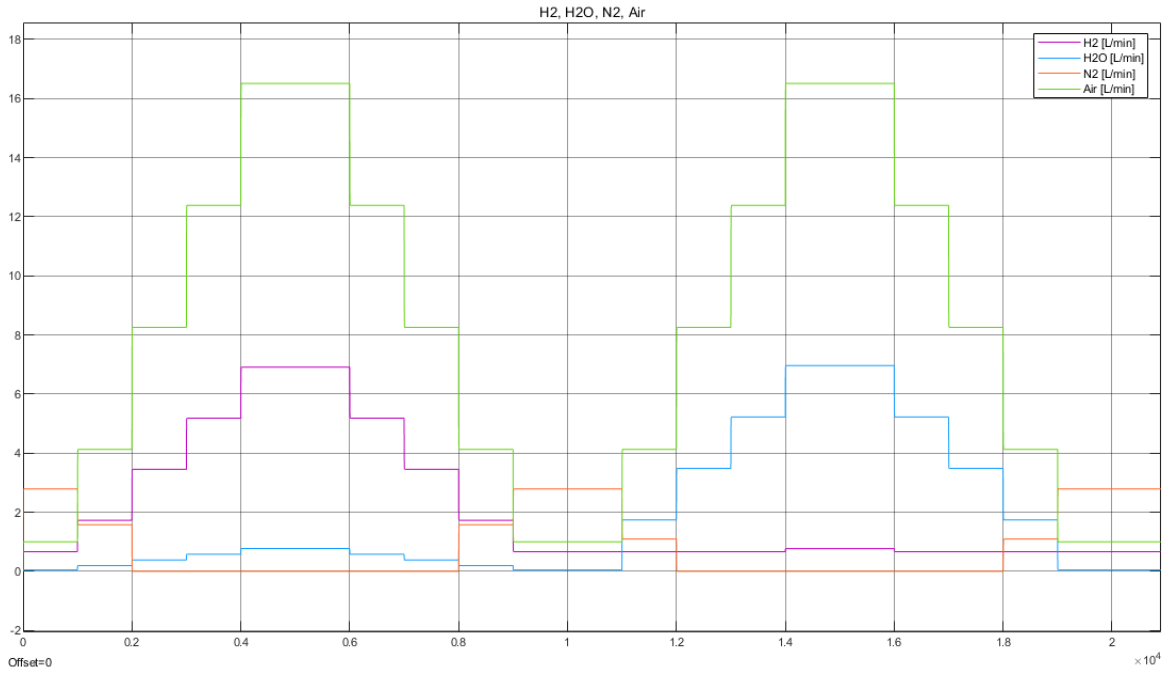
Figure 69. Total gas mass flow rates

The refrigeration control is responsible of choosing the amount air mass flow that is sent through the bypass, mixing later with the remaining air that passed through the heat exchanger. It only performs an action when the exothermic reaction in SOFC mode is large enough.
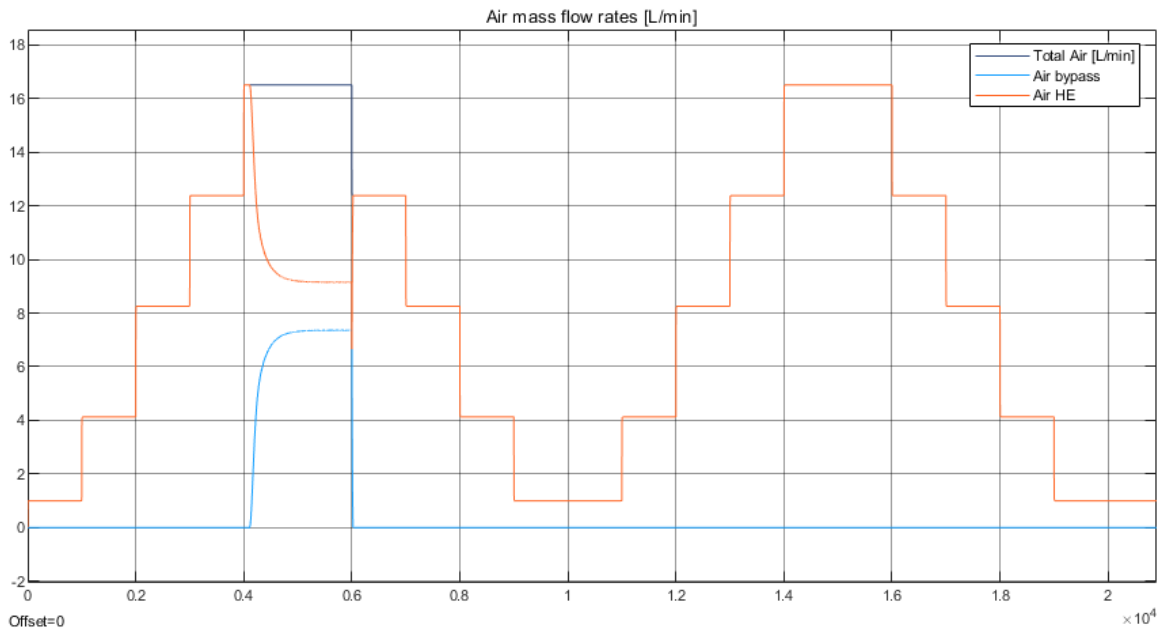

Figure 70. Air mass flow rates in L·min^{-1}

The gas temperatures in the air heat exchanger are shown in Figure 71. When the air bypass is active, the cold side exit temperature drops to cool down the stack by convection.
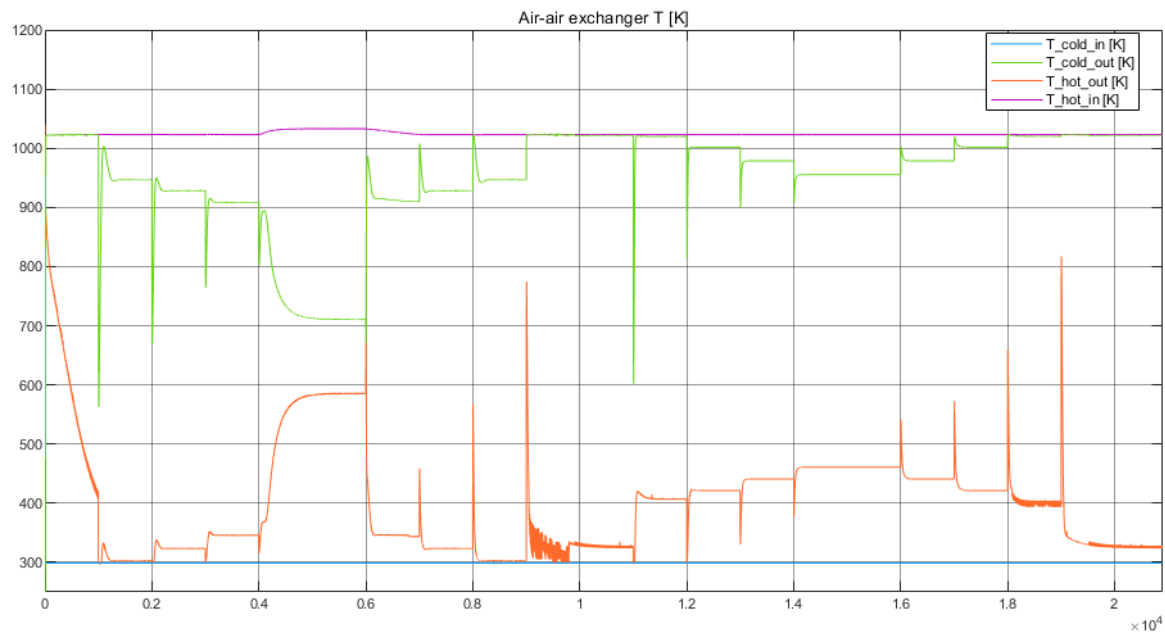

Figure 71. Air-air heat exchanger temperatures

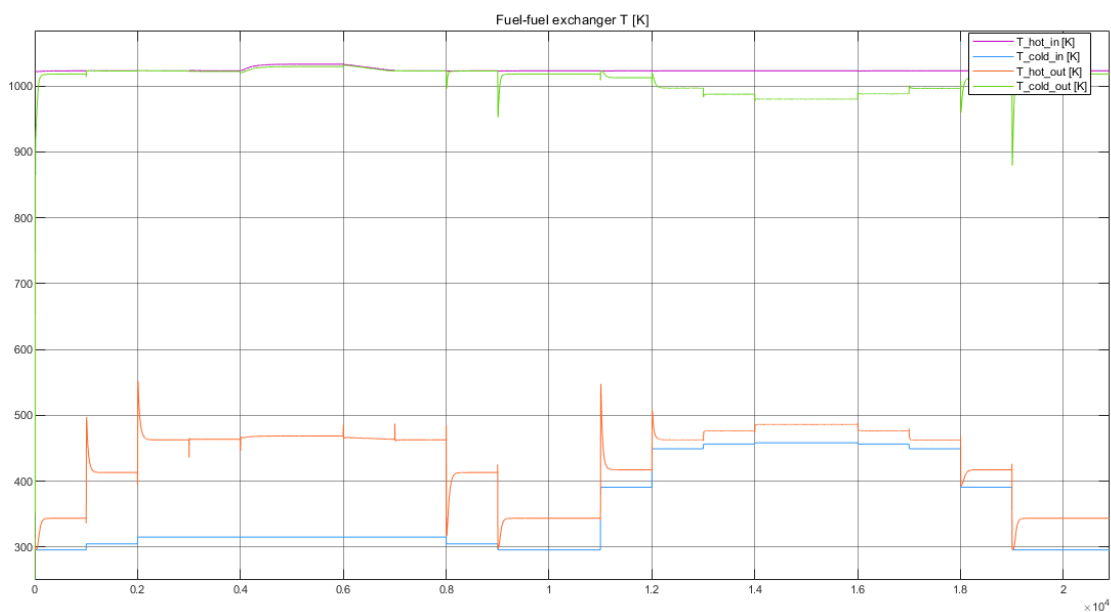The gas temperatures in the fuel heat exchanger are shown in Figure 72.

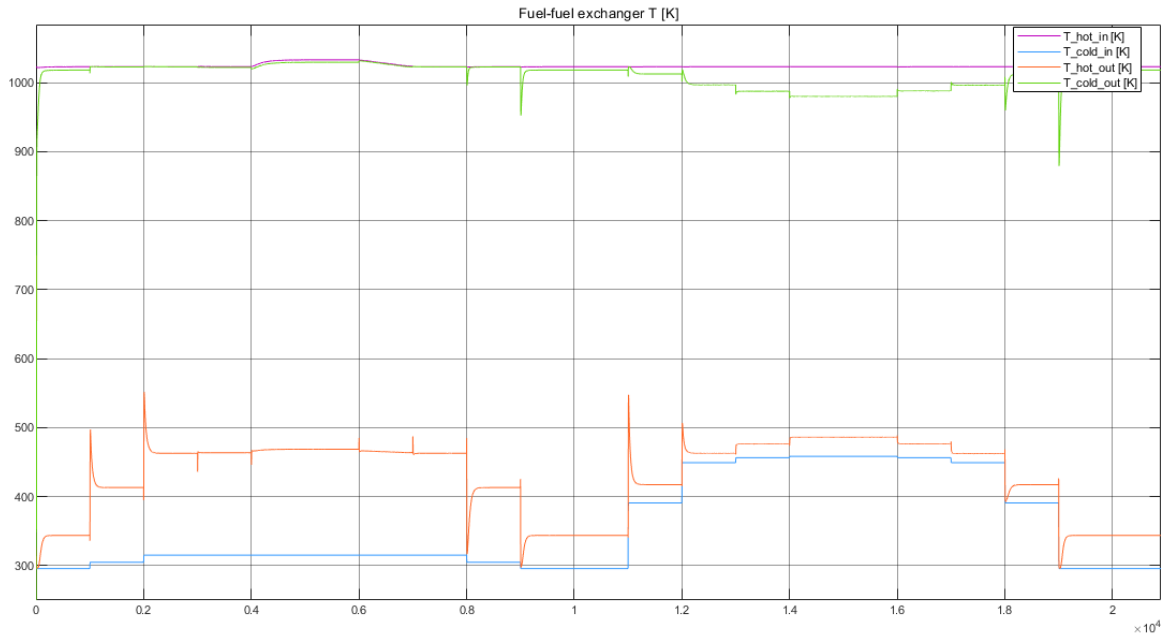*Figure 72. Fuel-fuel heat exchanger temperatures*

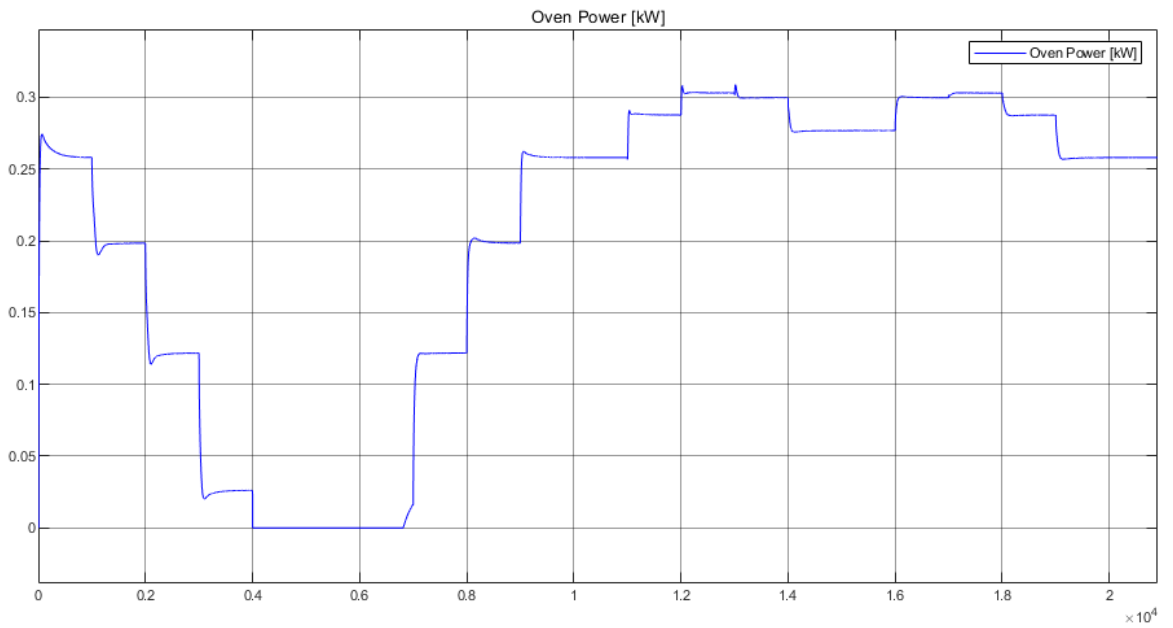*Figure 73. Fuel-fuel heat exchanger temperatures*

Figure 74. Oven power

An example of the heat balance resulting from the simulation is shown in Figure 75 the left half being a round-trip polarization curve in SOFC mode where the current goes from 0 A to 20 A and back, and the right half is operating in SOEC mode with the same current profile. The difference in gas convection losses and reaction heat can between both modes can be appreciated, which results in a much lower oven power required for SOFC mode in high currents.

In the left half, while the stack is working in fuel cell mode, it can be seen how the oven can be turned off during operation at high currents, since the reaction heat reaches values that compensate the losses. In fact, refrigeration is required for the stack to keep operating at the same temperature, and it is done by bypassing the heat exchangers to reduce the entrance temperature of air mass flow, as explained in more detail in section 4.4.1.

Meanwhile, the oven must work at higher power during electrolyser operation mode, since it must compensate the endothermic reaction, convection losses and losses to the environment.
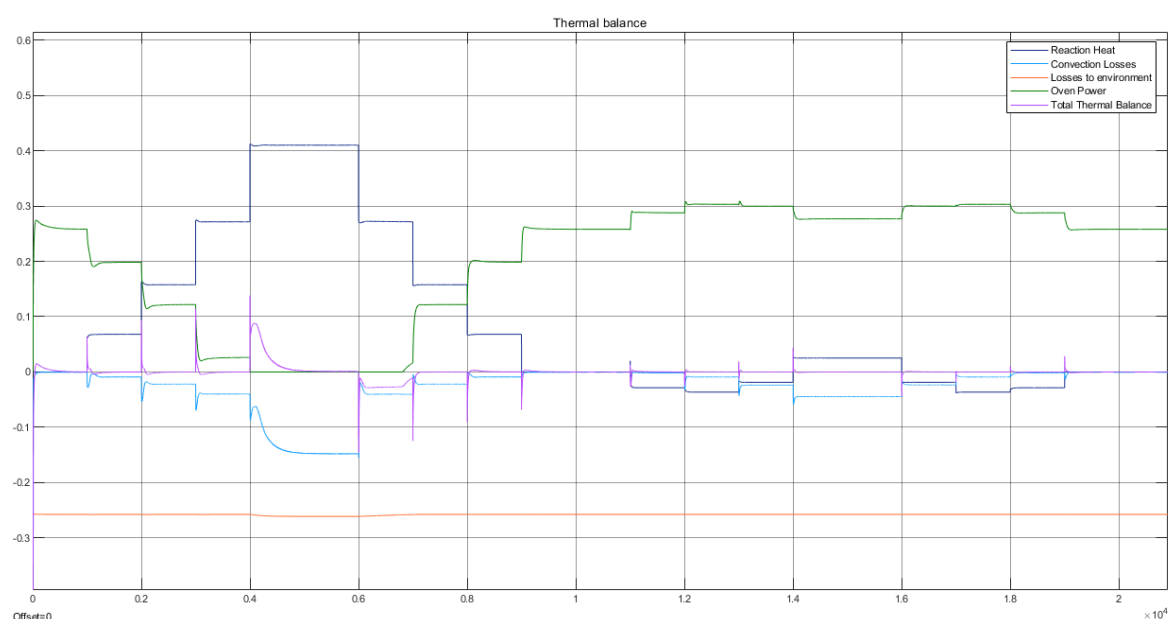
Figure 75. Thermal balance

And the resulting stack temperature is shown in Figure 76. As previously explained, the refrigeration setpoint is 10 K higher than the oven setpoint to avoid both control actions happening at the same time.
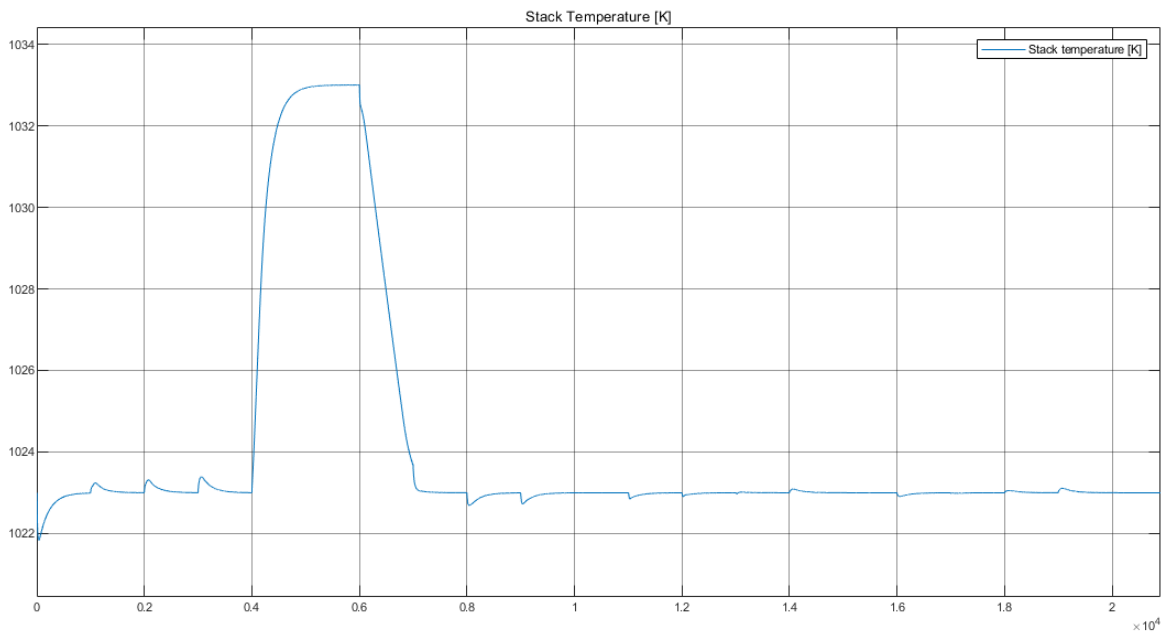
Figure 76. Stack temperature

The global efficiency is calculated, and it can be seen that in SOFC mode the best values are between 40 and 50% while in SOEC mode the efficiency is close to 70%.
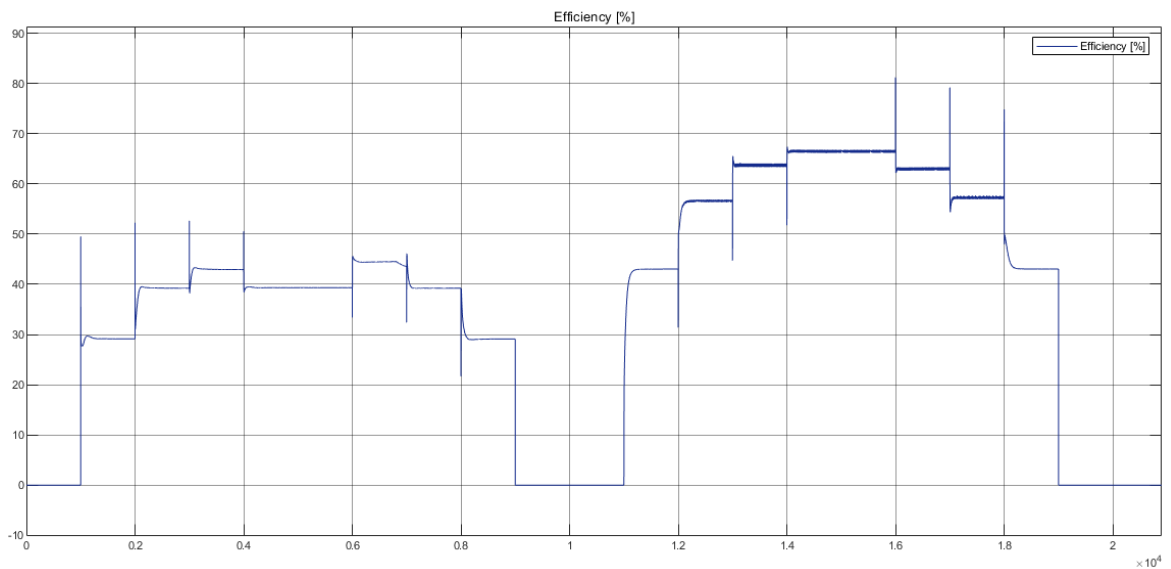
Figure 77. Global efficiency

6. Budget

The budget for the materialization of this work includes working hours, material provided by IRI or specifically acquired for this project, and necessary program licenses.

Concept	Unit Price	Units	Total Price
Engineer salary	15,00	900 hours	13500,00 €
LabVIEW License	433,00	1 u	433,00 €
MATLAB License	800,00	1 u	800,00 €
RSOC Stack	700,00	2 u	1400,00 €
Personal Computer	850,00	1 u	850,00 €
NI cRIO 9035	4295,00	1 u	4295,00 €
NI-9206	1627,00	1 u	1627,00 €
NI-9211	475,00	2 u	950,00 €
NI-9870	700,00	1 u	700,00 €
NI-9221	757,00	1 u	757,00 €
RS232 to RJ45 cable	20,00	1 u	20,00 €
Ethernet Switch	25,00	1 u	25,00 €
TOTAL BEFORE TAX			25357,00 €
TAX (21%)			5324,97 €
TOTAL PRICE AFTER TAX			**30681,97 €**

Table 20. Budget

ETSEIB

7. Environmental impact

The environmental impact from this work is directly related to the fabrication of all necessary instruments and electronic equipment, as well as electricity consumption related to the operation of the RSOC stack. During operation, the oven required about 1,5 kW of power to keep the stack at 750ºC. The fabrication of expensive components is also to be considered, but they can be re-used in later works. The electricity consumed by the personal computer during programming, modelling, simulation, and parameter estimation is very difficult to measure.

It is important to note that this work is helped develop the prototype of a RSOC system in the context of the HyBCN project, which will store renewable energy in the form of green hydrogen and produce clean electricity by transforming this hydrogen into water. RSOC technology is a promising solution to the intermittency of renewable energy. For this reason, we can conclude that this resulted in a positive impact on the environment.

8. Gantt diagram

Tasks	Start	Finish	01-09	15-09	01-10	15-10	01-11	15-11	01-12	15-12	01-01	15-01	01-02	15-02	01-03	15-03	01-04	15-04	01-05	15-05	01-06	15-06
Familiarization with RSOC technology and LabVIEW programming interface	01/09/2020	18/09/2020		▓																		
RSOC experimental station programming and testing	18/09/2020	07/12/2020			▓	▓	▓	▓	▓													
Installation of new RSOC stack and performing experiments	10/12/2020	28/02/2021							▓	▓	▓		▓									
Expansion of Simulink model	01/12/2020	31/01/2021							▓	▓	▓											
Parameter estimation	01/02/2021	30/06/2021											▓	▓	▓	▓	▓	▓	▓	▓	▓	▓
Control system design	01/02/2021	01/03/2021											▓	▓	▓							
Collaboration in the final stages of HyBCN project	01/04/2021	30/06/2021															▓	▓	▓	▓	▓	▓

ETSEIB

9. Conclusions

After months of work in different aspects related to RSOC operation, programming, modelling, control, and parameter estimation, the conclusions are explained below.

Firstly, a LabVIEW program to operate the RSOC was successfully developed. It fulfilled all the requirements and accomplished all objectives. This program allowed the user to perform polarization curve and sweep experiments automatically, as well as control the station manually when preferred. The author of this work supervised a total of 74 experiments, the data of which is available in Annex 1.

Then, the MATLAB/Simulink model was revised and expanded with the boiler, heat exchangers and efficiency calculation. The modelling of the condenser was discarded in accordance with other HyBCN members because it had no interaction with the control system and little relevance. The added elements brought relevant data and simulations helped make decisions for the construction and programming of the RSOC prototype.

In the MATLAB/Simulink model, the gas mass flow rate control was modelled and allowed the operation in both modes with different flow rate configurations. The temperature controller was also programmed with two simple PI controllers for heating and cooling, and a similar design has been used later in the prototype. Heating was achieved by the oven, while cooling was implemented with an air bypass valve that opened when needed, reducing the inlet temperature of air down to a minimum of 300ºC, cooling the stack by convection.

Finally, parameter estimation with the experimental data from six polarization curve experiments was performed using the Particle Swarm Optimization method, and the results are presented. More analysis is required, and data from more experiments will be considered in future works.

10. Acknowledgements

I would like to thank everyone who helped during its elaboration: Maria, Vicente, Lucile, Gotzon, Attila, Marc, Jaume, James. I prefer to address them in more detail in Catalan.

En primer lloc, vull agraïr l'ajuda i l'atenció rebuda per part de la meva directora, la Maria Serra. La seva constància i esforç han fet possible la realització d'aquest treball.

També vull agraïr especialment l'ajuda del Vicente Roda, que m'ha regalat moltes hores de treball al laboratori, i ha estat vital en la posada a punt de l'estació de proves.

Moltes gràcies a la Lucile i el Gotzon, que també han col·laborat al laboratori i m'han aconsellat sobre el treball quan ho he necessitat.

Finalment, vull agraïr a la resta de l'equip del projecte HyBCN (Attila, Marc, Jaume, James) la vostra dedicació i expertesa.

ETSEIB

Bibliography

[1]   A. Kahan, "EIA projects nearly 50% increase in world energy usage by 2050, led by growth in Asia," 2019. https://www.eia.gov/todayinenergy/detail.php?id=41433 (accessed Sep. 22, 2020).

[2]   "IRI - Hy-BCN." https://www.iri.upc.edu/project/show/236 (accessed Sep. 15, 2020).

[3]   E. Delgado Ferrer, M. Serra, and A. Husar, "Modelización y gestión térmica de una pila de combustible SOFC," 2017.

[4]   A. Cifuentes *et al.*, "Modelling of Solid Oxide Electrolizer and hydrogen leak estimation," 2019.

[5]   J. H. Gross, "The Issue : Fuel Cell Technology," *Jt. Legis. Air Water Pollut. Control Conserv. Comm.*, 2002.

[6]   "Fuel Cell History." https://fuelcellsworks.com/knowledge/history/ (accessed Nov. 20, 2020).

[7]   "Japan: A success story in deploying Fuel Cell micro-Cogeneration." http://www.pace-energy.eu/japan-a-success-story-in-deploying-fuel-cell-micro-cogeneration/ (accessed Nov. 23, 2020).

[8]   "Comparison of Fuel Cell Technologies." https://www.energy.gov/eere/fuelcells/comparison-fuel-cell-technologies (accessed Nov. 23, 2020).

[9]   K. Chen and S. P. Jiang, "Surface Segregation in Solid Oxide Cell Oxygen Electrodes: Phenomena, Mitigation Strategies and Electrochemical Properties," *Electrochem. Energy Rev.*, vol. 3, no. 4, 2020, doi: 10.1007/s41918-020-00078-z.

[10]   S. D. Ebbesen, X. Sun, and M. B. Mogensen, "Understanding the processes governing performance and durability of solid oxide electrolysis cells," *Faraday Discuss.*, vol. 182, 2015, doi: 10.1039/c5fd00032g.

[11]   S. P. S. Badwal, "Stability of solid oxide fuel cell components," *Solid State Ionics*, vol. 143, no. 1, pp. 39–46, 2001, doi: 10.1016/S0167-2738(01)00831-1.

[12]   S. P. S. Badwal, S. Giddey, C. Munnings, and A. Kulkarni, "Review of progress in high temperature solid oxide fuel cells," *J. Aust. Ceram. Soc.*, vol. 50, no. 1, pp. 23–37, 2014.

[13]   J. Larminie and A. Dicks, *Fuel Cell Systems Explained*. 2003.

[14]   R. Guidelli *et al.*, "Defining the transfer coefficient in electrochemistry: An assessment (IUPAC Technical Report)," in *Pure and Applied Chemistry*, 2014, vol. 86, no. 2, doi: 10.1515/pac-2014-5026.

[15]   J. Bernechea and M. Serra, "Modelling and Control of Reversible Solid Oxide Cell," Universitat Politècnica de Catalunya, 2020.

[16]   A. Gebregergis, P. Pillay, D. Bhattacharyya, and R. Rengaswemy, "Solid Oxide Fuel Cell Modeling," *IEEE Trans. Ind. Electron.*, vol. 56, no. 1, pp. 139–148, 2009, doi: 10.1109/TIE.2008.2009516.

[17]   S. Thomas, R. Thomas, A. K. Zachariah, and R. K. Mishra, *Spectroscopic Methods for Nanomaterials Characterization*, vol. 2. 2017.

[18]   R. Lan, P. I. Cowin, S. Sengodan, and S. Tao, "A perovskite oxide with high conductivities in both air and reducing atmosphere for use as electrode for solid oxide fuel cells," *Sci. Rep.*, vol. 6, 2016, doi: 10.1038/srep31839.

[19]   A. Cirera, C. Lpez-Gándara, and F. M. Ramos, "YSZ-based oxygen sensors and the use of nanomaterials: A review from classical models to current trends," *Journal of Sensors*, vol. 2009. 2009, doi: 10.1155/2009/258489.

[20]   P. Kazempoor, V. Dorer, and F. Ommi, "Modelling and performance evaluation of solid oxide fuel cell for building integrated co- and polygeneration," *Fuel Cells*, vol. 10, no. 6, 2010, doi: 10.1002/fuce.200900082.

[21]   J. R. Welty, C. E. Wicks, and R. E. Wilson, "Fundamentals of momentum, heat, and mass transfer. Fifth edition.," 2008.

[22]   F. R. Bianchi, A. Baldinelli, L. Barelli, G. Cinti, E. Audasso, and B. Bosio, "Multiscale modeling for reversible solid oxide cell operation," *Energies*, vol. 13, no. 19, 2020, doi: 10.3390/en13195058.

[23]   H. Yoshida and H. Iwai, "Thermal management in solid oxide fuel cell systems," *Fifth Int. Conf. Enhanc. Compact. Ultra Compact Heat Exch.*, no. September, pp. CHE2005-01, 2005.

[24]   R. O'Hayre, S.-W. Cha, W. Colella, and F. B. Prinz, *Fuel Cell Fundamentals.* 2016.

[25]   "National Instruments." https://www.ni.com/ (accessed Apr. 22, 2021).

[26]   "Temperature   Measurement." https://www.fierceelectronics.com/components/temperature-measurement (accessed May 15, 2021).

[27]   "Power   supply." https://en.wikipedia.org/wiki/Power_supply#Programmable_power_supply (accessed May 12, 2021).

[28]   "Programmable load." https://en.wikipedia.org/wiki/Programmable_load (accessed May 12, 2021).

[29]   "Modbus RTU." https://www.rtautomation.com/technologies/modbus-rtu/ (accessed May 16, 2021).

[30]   X.-Y. Miao, O. B. Rizvandie, and H. L. Frandsen, "Modelling of local mechanical failure in solid oxide cell stacks," *Appl. Energy*, vol. 293, no. March, p. 116901, 2021, doi: 10.1016/j.apenergy.2021.116901.

[31]   "Polarization curves."   https://www.fuelcellstore.com/blog-section/polarization-curves
         (accessed May 13, 2021).

[32]   Y. Zhu and K. Tomsovic, "Development of models for analyzing the load-following
         performance of microturbines and fuel cells," *Electr. Power Syst. Res.*, vol. 62, no. 1,
         pp. 1–11, 2002, doi: 10.1016/S0378-7796(02)00033-0.

[33]   J. T. Pukrushpan, H. Peng, and A. G. Stefanopoulou, "Control-oriented modeling and
         analysis for automotive fuel cell systems," *J. Dyn. Syst. Meas. Control. Trans. ASME*,
         vol. 126, no. 1, 2004, doi: 10.1115/1.1648308.

[34]   "Brazed plate heat exchangers - Boyd."   https://www.boydcorp.com/thermal/liquid-
         cooling/liquid-heat-exchangers/brazed-plate-heat-exchangers.html (accessed May 10,
         2021).

[35]   "NTU method." https://en.wikipedia.org/wiki/NTU_method (accessed May 10, 2021).

[36]   L. Hai, J. Chen, and L. Guo, "Particle swarm optimization," in *Comprehensive energy
         systems*, 2018.

[37]   "Particle   swarm   optimization."
         https://en.wikipedia.org/wiki/Particle_swarm_optimization (accessed May 22, 2021).

[38]   X. Zhang, D. Zou, and X. Shen, "A novel simple particle swarm optimization algorithm
         for global optimization," *Mathematics*, vol. 6, no. 12, 2018, doi: 10.3390/math6120287.

ETSEIB